Multiple attenuation using hyperbolic formulas

Dissertation with the aim of achieving a doctoral degree
at the Faculty of Mathematics, Informatics and Natural Sciences
Department of Earth Sciences
of Universität Hamburg

submitted by
Manizheh Vefaghnematollahy

2016 in Hamburg

Day of oral defense: 17.01.2017
The following evaluators recommend the admission of the dissertation:
Prof. Dr. Dirk Gajewski
PD. Dr. Claudia Vanelle

Abstract

The main objective of seismic data processing is to obtain information about the subsurface structure and properties from the recorded data. Almost all imaging methods assume that the recorded seismograms contain only primary reflections. Consequently, identification and suppression of multiples is of high importance in data processing. In this thesis, I use hyperbolic formulas to estimate travel times of the multiples in the prestack data. For this estimation, zero-offset traveltime of multiples are needed which can be obtained from the stacked section. The estimated traveltimes are used to adaptively subtract the multiples from the original data.

In this work, a new zero-offset picking approach is introduced which traveltime of the first layer multiples are picked directly from the stacked section. This method was applied to both synthetic and filed data. Moreover, a 3D dataset was examined to verify a new automatic picking approach. Conflicting dip situations are very challenging for automatic picking of an event. In order to obtain a stacked section with less conflicting dip situations, the application of this method in Common Scatter Point (CSP) domain was studied. To address other surface related multiples as well as first layer multiples, I proposed to use additional information like coherency or velocity as a guide for zero-offset traveltime picking.

The proposed approaches are considered interpretational. All the results are quite promising. Moreover, it is fast and robust and performs stably for dipping events. Furthermore, it is field applicable and does not require a high computational effort. Only surface related multiple attenuation was investigated but it could be applied to internal multiples as well. The method can be applied within any kind of stacking operator including Common Mid Point (CMP) or Common Reflection Surface (CRS) staking operator.

Zusammenfassung

Das Hauptziel der seismischen Datenverarbeitung ist es, aus den aufgezeichneten Daten Informationen über die Struktur und die Eigenschaften des Untergrunds zu erhalten. Fast alle digitalen Bildverarbeitungsverfahren gehen davon aus, dass die aufgezeichneten Seismogramme nur Primärreflexionen enthalten. Folglich ist bei der Datenverarbeitung die Identifikation und Unterdrückung von Multiplen von großer Bedeutung.

In dieser Arbeit werden die Laufzeiten von Multiplen in prestack Daten unter Verwendung hyperbolischer Formeln berechnet. Für diese Berechnung wird eine zero-offset Laufzeit von Multiplen benötigt, die aus der gestapelten Sektion erhalten werden können. Die berechneten Laufzeiten werden verwendet, um die Multiplen adaptiv von den ursprünglichen Daten zu subtrahieren. In dieser Arbeit wurde ein neues zero-offset Picking untersucht, bei dem die Laufzeit der Multiplen in der ersten Schicht direkt aus der gestapelten Sektion sowohl für synthetische Daten als auch für Felddaten ausgewählt wurde. Darüber hinaus wurde ein 3D-Datensatz untersucht, um eine neue automatische Bestimmung der Ersteinsätze zu verifizieren. Conflicting dip Situationen sind sehr schwierig für die automatische Ersteinsatzbestimmung eines Ereignisses. Um eine Stapelsektion mit weniger conflicting dip Situationen zu erhalten, wurde die Anwendung dieses Verfahrens in der Common Scatter Point (CSP) Domäne untersucht. Um andere oberflächenbezogene Multiplen sowie die Multiplen der ersten Schicht zu adressieren, wird die Verwendung eines Attributs wie zum Beispiel Kohärenz oder Geschwindigkeit als Orientierungshilfe für das zero-offset Picking vorgeschlagen.

Der vorgeschlagene Ansatz wird als interpretatorischer Ansatz betrachtet. Die Ergebnisse sind alle vielversprechend. Darüber hinaus ist diese Methode schnell und robust und führt zu Stabilität für Dippingfälle und große Offsets. Außerdem ist sie im Feld anwendbar und erfordert keinen hohen Rechenaufwand. Sie wurde auf oberflächenbezogene Multiplen angewandt, könnte aber auch für interne Multiplen verwendet werden. Das Verfahren kann mit jeder Art von Stapeloperator, z.B. Common Mid Point (CMP) oder Common Reflection Surface (CRS) verwendet werden.

Contents

Introduction

Seismic sections are affected by noise which can obscure reflections and diffractions. This is why it should be identified and suppressed prior to interpretation. One source of noise are multiple reflections. Their presence in the data can be misinterpreted as, or interfere with, primaries. Multiple attenuation, which has been a longstanding topic in seismic, is still partially solved (Landa et al., 1999). Many methods are available but every method uses different assumptions. These methods are applicable only when their assumptions and preconditions are satisfied. But there are many cases when these assumptions are not valid or where the preconditions are difficult or impossible to achieve. Therefore, multiple attenuation is still a challenging step in a seismic data processing workflow.

The method which is presented in this thesis is based on a previously published Common Reflection Surface (CRS) workflow (Dümmong and Gajewski, 2008). Their method is an entirely data driven approach and includes two steps of prediction: first, zero-offset multiples in a CRS stacked section are predicted, and in the second step, the obtained CRS attributes are used for pre-stack multiple prediction. They proposed multiple prediction in the CRS stacked section using a series of convolutions. This concept of multiple prediction by convolution of stacked traces i.e. poststack Surface Related Multiple Elimination (SRME) originates from the work of (Verschuur et al., 1992) and (Kelamis and Verschuur, 1996). They supposed that the stacked data result from propagation of a plane wave in a homogeneous medium. The workflow is restricted to 1D media; therefore, errors for dipping events are inevitable and it is necessary to correct the predicted data. This correction is not easy to determine. To resolve these issues, I proposed a method which includes picking the multiples directly in the stacked section or using an attribute as a guide. The zero-offset traveltime of multiples, the stacked section and the velocity section contribute to predicting the prestack traveltime of multiples using hyperbolic formulas. This approach can be applied to surface related multiples as well as internal multiples. The disadvantage of the proposed workflow is that it relies on interpretation.

Hyperbolic stacking operators are affected by spread length bias. To resolve this issue, I applied the method separately to different ranges of offset.

Chapter 1 gives a definition of multiples and an overview of common multiple attenuation methods. Then, the CRS workflow of (Dümmong and Gajewski, 2008) is reviewed. Afterwards, an adaptive filtering method which is a very powerful tool in seismic processing

including multiple attenuation is introduced. Besides from applying the method in CMP domain, I applied it in a Common scatter Point domain to encounter less conflicting dip situation in comparison with CMP domain. CSP data mapping is also introduced in this chapter.

In **Chapter 2**, I introduce a prestack multiple attenuation where multiples are picked directly in the stacked section. In this chapter, a 2D synthetic and a 2D field data example of application of this method, where the multiples are picked manually, are shown. A 3D synthetic example is provided as well, which verifies the method within a newly introduced automatic picking strategy. The last example in this chapter is an application of the method in the partially migrated domain. Since this domain contains less diffractions and conflicting dip situations, picking multiples is less challenging.

In **Chapter 3**, a method is proposed to address other surface related multiples as well as first layer multiples. In the first section coherency is used as a guide to pick the zero-offset traveltime of multiples. Then a synthetic and a field data example are provided. In the next step, a velocity section is used to provide guidance on picking multiples. Again a synthetic and a field data example of the application of the method within a CRS workflow are shown.

In this thesis, different examples of different approaches of the proposed method are investigated. **Chapter 4**, I compare these approaches and I give the conclusions and outlook.

In **Appendix A**, I review two of the most common methods for multiple attenuation, f-k filtering and Radon transform. Since these methods are based on Normal Move Out (NMO), prior to review these methods first I define the NMO concept. In **Appendix B** and in **Appendix C**, I explain the concepts of convolution and correlation which is very fundamental in adaptive filtering. In **Appendix D**, tables containing parameters which I used in this thesis to process the data are provided.

Chapter 1

Theory

In seismic reflection measurements a source is set off near or at the surface. Sound waves propagate in all directions from the source, this energy is then recorded by surface or borehole receivers. Seismic imaging methods focus on creating an image of the reflection properties of the subsurface.

Most of these methods assume that energy has been reflected only once as indicated by the yellow lines in the Figure 1.1 but sometimes reflection has more than one bounce which are depicted with the blue lines in Figure 1.1. These reflections are called multiples and cause additional reflections of events which are already present in the data. Although multiples contain information, that can be used, they are usually considered as noise and need to be removed in order to gain an untainted image of the subsurface. This process is often referred to as multiple attenuation, multiple suppression or demultiple.

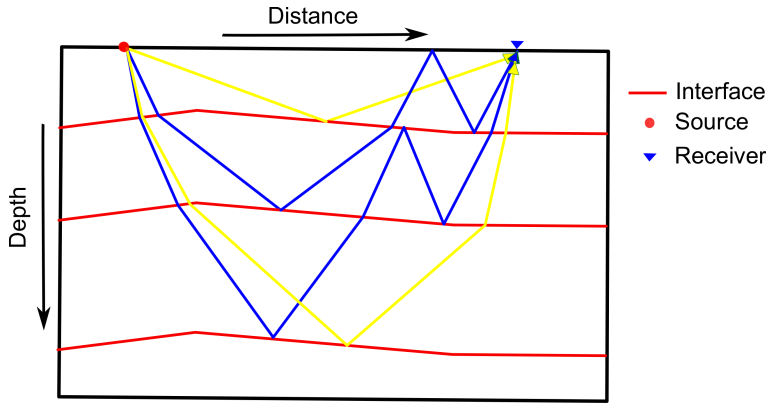

Figure 1.1: Yellow lines show primary reflections, that have only one upward reflection. Multiples, which have more than one downward reflection, are depicted with blue lines (modified after Verschuur, 2006).

1.1 Categorizing of multiples

There are different approaches to classify multiples. If we categorize the multiples according to the shallowest interface where the downward reflection occurs then we have two main categories:

1. Surface related multiples;
2. Internal multiples;

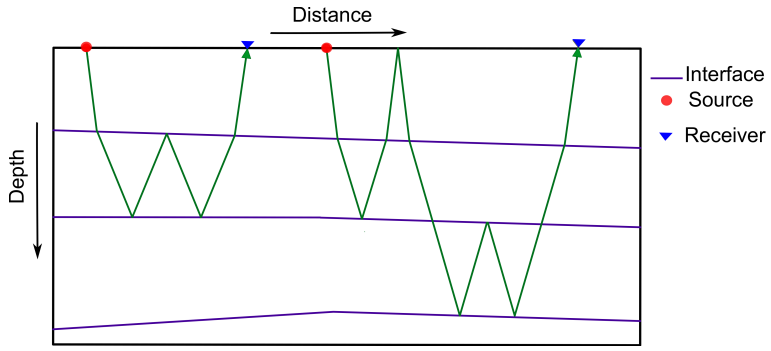

Figure 1.2: The multiple on the left side has one downward reflection below the surface so it is called an internal multiple. The multiple path on the right side has two downward reflections but the shallowest reflector, where the downward reflection occurs, is the free surface so that it is called a surface related multiple (modified after Verschuur, 2006).

In Figure 1.2 there are two multiples, the left side has one downward reflection below the surface so it is called internal multiple. The multiple on the right side has two downward reflections but the shallowest reflector, where the downward bounce occurs, is the free surface so that it is called surface related multiple. In other words, surface related multiples disappear if the free surface was replaced by a transparent surface. Since surface related multiples are mostly issue in marine data, they are divided into sub-categories:

1. First layer multiples or water layer multiples: the energy of such multiples propagate only in water. In other words, they never travel below the water bottom. Figure 1.3(a) shows an example of first order and second order water layer multiples.
2. First layer reverberation/ peg-legs: The energy of this multiple type propagates below the water bottom but there is only one reflection. Figure 1.3(b) illustrates an example of such multiples. Reverberations can occur at both the source or receiver side.
3. Other surface related multiples: These multiples, which have more than one reflection below the water bottom, are important in case of a strong reflector like salt layering below the water bottom. Figure 1.3(c) shows two examples of such multiples.

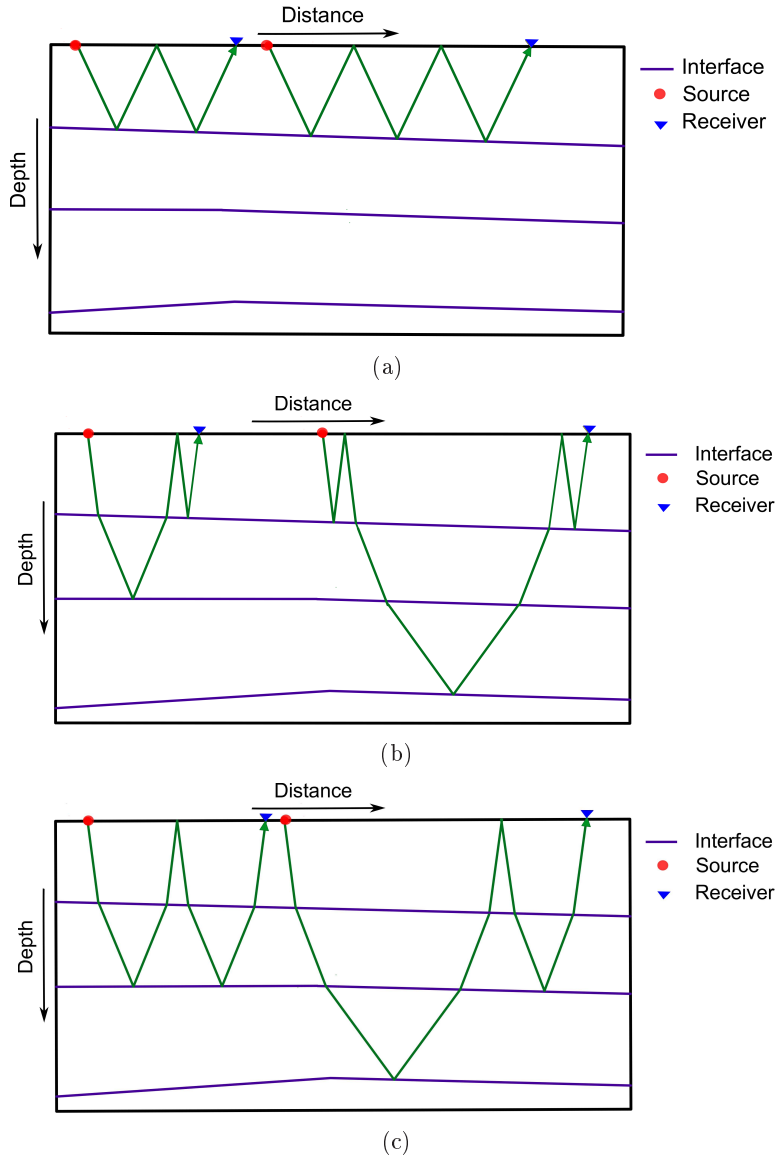

Figure 1.3: Classification of surface related multiples. (a) Multiples that travel only within the first layer. (b) Multiples with one reflection below the water bottom. (c) Multiples with more than one reflection below the water bottom (modified after Verschuur, 2006).

Furthermore, multiples can be categorized based on their period: there are long period and short period multiples. Long period multiples appear in the seismic data as separate events and behave more deterministically than short period multiple, Figure 1.4(a) is an example of this type of multiple. On the contrary, short period multiples do not appear separately from primaries that generate them. They occur due to the presence of thin layers and usually overlay the primaries, resulting in one effective event in the image leading to falsified defected wavelet, which is different from the source wavelet (O'Doherty and Anstey, 1971). As illustrated in Figure 1.4(b) these multiples are related to thin layers. There is no clear distinction between long period and short period multiples in the seismic image but they can be distinguished by the length of the source wavelet.

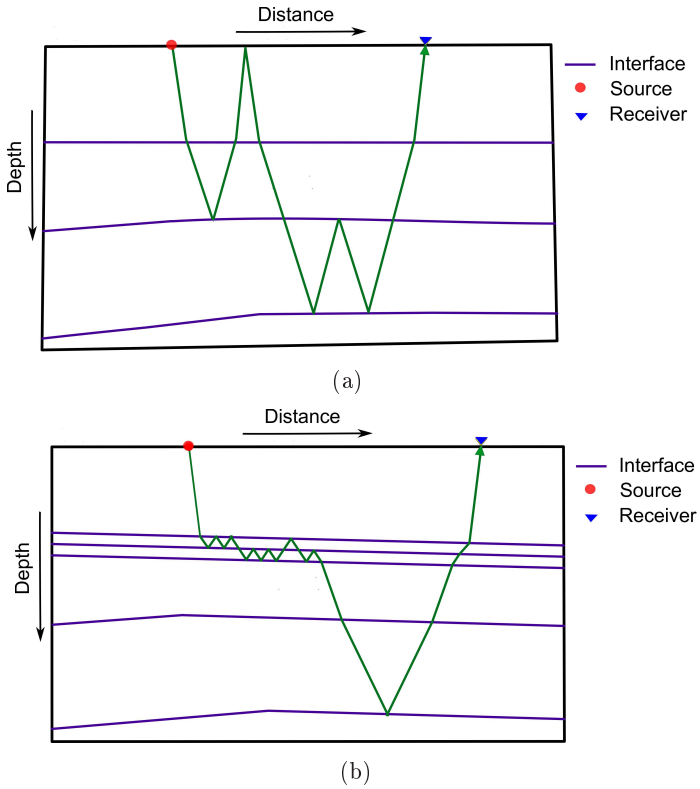

Figure 1.4: Classification of multiples. (a) Long period multiples. (b) Short period multiples which are related to thin layers (modified after Verschuur, 2006).

If the difference between arrival times of a multiple and the related primary is shorter than the period of the source wavelet then the multiple is called short period multiple otherwise we consider the multiple as a long period multiple. In this thesis, only long period multiples will be investigated. The effect of short period multiples can usually be removed with the help of source signature deconvolution techniques like spiking deconvolution or minimum phase deconvolution (Leinbach, 1995). Moreover, in thin layers short period multiples demonstrate another effect known as effective absorption. This influences the source signature by suppression and dispersion impact, which can be corrected by inverse-Q filtering (Bickel and Natarajan, 1985).

1.2 Characteristics of multiples in marine data

It is critical to recognize the effect that multiples can have on a stacked section. The following characteristics of multiples help us to distinguish multiples from primaries (Verschuur, 2006):

- Periodic repetition: if some reflections are replicated in a specific time interval and have amplitudes decreasing with time, they are likely to be multiples. Figure 1.5

shows a stack section of data from a synthetic velocity model including two horizontal layers, the upper event is primary and the other events are multiples related to this primary.

- Increasing dips: if primaries are dipping, the dip of multiples in every bounce increases by the same amount as the dip of primaries. An example of a synthetic model with a dipping reflector is shown in the Figure 1.6, where in the corresponding stack section the dip of multiples increases in every bounce.

- Conflicting dips: multiples may conflict with primary reflections from deeper interfaces. This is illustrated in Figure 1.7, which is a stack section of a synthetic model with two dipping reflectors. We can see that the first order multiple conflicts with the primary from the deeper reflector. However, any conflicting dip situation is not necessarily a sign for presence of multiples.

- Focusing and defocusing events: small fluctuations in primaries will be enhanced in high order multiples and will cause focusing and defocusing events. The synthetic model which is used here includes only one reflector with small geometry variations. Figure 1.8 shows the corresponding stack section.

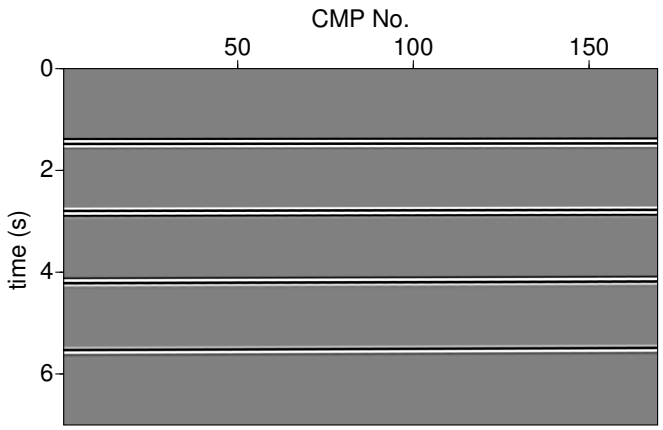

Figure 1.5: The stacked section of the data generated from a two horizontally layered medium. The upper event is a primary and multiples are repeated with a certain time interval.

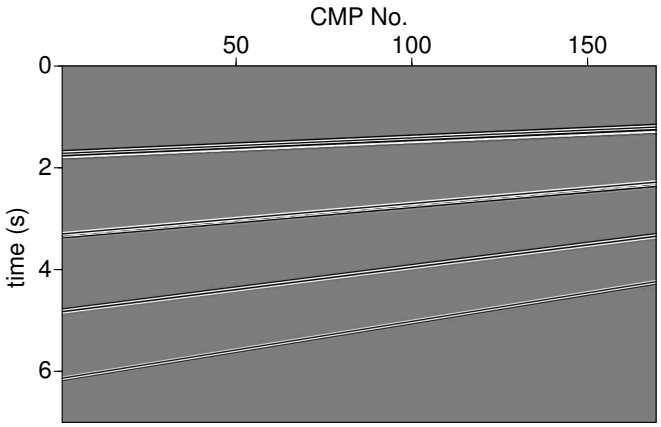

Figure 1.6: The stacked section of the data obtained from a synthetic model with one dipping reflector. Dip of multiples is increasing.Only three multiples are modeled here.

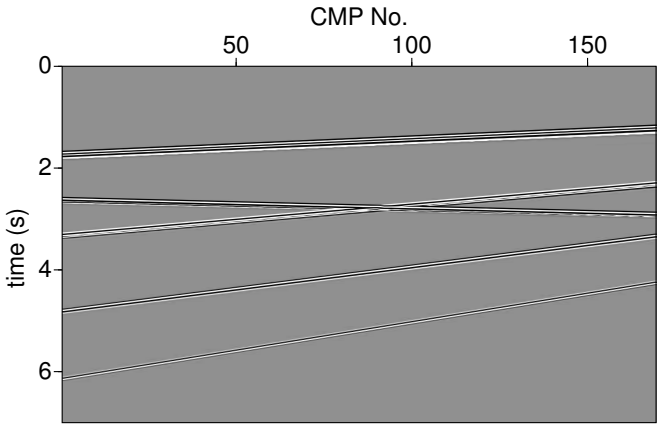

Figure 1.7: The stacked section of the data obtained from a synthetic model with two dipping reflectors: multiples conflict with the primary from the deeper reflector. Only three multiple related to the primary from the upper reflector are modeled.

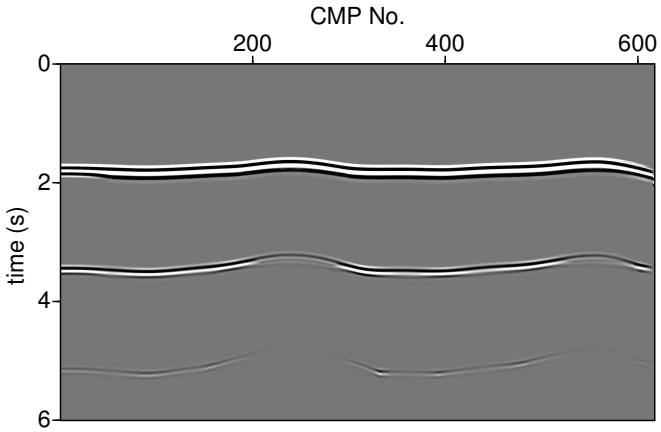

Figure 1.8: The stacked section of the data obtained from a synthetic model consisting of one dipping reflector with small geometry variations. In higher order multiples focusing and defocusing events are generated.

1.3 Conventional multiple attenuation methods

Standard stacking process, using a proper velocity profile, and prestack deconvolution suppress a large amount of multiple energy in the stacked section (Mayne, 1962). However, some multiples leak into the stacked section and application of some multiple attenuation methods is inevitable. The commonly used multiple attenuation approaches are:

- **Based on different spatial behavior between multiples and primaries:** Multiples travel along different paths in the subsurface, therefore they have come through different properties like velocity anomaly and depict different reflecting structures in comparison to primaries. So with filtering techniques they can be separated from primaries. This filtering can be applied in poststack domain or in prestack domain. Two of the most common methods related to this category are f-k filtering (Ryu, 1982) and Radon transform (Diebold and Stoffa, 1981) which are introduced in the **Appendix A**.

- **Based on the fact that multiples have periodic behavior and predictability:** Essentially there is a relationship between multiples and primaries. In other words, multiples are events that appear in a repetitive form. This fact is exploited in some multiple attenuation methods. Generally, these methods consist of two main steps: first, multiples are predicted exploiting the fact that primaries and multiples have an inherent relationship. In the next step, they are subtracted from the original data. Only in an ideal case of zero-offset data and horizontally layered media multiples appear in a periodic pattern. Even in horizontally layered media, in far offsets, periodicity is not preserved, that is why some assumptions should be made. Usually, these methods are used in prestack domain. However, it is possible to use them in poststack domain or after poststack migration but some further assumptions like subsurface behaves as a 1D medium, have to be made. One of the most common approaches in this category, which is also one of the oldest way of multiple attenuation, is predictive deconvolution (Robinson, 1957, 1967). Since then a plenty of methods has been developed including Common Reflection Surface (CRS) workflow (Dümmong and Gajewski, 2008), which I will review later in Section 1.5, after introducing the CRS stacking operator.

1.4 Common Reflection Surface (CRS) stacking

Since the main tool for workflow of (Dümmong and Gajewski, 2008) is CRS operator, before reviewing this method, CRS operator is introduced.

The CRS method is a powerful tool. Contrary to the CMP method where stacking is performed along a line, it sums up the data along a surface. In fact, the CRS method is a generalization of the CMP method. An example of a CRS stacking surface is shown in Figure 1.9. The CRS stack considers the subsurface as a curved reflector. As a result,

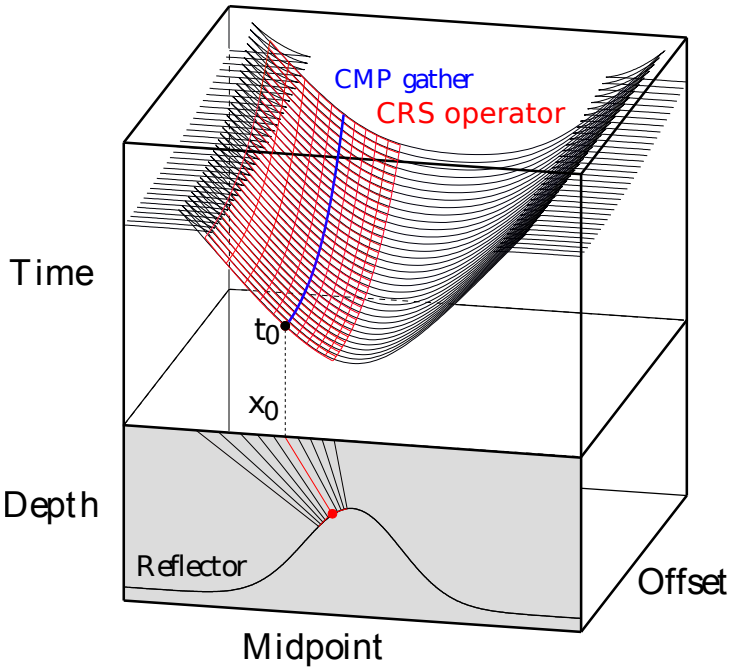

Figure 1.9: Example of a common reflection surface (red) (modified after Müller, 1999). Here, t_0 is the reference traveltime at the central midpoint x_0.

the local characterization of the subsurface like: dips, anticlines, synclines is included. There are different ways for CRS traveltime computation, such as hyperbolic and parabolic formulations. Both depend on the three CRS stacking parameters. The hyperbolic formula is given by

$$t^2(\Delta x_m, h) = (t_0 + \frac{2\sin\alpha}{v_0}\Delta x_m)^2 + \frac{2t_0\cos^2\alpha}{v_0}(\frac{\Delta x_m^2}{R_N} + \frac{h^2}{R_{NIP}}),$$

where $\Delta x_m = x_m - x_0$ is the displacement from the central midpoint x_0 and h is the half-offset, t_0 is the ZO traveltime and v_0 is equal to the near-surface velocity. The CRS stacking parameters are: α which represents the angle of emergence of a ZO ray, R_{NIP} and R_N are the Normal Incidence Point (NIP) wave and normal wave radii. The N-wave or normal wave is emitted by an imaginary exploding reflector segment around the NIP whereas the NIP-wave is emitted by a fictitious point source positioned at the reflector, i. e., point of the normal incidence (Müller, 1999). Figure 1.10 illustrates the physical concept of the kinematic wavefield. In the 2D case there are only three parameters for CRS attributes but in the 3D case the parameters increase to 8, since R_{NIP} and R_N have three dimensions in space and α is described by two elements dip and azimuth. For more information, see, e.g., Müller (1999); Mann (2002).

1.4.1 Implementation

There are different approaches for estimation of the three CRS attributes. To start with, there is pragmatic approach (Mann, 2002), that was initially applied in CRS workflow.

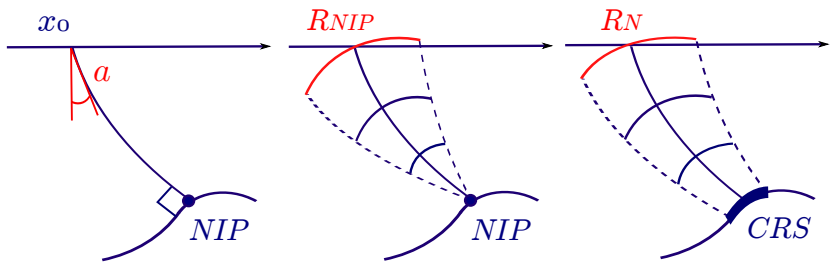

Figure 1.10: Physical meaning of the CRS parameters. α is the angle of emergence of a zero-offset ray and R_{NIP} and R_N are the Normal Incidence Point (NIP) wave and normal wave radii (Schwarz, 2011).

Another approach is simultaneous search, which is a challenging task and has been developed recently. Simultaneous search may be more expensive in comparison with pragmatic approach but it provides more reliable attributes and yields a stack section with higher resolution (e.g., Walda and Gajewski, 2015a). An example of this approach will be presented in **Chapter 3**.

Pragmatic approach

In many cases, if the starting point is already available and the search space of possible solutions is small, it is sufficient to search the nearest minimum/maximum. These algorithms are often referred to as local optimization methods. Pragmatic approach, that was initially applied in the CRS workflow (Mann, 2002), is based on this strategy.

CMP search

One of the solutions for the CRS equation with three parameters is to decompose it into three separate equations. In Equation 1.1 if $x_m = 0$, then

$$t^2(h) = t_0^2 + \frac{2t_0 \cos^2 \alpha h^2}{v_0 R_{NIP}}. \tag{1.1}$$

If:

$$v_{stk}^2 = \frac{2v_0 R_{NIP}}{t_0 \cos^2 \alpha}, \tag{1.2}$$

we can obtain conventional CMP formula with a simple substitution. It shows that CMP traveltimes to the second order are not dependent on the curvature of reflectors (Hubral, 1983)

$$t^2(h) = t_0^2 + \frac{4h^2}{v_{stk}^2}. \tag{1.3}$$

Therefore, the first step of the parameter search is standard velocity analysis.

Zero offset search

The second step in the pragmatic search strategy is done in zero offset configuration, i.e., for $h = 0$. In this case, parameters are estimated in the post stack domain

$$t^2(\Delta x_m, h = 0) = (t_0 + \frac{2 \sin \alpha}{v_0} \Delta x_m)^2 + \frac{2 t_0 \cos^2 \alpha x_m^2}{v_0 R_N}.$$

Now there are two unknown parameters, with the assumption of a plane wave (Hubral and Krey, 1980) the equation can be simplified to

$$t^2(\Delta x_m, h = 0) = t_0 + \frac{2 \sin \alpha}{v_0} \Delta x_m^2. \tag{1.4}$$

In this equation, only the emergence angle is unknown which is estimated in one parameter optimization. Afterwards, R_N can be determined from Equation 1.4. Then, R_{NIP} can be calculated from Equation 1.2.

CRS stack search

Now, as the three initial values are available, the final values can be optimized. Nowadays, different optimization algorithm are available such as flexible polyhedron search (Nelder and Mead, 1965), which was used by (Mann, 2002). Three final attributes are used in Equation 1.1 to stack the data.

Global optimization search

To obtain a better result, global optimization can be applied. In this case number of possible solution is higher than local optimization, therefore, it is more computationally demanding. Since computing facilities are improving steadily, global optimization methods become more popular. There are different algorithms like differential evolution, which has been already applied to field data by (Barros et al., 2015), or genetic algorithm (Walda and Gajewski, 2015b).

1.5 CRS workflow for multiple attenuation

Because the CRS workflow of (Dümmong, 2010) was our motivation to start working in multiple attenuation field, we will introduce their method here. It includes two steps of prediction: first, zero-offset multiples in a CRS stacked section are predicted by series of convolutions, and in the second step, the obtained result is used for prestack multiple prediction.

1.5.1 Multiple prediction

The first step of CRS workflow after stacking is to predict the zero offset traveltime of a multiple. The raypath of the multiple in Figure 1.11 can be seen as two individual primary paths that are connected at the surface. Therefore, it is possible to construct multiples by connecting the primaries. Based on this, (Dümmong and Gajewski, 2008) introduced a prediction method by a series of convolutions which is limited to 1D media. The idea originates from the work of (Verschuur et al., 1992) and (Kelamis and Verschuur, 1996). In this case, it is assumed that the earth is horizontally layered and the waves are horizontal planes. The original idea of predicting multiple in 1D media is reviewed in the following section.

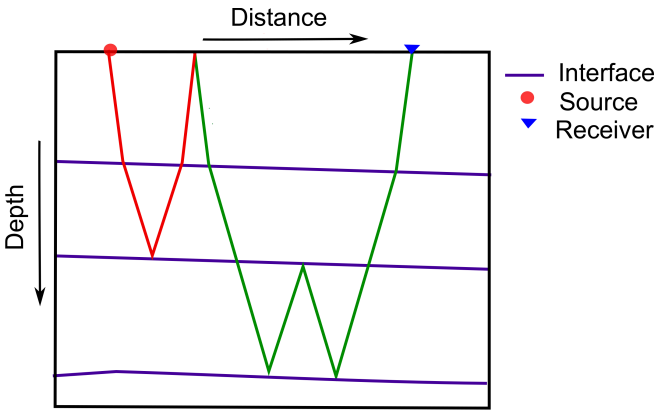

Figure 1.11: The first order surface related multiple can be seen as two individual primary paths that are connected at the surface.

Prediction in 1D Media

For simplicity, we suppose the impulse response of the earth for a horizontal plane wave with infinite frequency is $x(t)$, which includes primaries and internal multiples and different orders of surface related multiples (Verschuur, 2006), then

$$x(t) = x_0(t) + m_1(t) + m_2(t) + m_3(t) + \cdots , \tag{1.5}$$

where $x_0(t)$ includes primary response and internal multiple and $m_1(t)$, $m_2(t)$, and $m_3(t)$ are first, second, and third order of multiples. Autoconvolution of $x_0(t)$ generates the first order multiple

$$m_1(t) = -x_0(t) * x_0(t), \tag{1.6}$$

assuming that the sea surface reflection coefficient is -1. This multiple will arrive at the surface and will be the source for the second order multiple. Then we get

$$m_2(t) = -x_0(t) * m_1(t) = x_0(t) * x_0(t) * x_0(t). \tag{1.7}$$

Then Equation 1.5 can be written as

$$x(t) = x_0(t) - x_0(t) * x_0(t) + x_0(t) * x_0(t) * x_0(t) + \cdots , \tag{1.8}$$

or

$$x(t) = x_0(t) * [\delta - x(t)] = x_0(t) - x_0(t) * x(t), \tag{1.9}$$

It indicates that all surface related multiples can be produced by convolving the primary response with the whole response. Since in frequency domain convolutions become multiplication, then Equation 1.8 can be formulated as

$$X(f) = X_0(f) - X_0^2(f) + X_0^3(f) - X_0^4(f) + \cdots , \tag{1.10}$$

then Equation 1.9 becomes

$$X(f) = X_0(f) - X_0(f)X(f), \tag{1.11}$$

or

$$X_0(f) = X(f)[1 - X(f)]^{-1}. \tag{1.12}$$

This is the equation for calculating surface related multiple free response from the total response. The expansion of this equation is

$$X_0(f) = X(f) + X^2(f) + X^3(f) + X^4(f) + \cdots . \tag{1.13}$$

This equation in time domain look like (Verschuur, 2006)

$$x_0(t) = x(t) + x(t) * x(t) + x(t) * x(t) * x(t) + \cdots . \tag{1.14}$$

This indicates that the multiple free response can be obtained by a series of convolutions. A simple example is provided in Figure 1.12a where there is a primary response and two related multiples $x(t)$. Figure 1.12b is the autoconvolution of the total response $x(t) * x(t)$, Figure 1.12c is the convolution of the result in Figure 1.12b with the total response $x(t) * x(t) * x(t)$ and Figure 1.12d is the result of summation of a, b, and c which gives us the impulse response without multiples. In the following section, to be more realistic, the source signature is included.

Prediction in 1D Media including source signature

In the example with a perfect impulse response, the amplitudes did not change in the generation step. With the consideration of source signature the process becomes more complex. The response of the earth with $s(t)$ being the source signature can be written as (Verschuur, 2006)

$$p_0(t) = x_0(t) * s(t), \tag{1.15}$$

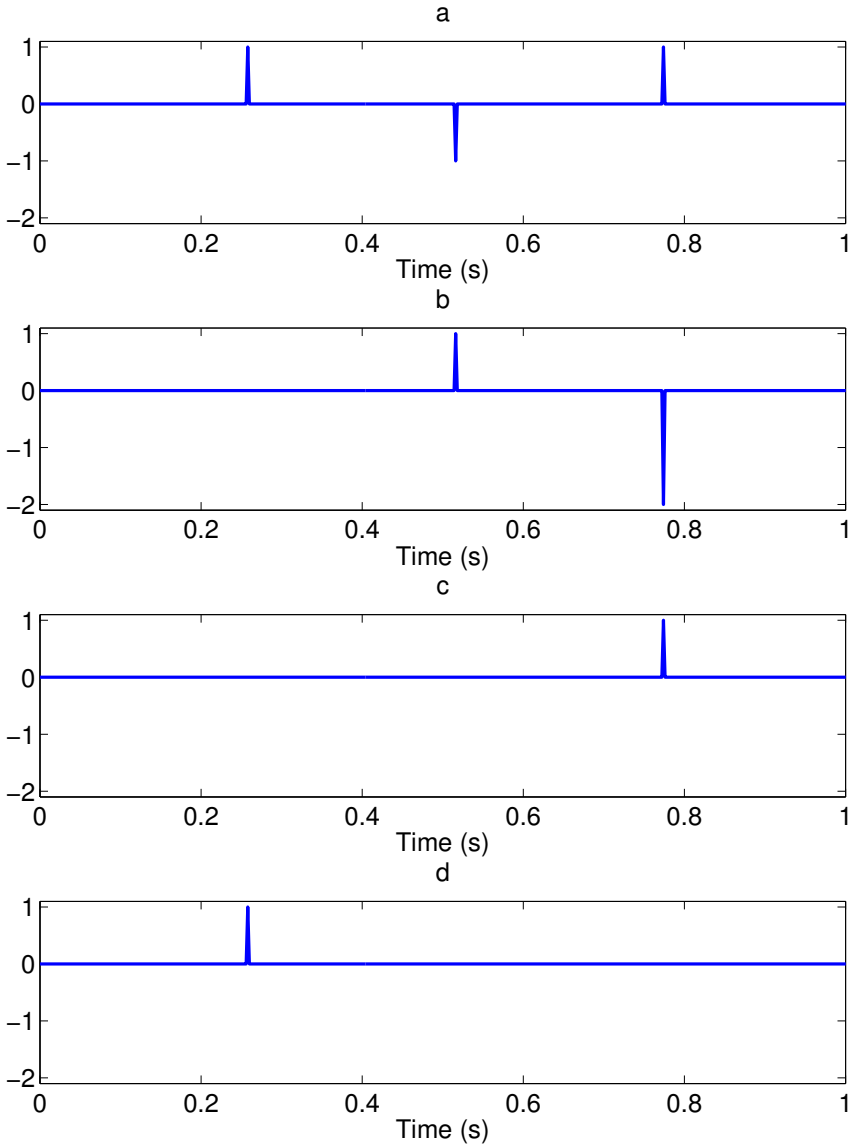

Figure 1.12: (a) is a primary response and two multiples $x(t)$, (b) is the autoconvolution of total response $x(t) * x(t)$, (c) is the convolution of the result in (b) with total response $x(t) * x(t) * x(t)$ and (d) is the result of summation of (a), (b), and (c) which gives us the impulse response without multiple.

and the response of the earth including multiples as

$$p(t) = x(t) * s(t), \tag{1.16}$$

then Equation 1.9 becomes

$$p(t) = x_0(t) * [s(t) - p(t)] = p_0(t) - x_0(t) * p(t). \tag{1.17}$$

With defining a new operator $a(t)$ as

$$a(t) * s(t) = -\delta(t), \tag{1.18}$$

we can rewrite Equation 1.17 in terms of the response without surface related multiples and the response with all multiples as

$$p(t) = p_0(t) + p_0(t) * a(t) * p(t), \tag{1.19}$$

where the $a(t)$ is a convolution filter. Equation 1.14 including source signature can be formulated as

$$p_0(t) = p(t) - a(t) * p(t) * p(t) + a(t) * a(t) * p(t) * p(t) * p(t) - \cdots . \tag{1.20}$$

This equation can also be described in the frequency domain (Verschuur, 2006) as

$$P_0(f) = P(f) - A(f)P^2(f) + A^2(f)P^3(f) - A^3(f)P^4(f) + \cdots , \tag{1.21}$$

where $A(f)$ is

$$A(f) = -[S(f)]^{-1}, \tag{1.22}$$

and $S(f)$ is defined as the Fourier transform of the source signature $s(t)$.

1.5.2 Correction of the 1D Prediction

Since prediction of multiples by a series of convolutions is restricted to 1D media, the errors for dipping events are inevitable and it is necessary to correct the predicted data according to the stacked section. This is done by a crosscorrelation algorithm. This problem can be connected to finding the best overlap between two images. Crosscorrelation algorithms are widely used, e.g., for time-laps imaging (Hale, 2009), cell tracking in nano-biology (Perez-Careta et al., 2008). The normalized crosscorrelation can be formulated as follows

$$CC(\delta_x, \delta_t) = \frac{1}{ntr * nt} * (\sum_{x=0}^{ntr-1} \sum_{t=0}^{nt-1} A_{x,t} * B_{x+\delta_x, t+\delta_t}), \tag{1.23}$$

where $A_{x,t}$ represents the stacked section, $B_{x,t}$ is the predicted multiple section, δ_t and δ_x denote the shift in time and space, ntr the number of traces , and nt the time sample (Hale, 2009). The maximum correlation makes an estimation of the total shift in time and space to best align the two sections. Since with this formula only global shift can be estimated, it can only be applied in cases where geological setting is not too complex and a global shift is sufficient. In case of more complex geology, the process can be implemented in a windowed way (Hale, 2009).

1.5.3 Prestack multiple prediction

As CRS attributes and ZO traveltime of multiples are available, it is possible to estimate traveltimes of multiples using the following formula

$$t^2 = t_0^2 + \frac{2t_0 \cos^2 \alpha h^2}{v_0 R_{NIP}}. \tag{1.24}$$

Note that CRS attributes at t_0 are used to estimate traveltimes of multiples.

1.5.4 Adaptive subtraction

The predicted multiples are then adaptively subtracted from the data. Adaptive filtering is widely used in different steps of processing, including the subtraction of multiples from the original data (e.g., Yilmaz, 2001). In the following, I will introduce the concept of adaptive filtering .

Designing an adaptive filter

An important tool that is needed for multiple subtraction is designing a filter to match the predicted multiples to the original data. Put another way, the problem is designing a convolution filter $f(t)$ to reshape an input signal $x(t)$ into a desired output signal $y(t)$

$$y(t) = f(t) * x(t). \tag{1.25}$$

The first scientist who reported this method was Wiener (1964), therefore, this technique is often referred to as Wiener filter design. For more historical details see, e.g., (Webster, 1978). The difference between the energy of filtered input and desired output can be expressed as

$$E = \sum_n (y[n] - f[n] * x[n])^2, \tag{1.26}$$

assuming that signals are discrete, which means $x[n]$ has values for $t = n\Delta t$ where Δt is the sampling interval and n denotes the total number of samples in the signal. This equation can be written as

$$E = \sum_{n=0}^{M} (y[n] - \sum_{k=0}^{N} f[k]x[n-k])^2. \tag{1.27}$$

The value of E is minimum if the partial derivatives with respect to each of the filter coefficient $f[n]$ are equal to zero

$$\frac{\partial E}{\partial f[n]} = 0. \tag{1.28}$$

The partial derivative of E with respect to $f[1]$ is

$$\frac{\partial E}{\partial f[1]} = \sum_{n=0}^{M} \Big(2\Big(y[n] - \sum_{k=0}^{N} f[k]x[n-k]\Big) \frac{\delta}{\delta f[1]} \Big(y[n] - \sum_{k=0}^{N} f[k]x[n-k]\Big)\Big)$$

$$= 2\sum_{n=0}^{M} \Big(\Big(y[n] - \sum_{k=0}^{N} f[k]x[n-k]\Big)\Big(- x[n-1]\Big)\Big)$$

$$= 2\sum_{n=0}^{M}\left(y[n](-x[n-1]) - \sum_{k=0}^{N} f[k]x[n-k](-x[n-1])\right)$$

$$= 2\sum_{n=0}^{M} -y[n]x[n-1] + \sum_{k=0}^{N} f[k]\sum_{n=0}^{M} x[n-k]x[n-1]. \tag{1.29}$$

This equation can be written as

$$= 2(-\phi_{yx}[1] + \sum_{k=0}^{N} f[k]\phi_{xx}[1-k]), \tag{1.30}$$

where ϕ_{yx} is the crosscorrelation of signal y with signal x and ϕ_{xx} denotes the autocorrelation of signal x. This equation should be equal to zero then

$$\sum_{k=0}^{N} f[k]\phi_{xx}[1-k] = \phi_{yx}[1]. \tag{1.31}$$

In this way, we can compute all the derivatives of E with respect to the $f[i]$ for $i = 0, 1, 2, \cdots, n$.

$$\sum_{k=0}^{N} \phi_{xx}[i-k]f[k] = \phi_{yx}[i], \qquad \text{for} \quad i = 0, 1, 2, \cdots, N. \tag{1.32}$$

This equation can be written in a matrix form, which makes it easier to understand the structure of the equation:

$$\begin{pmatrix} \phi_{xx}[0]+\epsilon^2 & \phi_{xx}[1] & \phi_{xx}[2] & \cdots & \phi_{xx}[N] \\ \phi_{xx}[1] & \phi_{xx}[0]+\epsilon^2 & \phi_{xx}[1] & \cdots & \phi_{xx}[N-1] \\ \phi_{xx}[2] & \phi_{xx}[1] & \phi_{xx}[0]+\epsilon^2 & \cdots & \phi_{xx}[N-2] \\ \vdots & \vdots & \vdots & \ddots & \vdots \\ \phi_{xx}[N] & \phi_{xx}[N-1] & \phi_{xx}[N-2] & \cdots & \phi_{xx}[0]+\epsilon^2 \end{pmatrix} \begin{pmatrix} f[0] \\ f[1] \\ f[2] \\ \vdots \\ f[N] \end{pmatrix} = \begin{pmatrix} \phi_{yx}[0] \\ \phi_{yx}[1] \\ \phi_{yx}[2] \\ \vdots \\ \phi_{yx}[N] \end{pmatrix}, \tag{1.33}$$

where the left-side matrix represents autocorrelation lags of the input wavelet multiplied by the Wiener filter coefficients and the right-side vector shows the crosscorrelation lags of the input wavelet with the desired output. For stabilization, ϵ^2 is added to the diagonal elements of the matrix. A certain fraction of the maximum value of $f[k]$ (typically a few percent of the maximum value) is a good choice for stabilization constant (Verschuur, 2006). To solve this equation, the inverse form of the autocorrelation matrix is multiplied

to the vector of the crosscorrelation lags. The left-side matrix is called Toeplitz matrix, since all the values along a certain diagonal are constant. For solving such a special equation (Levinson, 1947) has suggested a recursion algorithm that reduces the number of calculations from the order N^3 to the order N^2.

Least-square subtraction strategies

Adaptive filtering is used for matching the predicted multiples with the original data. For this purpose some modifications and strategies have to be made. Equation 1.32 considers only one trace but in adaptive subtraction usually an ensemble (e. g., common offset gather) is taken into account. Therefore, the energy that is minimized in this case should contain the sum of the energy of all traces, so Equation 1.26 is modified into

$$E = \sum_j \sum_n (p[j,n] - a[n] * m_0[j,n])^2, \tag{1.34}$$

where p denotes the original data, m_0 is predicted multiple, j indicates the trace number in the section, and n describes the time sample. Considering this extra summation, Equation 1.32 will be expanded into

$$\sum_j \sum_{n=0}^{N} \phi_{mm}[j, i-n] f[n] + \epsilon^2 a[i] = \sum_j \phi_{pm}[j,i], \qquad for \quad i = 0, 1, 2, \cdots, N, \tag{1.35}$$

where $\phi_{mm}[j,n]$ indicates the autocorrelation of the predicted multiples for trace j and $\phi_{pm}[j,n]$ describes the crosscorrelation of the predicted multiple and the input data for trace j (Verschuur, 2006).

Two stages least-square subtraction

In 1997, Berkhout and Verschuur suggested to apply adaptive subtraction in two stages to obtain a better result:

1. Global subtraction in every shot gather to find the deconvolution filter for source signature.
2. Local subtraction within a smaller space-time windows that overlap with each other in both space and time directions.
   For global subtraction a long filter (e.g., 200 ms) is determined, while in local subtraction a small variation from the overall filter is determined. The size of the

local window size could be 25 traces in space and up to hundreds of ms in time (Verschuur, 2006).

1.5.5 Processing tuned to the primaries

After subtracting multiple, the prestack multiple free data is available for further processing steps tuned to image primaries. Figure 1.13 is a schematic illustration of the approach.

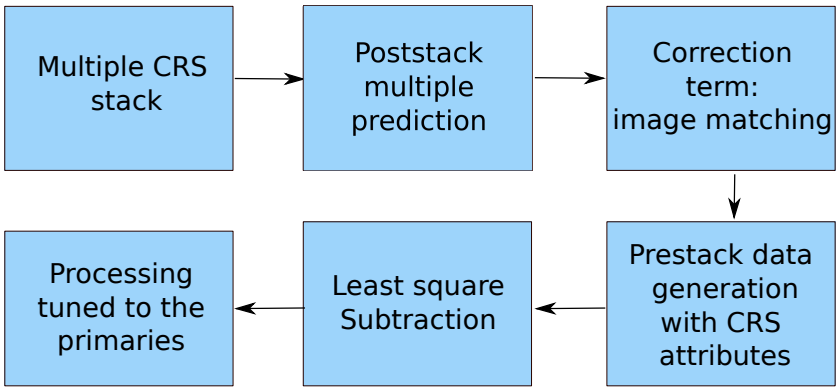

Figure 1.13: Schematic sketch of the CRS multiple attenuation workflow (after Dümmong and Gajewski, 2008).

In this thesis, I will introduce a zero-offset picking approach for multiple attenuation. Besides from applying the method in CMP domain, I also applied it in a Common Scatter Point (CSP) domain to encounter less conflicting dip situations comparing to CMP domain. This domain is introduced in the following section.

1.6 Common Scatter Point (CSP) domain

In this section, I will introduce the Common Scatter Point (CSP) domain but before that, the concept of time migration is described.

1.6.1 Time migration

The aim of migration is to move reflections to their true spatial positions by correcting their dip and length, to collapse diffractions, and to unfold triplications. Thus, it not only provides an image with a better spatial resolution, but also helps to remove the misleading features. There are two main concepts for migration, i.e., time migration and depth migration.The migration process that produces a migrated time section is called time migration while in depth migration the output is a depth section. Depth migration makes the section look similar to the geologic cross section in depth. However, migration

is commonly performed in time. Prestack time migration (PreSTM) is a classical and preferable tool in seismic processing. This is because it is rapid and robust and has the ability to focus seismic events for most geological settings. One of the conventional PreSTM migration types is the Kirchhoff Diffraction Stack. The physical explanation for this method is as follows: a reflector is assumed to be composed of a sufficiently dense set of imaginary point diffractors. The reflective response is obtained by superposition of the diffraction responses from these points, so that the envelope of the diffraction traveltimes is the reflection traveltime surface. In this case, the diffractions superimpose constructively through reflectors and destructively elsewhere. As previously mentioned, the diffractors are imaginary and can not be detected separately. For each diffractor, the traveltime is estimated separately with the time migration operator using Double Square Root (DSR) formula. The amplitudes are summed up along the diffraction traveltimes and the result is assigned to the ZO apex of the migration operator. The 2D DSR equation reads as

$$t_D = \sqrt{\frac{t_0^2}{4} + \frac{(m-h)^2}{v^2}} + \sqrt{\frac{t_0^2}{4} + \frac{(m+h)^2}{v^2}}, \tag{1.36}$$

where h is the half source-receiver offset, m is the midpoint displacement with respect to the considered CMP position, t_0 is the zero-offset traveltime and v is assumed to be the migration velocity. Please note, the time migration velocity does not have a real physical meaning comparing to the depth migration velocity. Time migration velocity is a parameter which provides the best fit of the Kirchhoff migration operator to the data.

1.6.2 CSP data mapping

In 1998, Bancroft et al. reformulated the DSR operator into a single square root as

$$t_D = 2\sqrt{\frac{t_0^2}{4} + \frac{h_e^2}{v^2}}, \tag{1.37}$$

where h_e denotes the equivalent offset which is defined as

$$h_e^2 = m^2 + h^2 - (\frac{2mh}{tv})^2. \tag{1.38}$$

This offset represents the surface distance from the scatter point to the collocated source and receiver. They also developed a physical explanation for the generated gather, which they called Common Scatter Point (CSP) gather. Following this idea, Dell et al. (2010) proposed a new approach to generate CSP gathers by using partial time migration. The main concept of this method is a new parametrization of the Double Square Root (DSR) operator using the common offset apex of migration operator. Since moveout is preserved in CSP domain, it is a suitable domain for further seismic processing steps. The common offset (CO) of the time migration operator is obtained by a hyperbolic formula (Dell et al., 2009)

$$t_{apex} = \sqrt{t_0^2 + \frac{4h^2}{v^2}}. \tag{1.39}$$

Equation 1.36 can be written as

$$t_D = \sqrt{\frac{1}{4}\Big(t_0^2 + \frac{4h^2}{v^2}\Big) + \frac{m(m-2h)^2}{v^2}} + \sqrt{\frac{1}{4}\Big(t_0^2 + \frac{4h^2}{v^2}\Big) + \frac{m(m+2h)^2}{v^2}}. \tag{1.40}$$

With Equation 1.39 one can obtain

$$t_D = \sqrt{\frac{t_{apex}^2}{4} + \frac{m(m-2h)^2}{v^2}} + \sqrt{\frac{t_{apex}^2}{4} + \frac{m(m+2h)^2}{v^2}}. \tag{1.41}$$

Figure 1.14 visualizes the difference between full and partial time migration for a model of a homogeneous medium with a dipping reflector. The reflection response for a dipping reflector is depicted in dark blue. The migration operator is depicted in light blue. In Figure 1.14(a) the migration output is assigned to the ZO operator apex for every CO section (pink line). While in Figure 2.19(b) the CSP mapped output is assigned to the CO operator apex for every CO section (orange line).

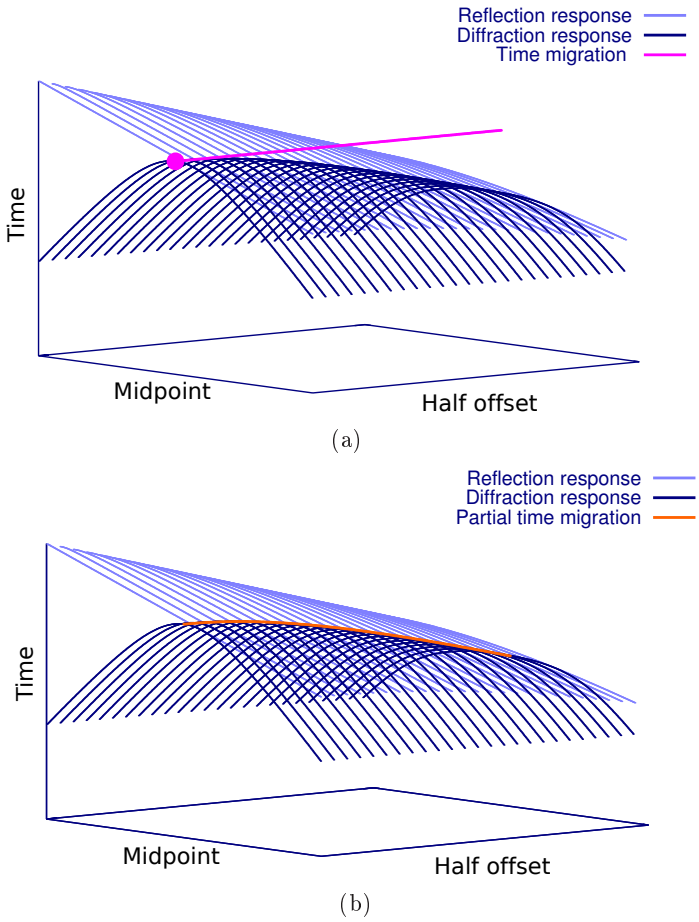

Figure 1.14: The figure compares the principles of time migration and data mapping for a homogeneous medium with a dipping reflector. The reflection response for the dipping reflector is depicted in dark blue and the migration operator is depicted in light blue. In (a) the migration output is assigned to the ZO operator apex for every CO section (pink line). In (b) the CSP mapped output is assigned to the CO operator apex for every CO section (orange line) modified after (Dell et al., 2009).

In the following chapter, I will introduce a zero-offset picking approach for multiple attenuation which can be applied within any stacking operator and is not restricted to 1D media, it can be also applied to internal multiples.

Chapter 2

Zero-offset picking approach

In this chapter, I present a rapid and robust approach based on a workflow for multiple attenuation of (Dümmong and Gajewski, 2008). Their method is an entirely data driven approach and includes two steps of prediction: first, zero-offset multiples in a Common Reflection Surface (CRS) stacked section are predicted, and in the second step, the obtained result is used for prestack multiple prediction these multiples are then subtracted from the original. They proposed multiple prediction in the CRS stacked sections using a series of convolutions. This workflow is restricted to 1D media; therefore, errors for dipping events are inevitable and it is necessary to correct the predicted data. This correction is not easy to determine. To resolve these issues, I propose to pick multiple events in the stacked section instead of predicting them by a convolution approach. Picking multiple events allows one to avoid the above described restrictions and to omit the correction. Another advantage is that this method can be applied to surface related multiples as well as internal multiples. In contrast to the above mentioned data driven approach, the proposed workflow relies on interpretation.

Since hyperbolic stacking operators are affected by spread length bias, I apply the workflow separately to two different range of offsets. The method, which is outlined in the following section, can be applied with any stacking operator.

2.1 Method

Several multiple attenuation methods are based on periodicity of multiples or moveout discrimination between multiples and primaries. My method is based on the fact that multiples, like primaries, can be described with a hyperbolic approach. Thus, it is possible to estimate traveltimes of multiples in the prestack domain, if zero-offset traveltimes of multiples and stacking velocities are available.

As an initial step of the zero-offset traveltime picking approach, I apply a stacking operator

to prestack data in order to obtain a stacked section, a stacking velocity profile, and a coherency section. The stacking velocity and the coherency section are estimated by an automatic semblance optimization (Neidell and Taner, 1971), i.e., the standard data processing sequence. Since the stacking process should be steered in a way that multiple events are imaged, the velocity search interval is adjusted accordingly. For example, if we aim at predicting surface related multiples, the velocity search interval should be set to a lower range. The velocity analysis step also provides a coherency section. This section is then used to differentiate between signal and multiples. For this purpose, a threshold factor is used to cut off the events with low coherency. In the next step, zero-offset traveltimes are picked in the obtained stacked section. Picking surface related multiples may be guided by the 1D convolution prediction.

It is critical to recognize multiples in a stacked section. The following characteristics of multiples help us to distinguish them from primaries (Verschuur, 2006):

- Periodic repetition
- Increasing dips
- Conflicting dips
- Focusing and defocusing events

In some cases multiples are more continuous in the coherency section in comparison with the stacked section so they are more distinguishable and easier to pick. It is possible to pick the multiples in the coherency section instead of the stacked section. In this case first the multiples are recognized in the stacked section then the corresponding events are picked in the coherency section. After zero-offset traveltime picking which can be done manually or automatically, prestack traveltimes of the multiples are predicted. The stacking velocity section, the picked traveltimes, the coherency section, and the selected threshold factor contribute to the prediction using the following well-known equation

$$t(h) = \sqrt{t_0^2 + \frac{4h^2}{v_0^2}}, \tag{2.1}$$

where h is the half offset, t_0 is the ZO traveltime and v_0 is the stacking velocity.
After multiple prediction, I employ an adaptive filtering method to match the predicted multiples with the input data. A Wiener optimum filter (Wiener, 1964) is used to fit the input seismogram to the desired output, which in our implementation is the original data. After that, multiples are subtracted from the data. This process is controlled by a space-time window and an operator length. The window size is the amount of traces that is used to determine the filter. A single trace, as well as several traces in space and up to hundreds of ms in time are valid space-time window sizes. The operator length is the length of the deconvolution operator applied to the data. The operator length is a critical parameter: if it is chosen too large, the operator matches any predicted trace with the

input data. Therefore, primaries in the vicinity of the multiples will also be subtracted. However, with a very short operator length, predicted data will not be properly matched to the input data. Consequently, multiples will not be subtracted from the data. The best result is obtained empirically; a window length matching the prevailing period of the data is a good choice in many cases. An example is provided in the next section. Figure 2.1 shows a schematic illustration of the method.

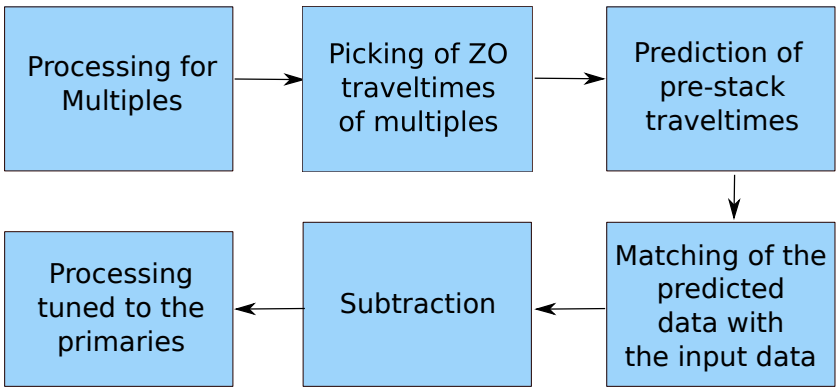

Figure 2.1: Schematic illustration of the ZO picking approach

It has been shown that the hyperbolic formula (Equation 2.1) is limited to near offsets and is affected by spread length bias. To use this method for larger offsets, I apply the method to different range of offsets separately. In the next section, the method is applied to a synthetic dataset.

2.2 Synthetic data example from Sigsbee2B

To illustrate the method, I first applied it to the well known synthetic Sigsbee2B dataset, which was created by Subsalt Multiple Attenuation And Reduction Technology Joint Venture (SMAART JV). It was designed to better understand the problems related to demultiple and subsalt imaging (Stoughton et al., 2001). It includes a large salt body with a very complex geometry that generates many diffractions and bow-ties. Figure 2.2 shows the interval velocity and table 2.1 shows the acquisition parameters of the data.

As an initial step, the stacked section, the corresponding coherency section, and the stacking velocity profile were generated for offsets from 0 m to 4500 m. I set the velocity search interval between from 1450 m/s to 1700 m/s because the aim was to image surface related multiples (Processing parameters are provided in **Appendix D**). Figure 2.3 displays the stacked section and the coherency section of the Sigsbee2B dataset for offsets from 0 m up to 4500 m and Figure 2.4 shows the corresponding velocity section. I manually picked ZO traveltimes of multiples in the stacked section then prestack traveltimes of multiples were predicted using the stacking velocity profile and the coherency section. Afterwards, the multiple were adaptively subtracted from data. I applied

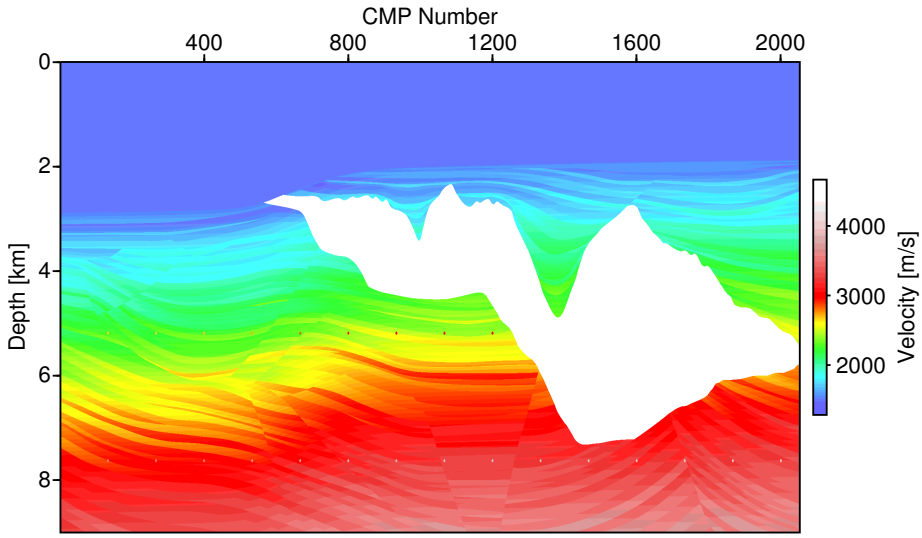

Figure 2.2: Interval velocity of the Sigsbee2B model

Table 2.1: Acquisition parameters from Sigsbee2B

Number of shots	496
Shot interval	45.72 m (150 ft)
Minimum offset	0 m (0 ft)
Maximum offset	7932 m (26025 ft)
No. of receivers	348
Max. fold	87
Receiver spacing	22.86 m (75 ft)
CMP interval	11.43 m (37.5 ft)
CDP range	25-2069
Sample rate	8 ms
Peak frequency	20 Hz
Max. frequency	40 Hz

adaptive subtraction in the common offset (CO) domain to investigate the result of the implementation at different offsets. As I mentioned previously, the length of the operator in adaptive filtering should be chosen carefully to keep the primaries untouched while attenuating the multiples. To illustrate this, an example is provided. Note that for a better visualization a close up of the sections is shown. Figure 2.5(a) shows a CO section at 4000 m for a CMP range between 400 to 850, before multiple attenuation and Figure 2.5(b) shows the same section after multiple attenuation with a suitable operator length (10 samples). The blue square specifies a part of the multiple event that is attenuated properly while the event in the vicinity of a multiple is preserved and marked by a red square. An example of too short (5 samples) and too long (100 samples) operator length is also provided. Figure 2.6(a) shows the same CO section after multiple attenuation with a short operator length. The blue square specifies a part of a multiple event that is not attenuated properly and the red square specifies a part of a primary event that is untouched after the multiple attenuation. Figure 2.6(b) shows this section after multiple attenuation with a too long

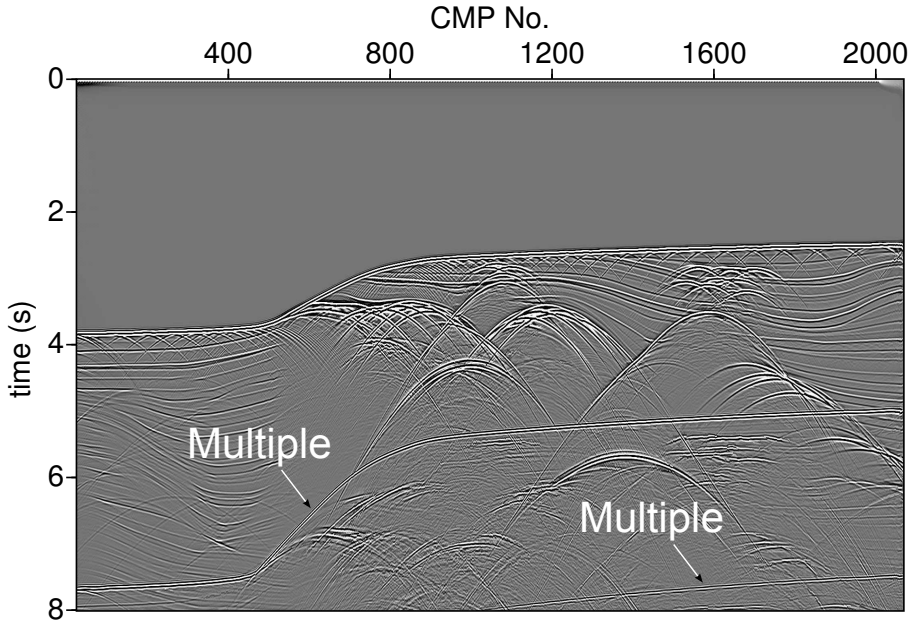

(a)

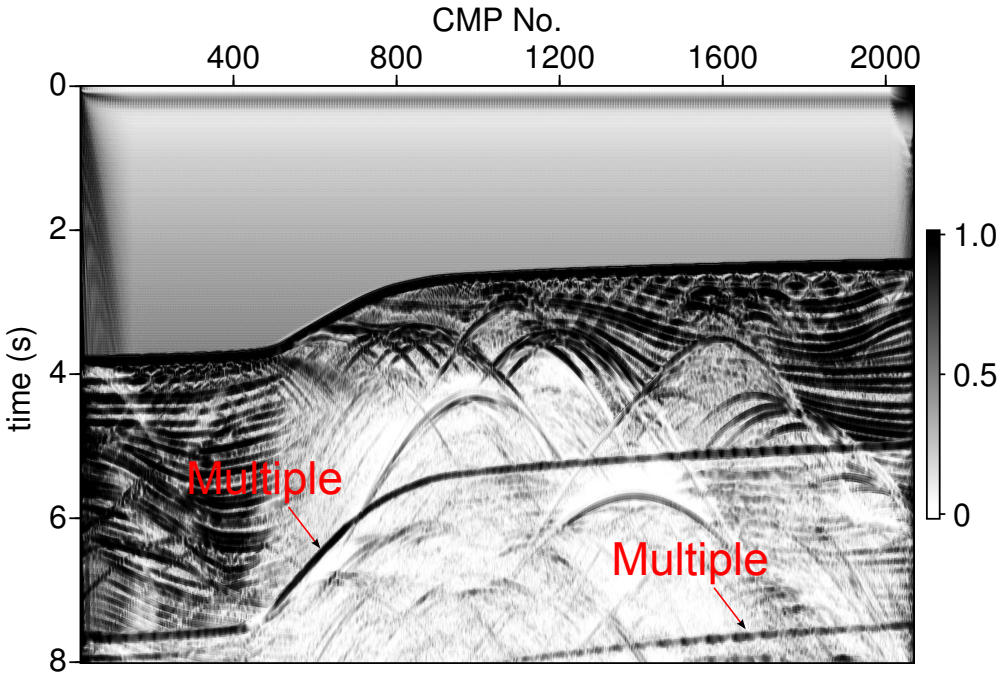

(b)

Figure 2.3: In (a) the stacked section of the Sigsbee2B dataset for offsets from 0 m up to 4500 m is shown. In (b) the corresponding coherency section is displayed.

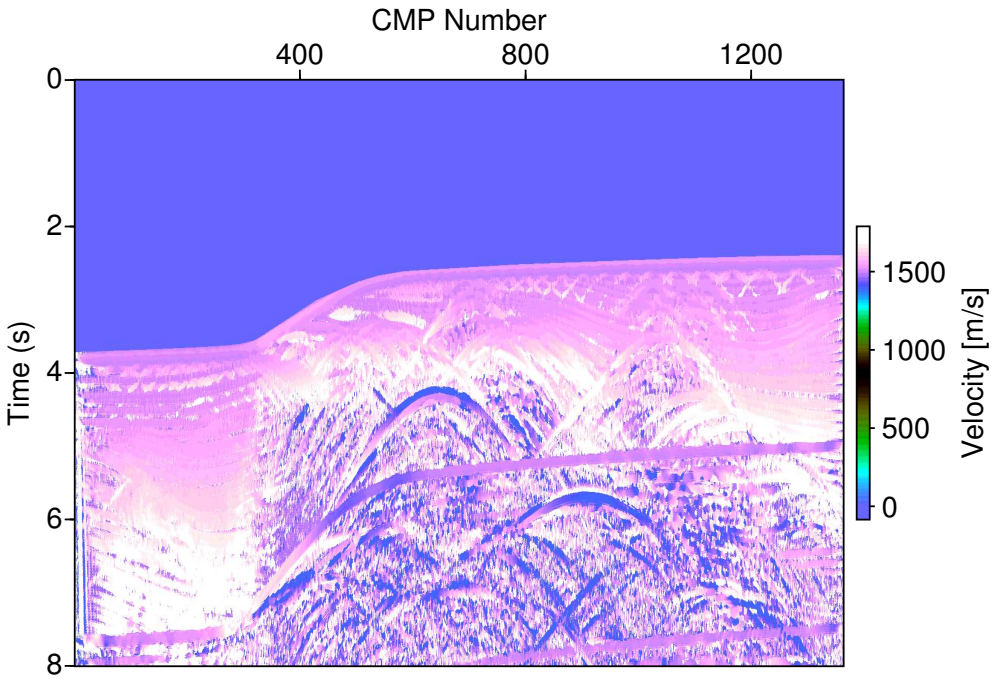

Figure 2.4: The velocity section of the Sigsbee2B dataset, offsets from 0 m to 4500 m. The velocity search interval is set from 1450 m/s to 1700 m/s.

operator length. The blue square specifies a part of the multiple event that is strongly attenuated, and the red square specifies a part of a primary event in the vicinity of the multiple that is also suppressed after the multiple attenuation.

As indicated before, the stacking operator is affected by spread length bias. This limitation is visualized in Figure 2.7 and Figure 2.8. Figure 2.7(a) displays a CO section at 500 m for the CMP range between 400 to 850 from the Sigsbee2B dataset before multiple attenuation and Figure 2.7(b) displays this section after multiple attenuation. The first order multiple, which is indicated by an arrow in Figure 2.7(a), is attenuated and not visible in Figure 2.7(b). Since the primary event crosses the multiple in the area specified by a square, it is also attenuated but only in the crossing spot. Considering that it is a prestacked section, other offsets of this primary will compensate this effect. Thus, the event will not be affected in the stacked section. Figure 2.8(a) shows a CO section at 6000 m for the CMP range between 400 to 850 from the Sigsbee2B dataset before multiple attenuation, and Figure 2.8(b) shows the same section after multiple attenuation. In Figure 2.8(b) the first order multiple, which is depicted with an arrow in Figure 2.8(a) are visible. In multiple prediction for both CO sections (500 m and 6000 m), the stacking velocity and stacked section are determined utilizing offsets shorter than 4500 m. To resolve this limitation, I applied the method to the offsets larger than 4500 m separately. Since I adjusted the velocity search interval and the apertures with a focus on the best possible multiple imaging result, primaries may not be properly imaged. Figure 2.9 shows the stacked section using only offsets from 4500 m up to 7000 m. Figure 2.10 displays the result of multiple attenuation in the CO section for the offset of 6000 m, Figure 2.10(a) shows the CO section after multiple attenuation using the stacked section and the velocity model

from the data including offsets from 0 m up to 4500 m, we can still see the multiple, which is indicated by an arrow. Figure 2.10(b) shows the CO section after multiple attenuation using the stacked section and stacking velocities determined from the data including only offsets from 4500 m up to 7000 m. Most of the multiple energy is successfully removed from the section.

The Sigsbee2B data was processed according to the above described procedure. The data with the offset larger than 4500 m and offset shorter than 4500 m are summed up. Now the prestack multiple attenuated data is available for further processing steps. To visualize the result I stacked the multiple attenuated data and also the data before multiple attenuation. In both cases, the stacking parameters are similar.The result is shown in Figure 2.11. In Figure 2.11(a), the stacked section including multiples is displayed and in Figure 2.11(b) the corresponding stacked section after multiple attenuation is shown. The energy from the first order multiple, which is indicated by an arrow in Figure 2.11(a), has been removed, and it is not recognizable in the stacked section in Figure 2.11(b), while the primaries in the vicinity of multiples are left untouched. Generally, the result is encouraging. For further investigation of the method, I applied it to field data in the following section.

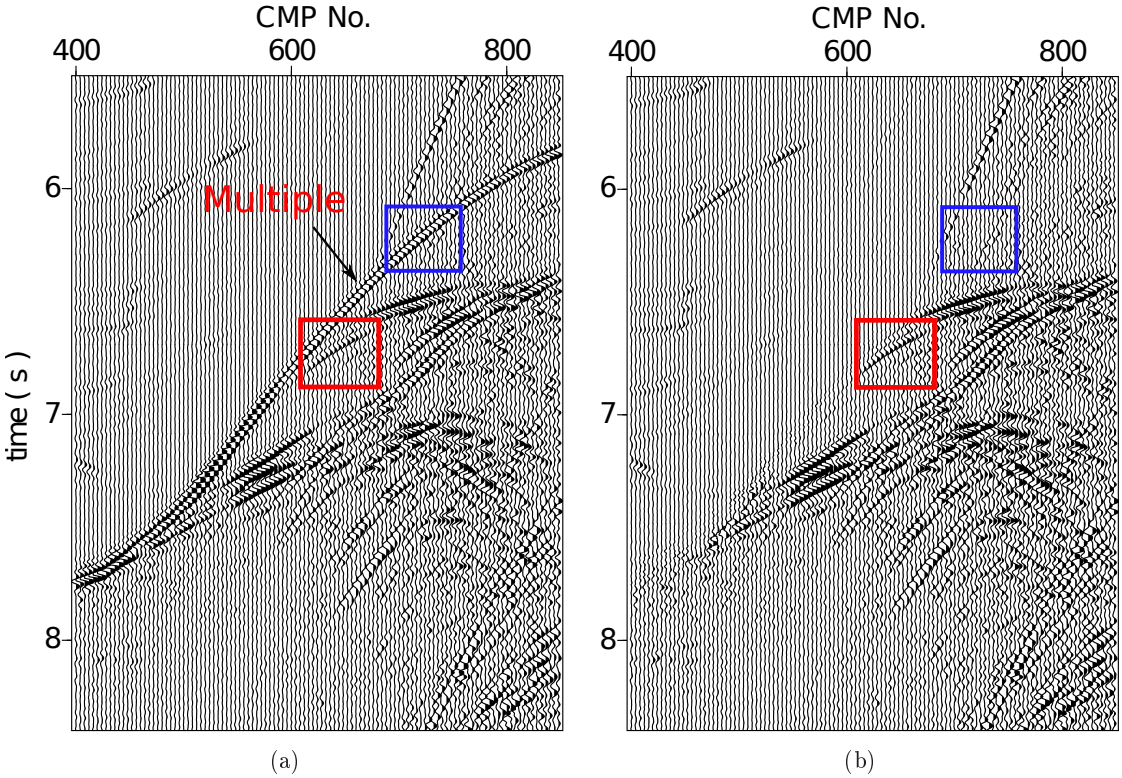

(a) (b)

Figure 2.5: Sigsbee2B dataset CO section at 4000 m for the CMP range between 400 to 850. (a) before multiple attenuation. (b) after multiple attenuation with a suitable operator length (10 samples). The blue square specifies a part of the multiple event that is attenuated properly and the red square specifies a part of a primary event in the vicinity of multiple that remains intact.

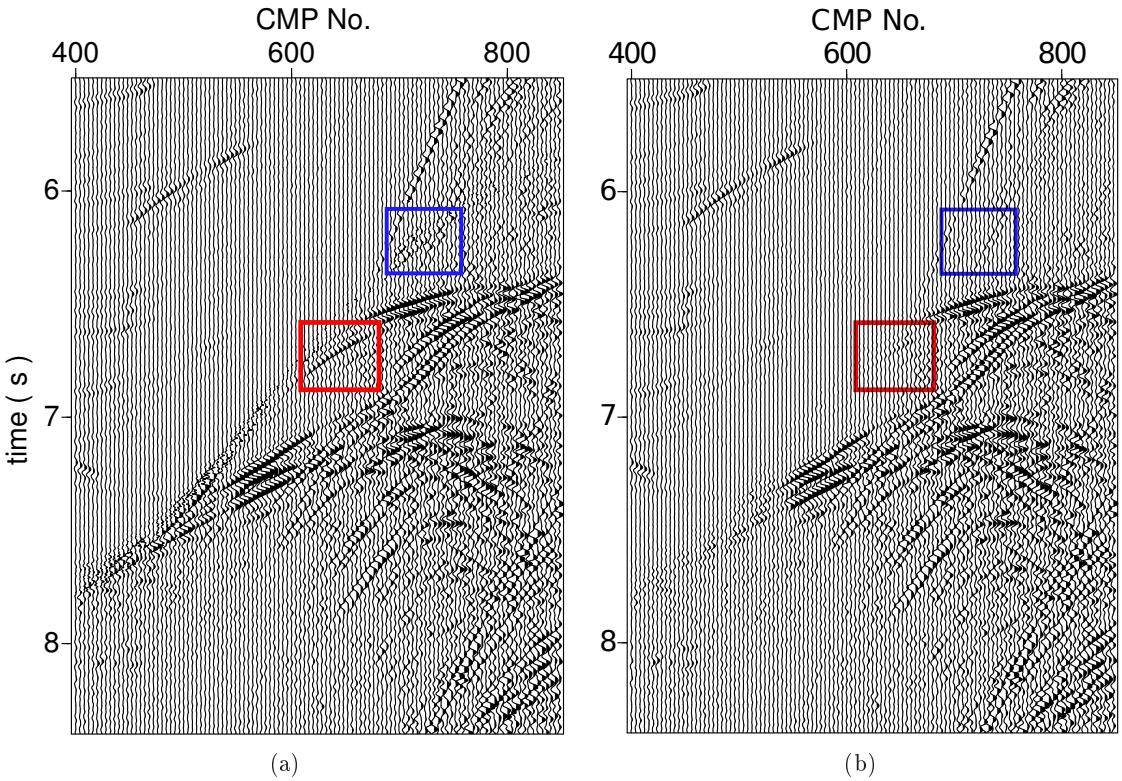

(a) (b)

Figure 2.6: Sigsbee2B dataset CO section at 4000 m for the CMP range between 400 to 850, after multiple attenuation. (a) with a short (5 samples) operator length. The blue square specifies a part of a multiple event that is not attenuated properly and the red square specifies a part of a primary event that is untouched. (b) with a too long (100 samples) operator length. The blue square specifies a part of a multiple event that is strongly attenuated, and the red square specifies a part of a primary event in the vicinity of a multiple which is also suppressed.

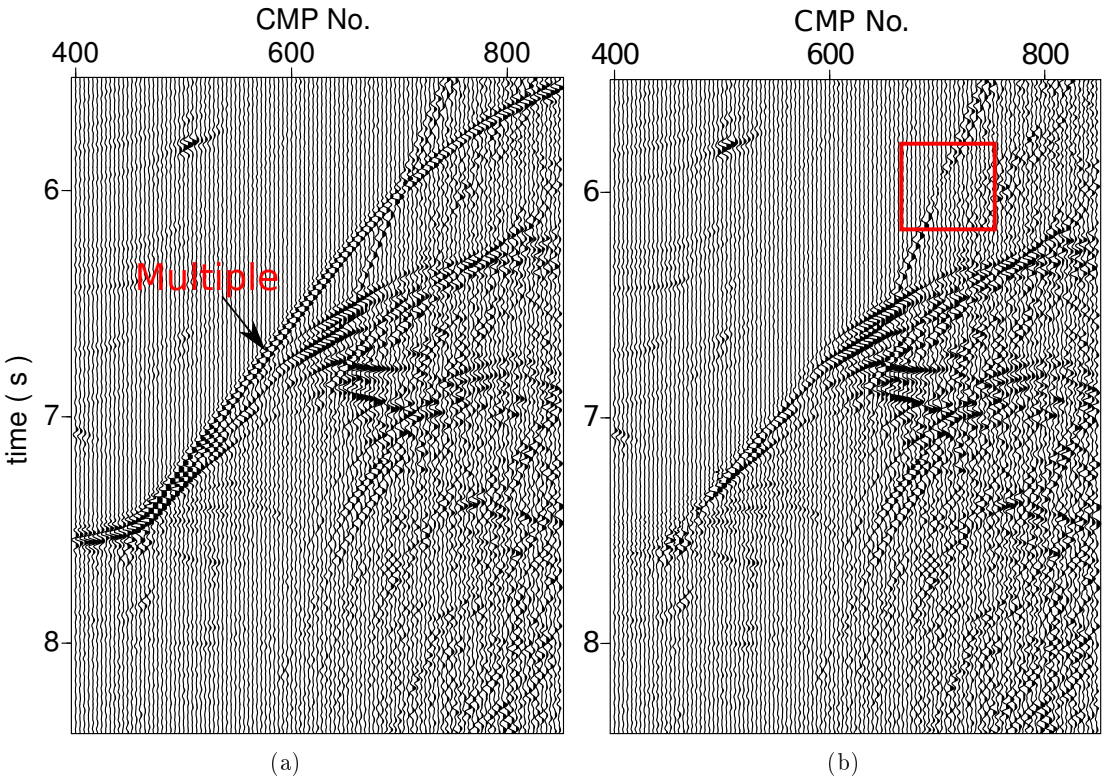

Figure 2.7: (a) displays a CO section at 500 m from the Sigsbee2B dataset CMPs between 400 to 850 before multiple attenuation. (b) displays this section after multiple attenuation using the stacked section and velocity model from the data, including offsets from 0 m up to 4500 m, the first order multiple, which is indicated by an arrow in (a), is attenuated and not visible in (b). Since a primary event conflicts with multiple in the area specified by a square, it is also attenuated. Considering that it is a prestacked section other primaries offsets of this primaries will compensate this and there will be no effect in the stacked section.

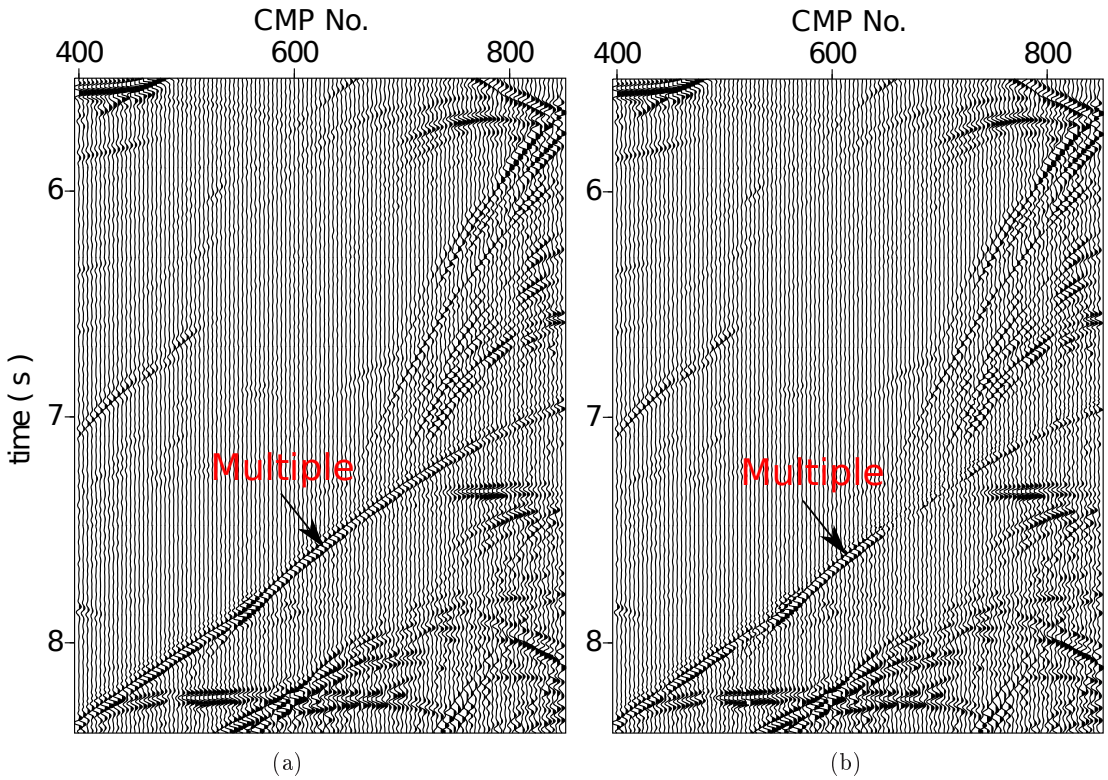

Figure 2.8: (a) displays a CO section at 6000 m from the Sigsbee2B dataset CMPs between 400 to 850 before multiple attenuation and (b) shows the same section after multiple attenuation using the stacked section and velocity model from the data, including only offsets from 0 m up to 4500 m. In (b), we can still see the first order multiple, which is depicted by an arrow.

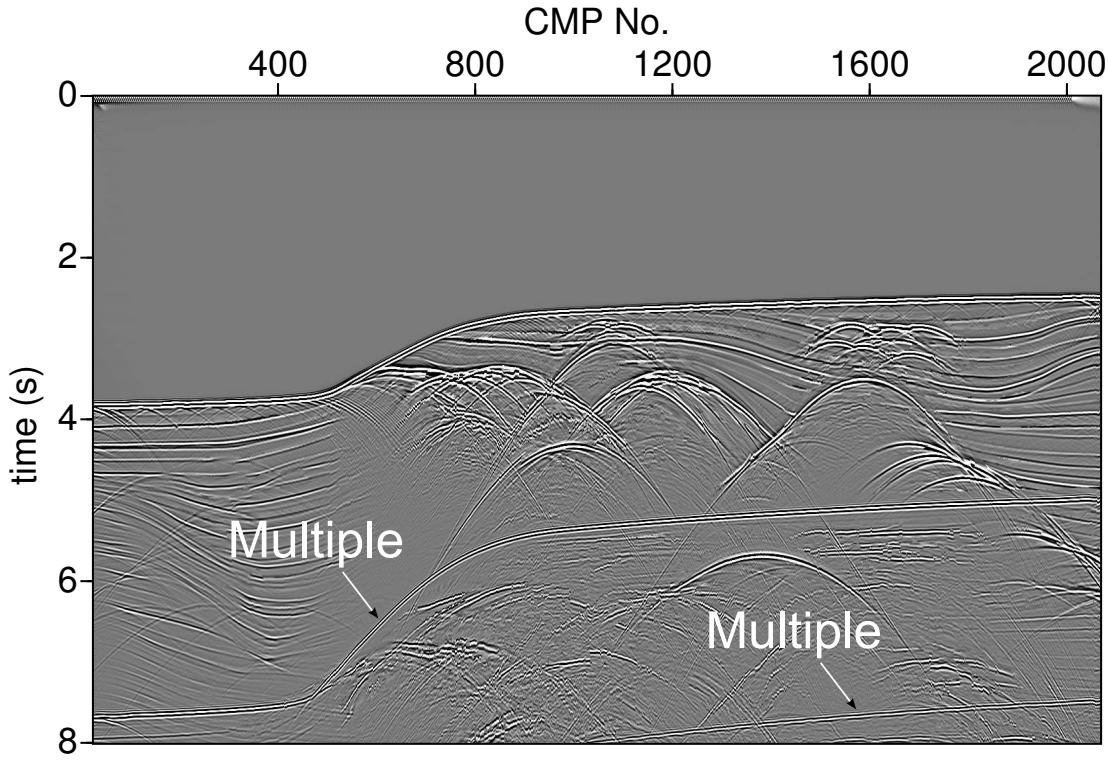

Figure 2.9: The stacked section of Sigsbee2B dataset including only offsets from 4500 m up to 7000 m; the stacking process is optimized with regard to multiple imaging.

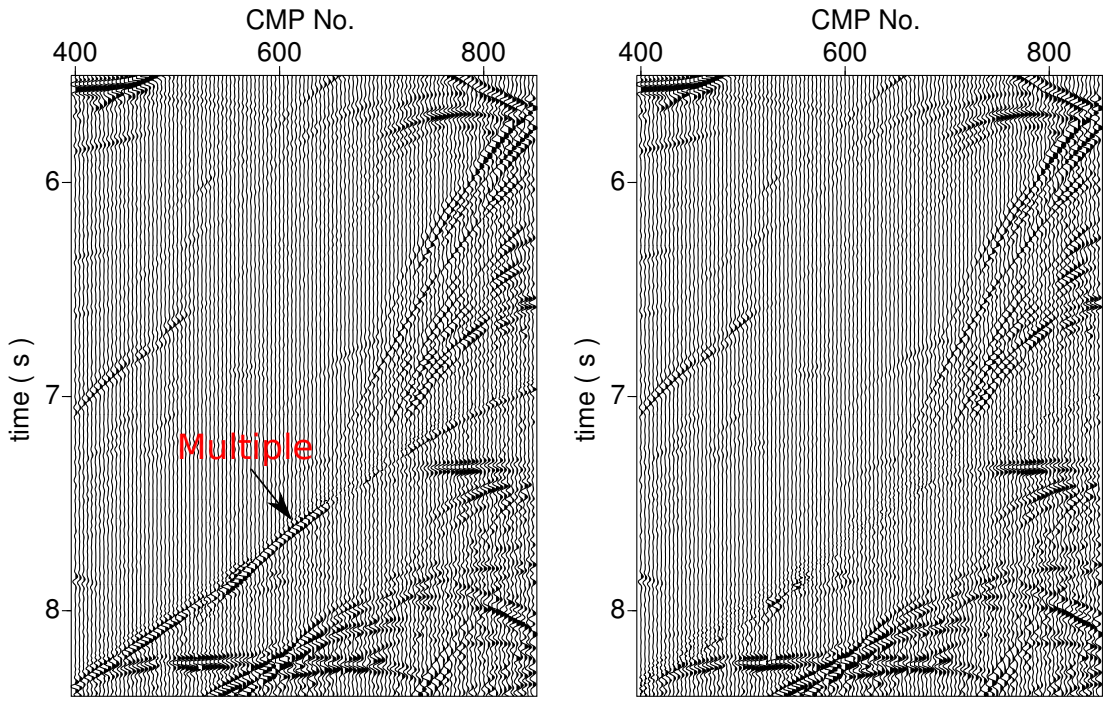

(a) (b)

Figure 2.10: The result of multiple attenuation at the offset of 6000 m from the Sigsbee2B dataset CMPs between 400 to 850. (a) using the stacked section and velocity model from the data, including only offsets from 0 m up to 4500 m. We can still see the multiple, which is shown by an arrow, in the section. (b) using the stacked section and velocity model from the data, including only offsets from 4500 m up to 7000 m. Multiple energy has been removed from this section.

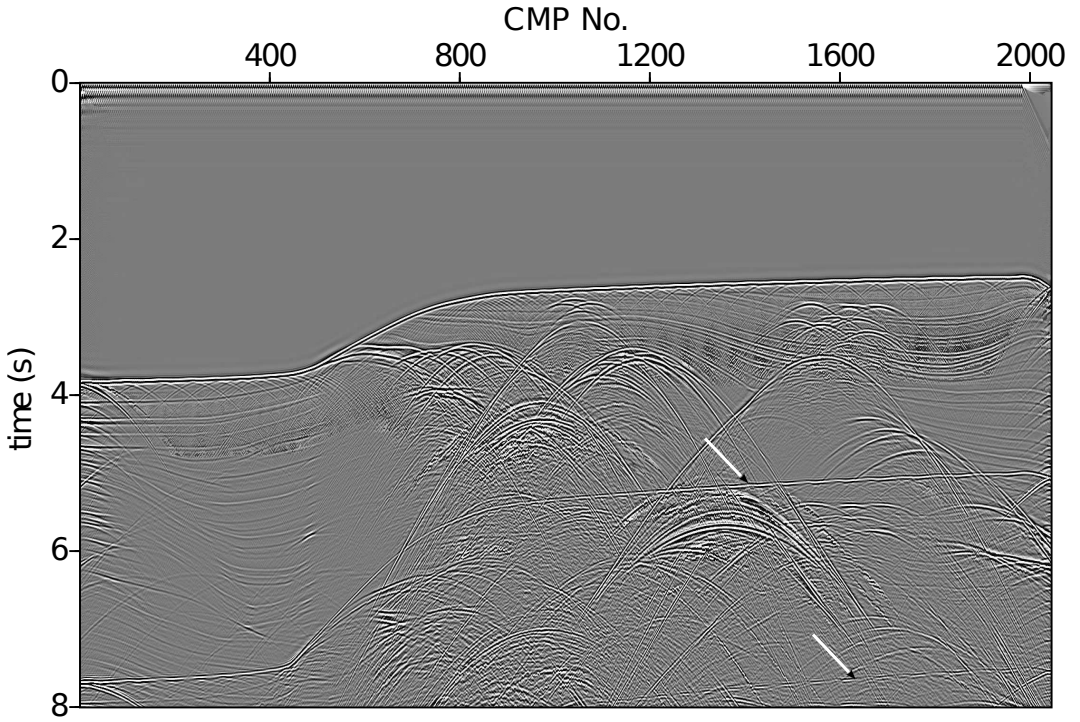

(a)

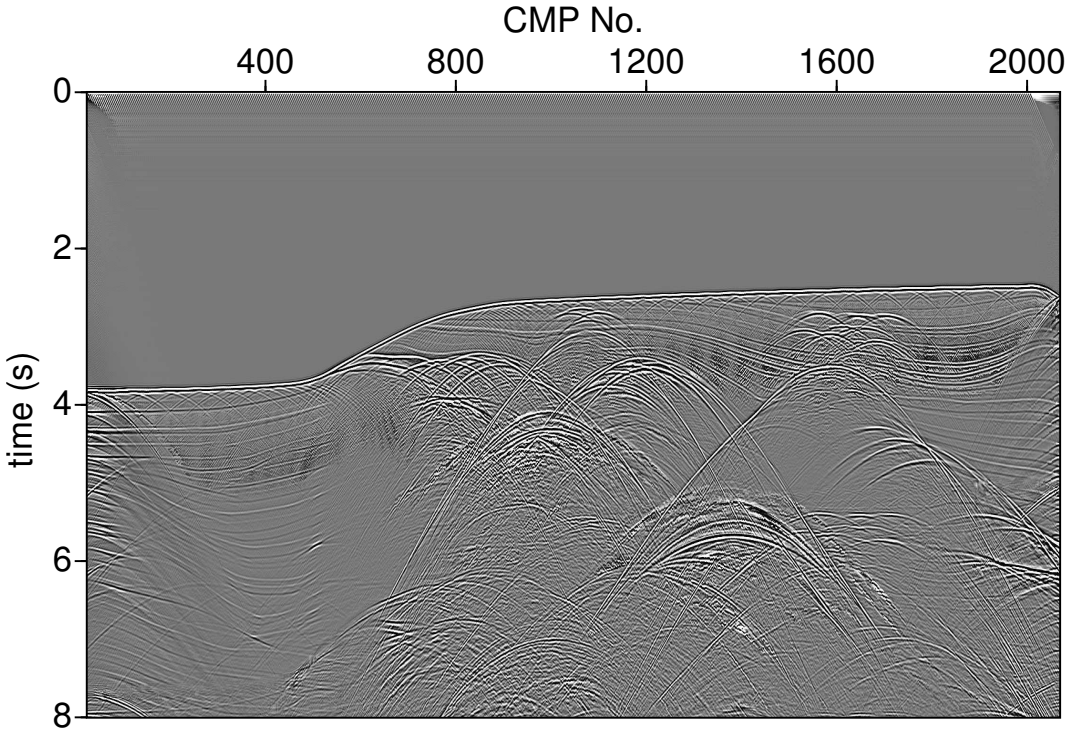

(b)

Figure 2.11: Sigsbee2B dataset. In (a) the stacked section including multiples (indicated by arrows) is displayed. In (b) the corresponding stacked section after multiple attenuation is shown. Most of multiple energy has been removed from the section.

2.3 Field data example

For further investigation, I applied the method to a marine seismic dataset. The data originates from the Levantine basin in the eastern Mediterranean Sea which is limited by the borders of Lebanon, Israel and Egypt to the east and south and by Cyprus in the north. Figure 2.12 shows the Eastern Mediterranean sea with black line indicating the approximate position of the seismic profile. This commercial data is provided by TGS-NOPEC and features a large offset of about 7300 m with a maximum fold of 288. In this thesis, I will refer to this data as TGS data. Table 2.2 shows the acquisition parameters from TGS data. The processing parameters are also provided in **Appendix D**. The Levantine Basin covers a basinal succession or mobile unit of the Messinian succession. The deformation pattern of this unit contains folds and thrust faulting which proves extensive salt tectonics and shortening in the depositional phase. Post-positional gravity gliding also created salt rollers in the extensional marginal, compressional folds, and faults within the Levantine basin (Gradmann et al., 2005; Netzeband et al., 2006b). Figure 2.13 shows a structural sketch of the seismic line. The parallel pretectonic units (green), above the salt body (red), are separated from the divergent syntectonic units (green) by a slump complex (gray). For further information on the geological setting, see, e.g., Clauzon et al. (1996); Krijgsman et al. (1999).

Table 2.2: Acquisition parameters from TGS data

Minimum offset	150 m
Maximum offset	7338 m
No. of receivers	576
Max. fold	288
Receiver spacing	25 m
CMP interval	12.5 m
CDP range	2351-4739
Sample rate	2 ms

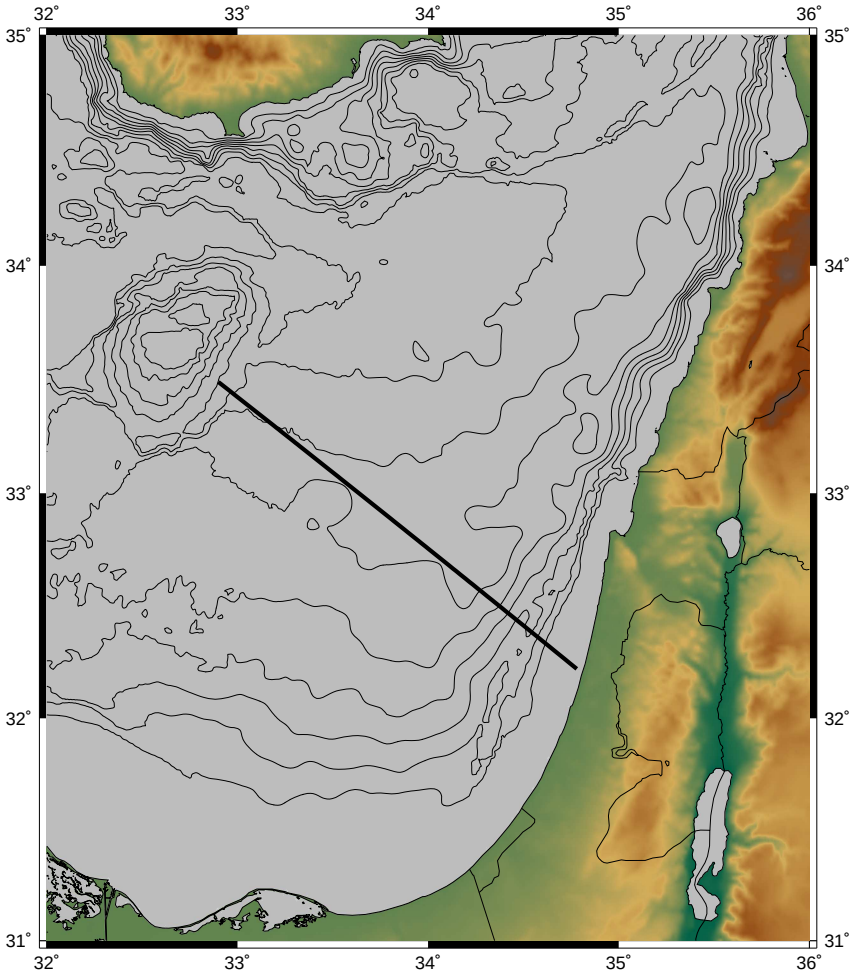

Figure 2.12: Map showing the eastern Mediterranean Sea. The black line indicates the approximate position of the seismic line (Netzeband et al., 2006a).

At the first step of applying the method to the presented TGS data, standard preprocessing steps applied to the data. Then, the stacked section, the corresponding coherency section, and the stacking velocity profile were generated for offsets from 150 m up to 3638 m. Since in this case our target was to image surface related multiples in marine data, I set the velocity search interval from 1450 m/s to 1550 m/s, which is the water velocity. The ZO traveltimes were picked in the stacked section then prestack traveltimes of multiples were predicted using the stacking velocity profile and the coherency section. In order to predict multiples for larger offsets, the method was applied once again to offsets from 3638 m up to 7338 m. Stacking velocity range was chosen with the intention to enhance multiples. Figure 2.14(a) shows the stacked section of the far offset data. As mentioned before, it is possible to use the coherency section to pick multiples. This section was used in this case, since picking multiples was more convenient in this section. Figure 2.14 shows the stacked section of offsets from 3638 m up to 7338 m in the TGS data and corresponding coherency section. It is easier to pick the multiple which is indicated by an arrow in the coherency

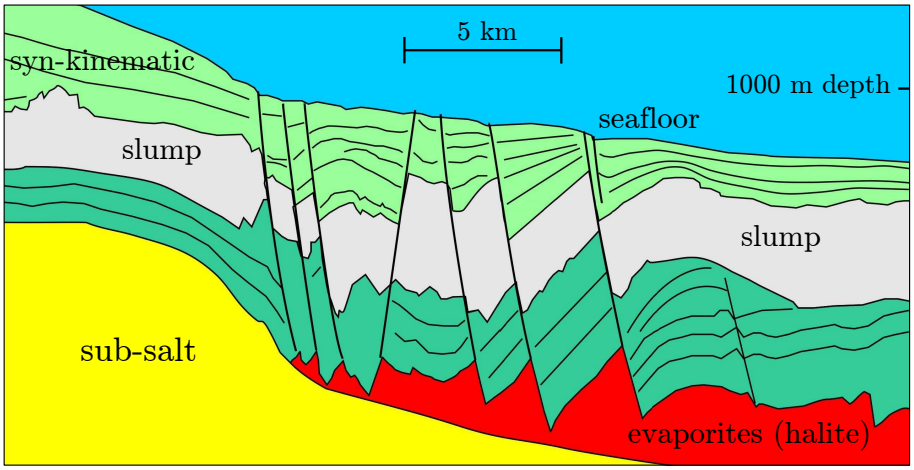

Figure 2.13: Structural sketch of subsurface. The parallel pretectonic units (green), above the salt body (red) are separated from the divergent syntectonic units (green) by a slump complex (gray) (Netzeband et al., 2006a).

section. In Figure 2.15(a), the stacked section before multiple attenuation is presented, and in Figure 2.15(b) the corresponding stacked section after multiple attenuation is shown. Overall, most of the multiple energy, which is depicted with an arrow in Figure 2.15(a), is removed from the stacked section in Figure 2.15(b). Although there are some residuals of the multiples, the result is quite promising for the future development of this approach. In the next section, I will apply the method to a 3D synthetic data.

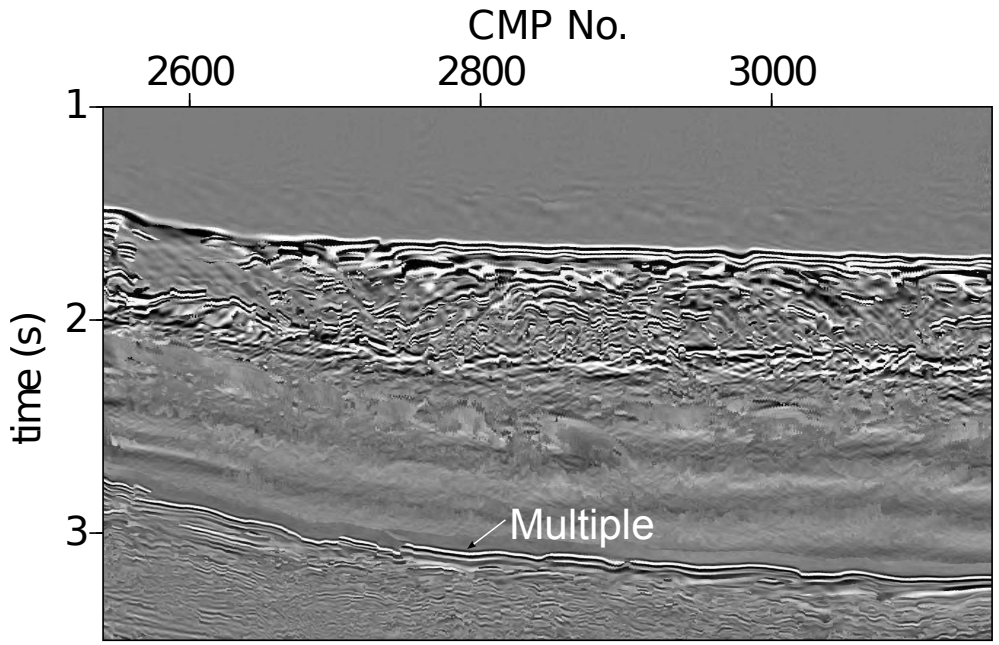

(a)

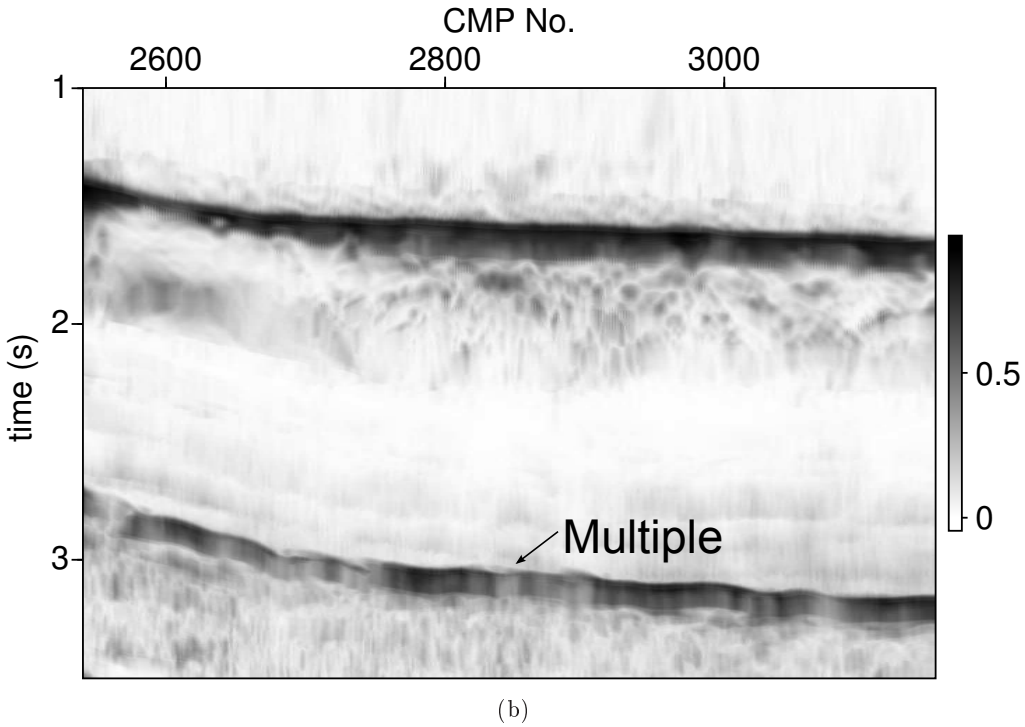

(b)

Figure 2.14: The coherency section and stacked section of the TGS data including offsets from 3638 m up to 7338 m. The stacking process has been optimized to image multiples so primaries may not be optimally imaged. In (a) the stacked section presented the multiple which is indicated by an arrow is not continuous. In (b) the corresponding coherency section is displayed. The multiple which is indicated by an arrow is more continuous in comparison with the stacked section.

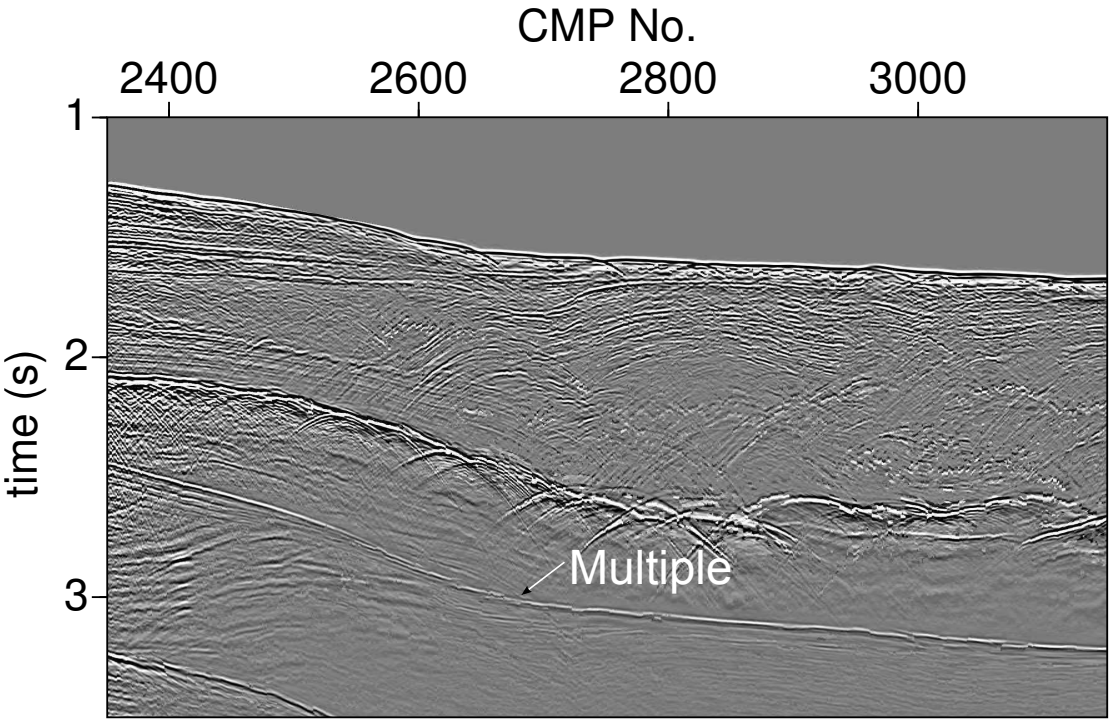

(a)

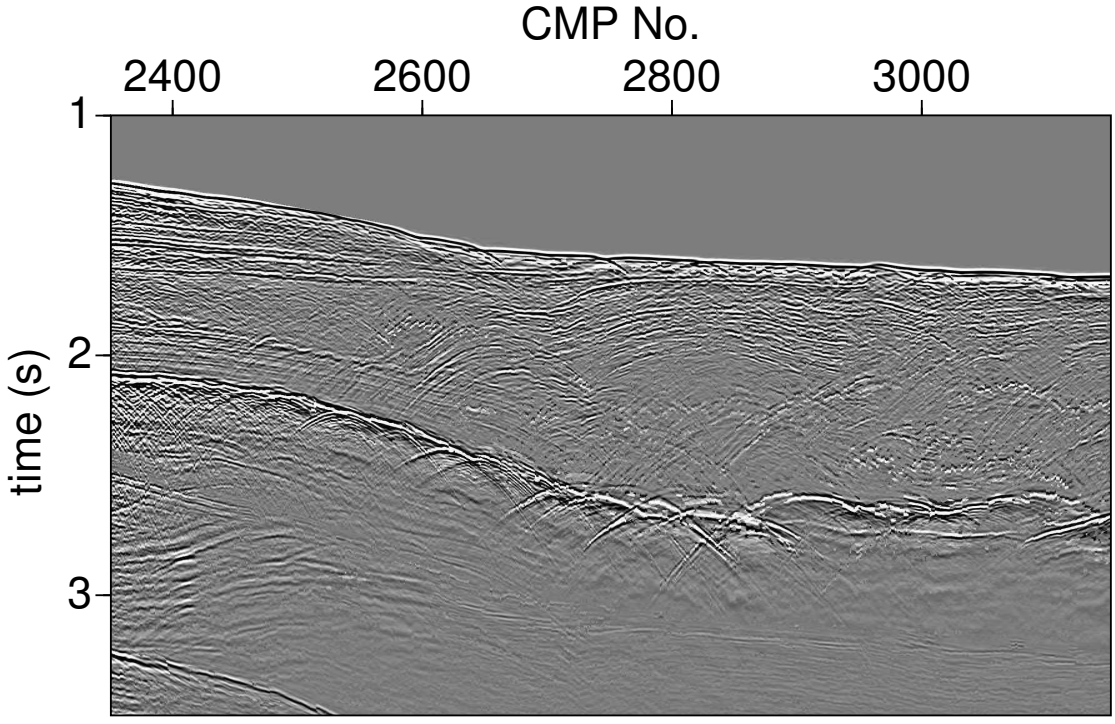

(b)

Figure 2.15: Marine data example. In (a) the stacked section including multiples is displayed. In (b) the corresponding stacked section after multiple attenuation is shown. we can see that most of the multiple energy (indicated by an arrow in (a)) has been removed from the stacked section in (b).

2.4 3D example

In the previous section, I presented 2D examples, where multiples were picked manually. This may raise the question of the method applicability to 3D data where manual data picking is hardly feasible. For further investigation I have provided a simple synthetic 3D example. In this case, multiples are picked automatically. To generate this data I used Norsar 3D software. The velocity model consists of to layers which is shown in the Figure 2.16. The velocity of the upper layer is 1500 m/s, velocity of and the lower layer is 2000 m/s. The receiver interval and source interval are 50 m. The number of inlines and crosslines are 41 and the distance between two lines is 50 m. As a source wavelet, I used zero phase Ricker wavelet with dominant frequency of 20 Hz. The primary and only first order multiples are modeled. I applied the method as previously described, the only difference

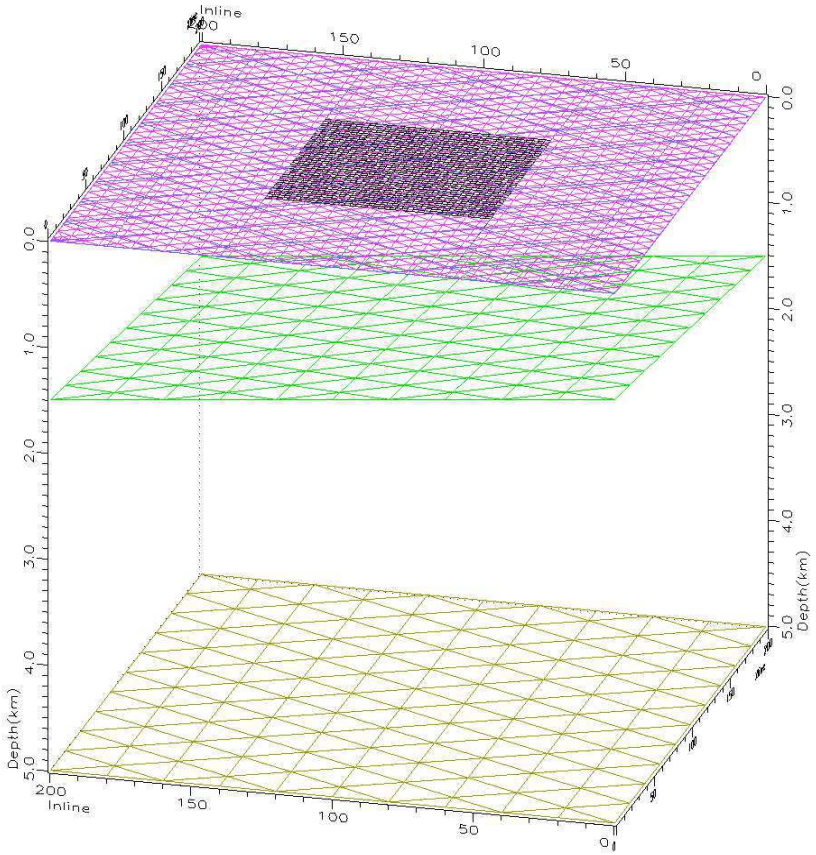

Figure 2.16: The synthetic 3D velocity model. The velocity in the upper layer is 1500 m/s and the lower layer is 2000 m/s. The receiver interval and source interval are 50 m. There are 41 crosslines and inlines and the distance between two lines is 50 m. The black lines show the acquisition geometry, the purple lines show the surface, and the green lines show the interfaces.

is that for multiple picking the Petrel software was used. In Figure 2.17(a), the stacked section before multiple attenuation is presented, and in Figure 2.17(b) the corresponding

stacked section after multiple attenuation is shown. Generally, I the multiples, which are indicated by an arrow in Figure 2.17(a), are properly attenuated, and are not visible in the stacked section in Figure 2.17(b).

Automatic picking is a very challenging task in presence of conflicting dip situations, one can apply this method in a migrated domain, where the diffractions are focused and triplications are unfolded, thus, there will be fewer conflicting dip situations. In the following section, I investigate the application of the proposed method in the CSP domain which is a partial time migrated domain.

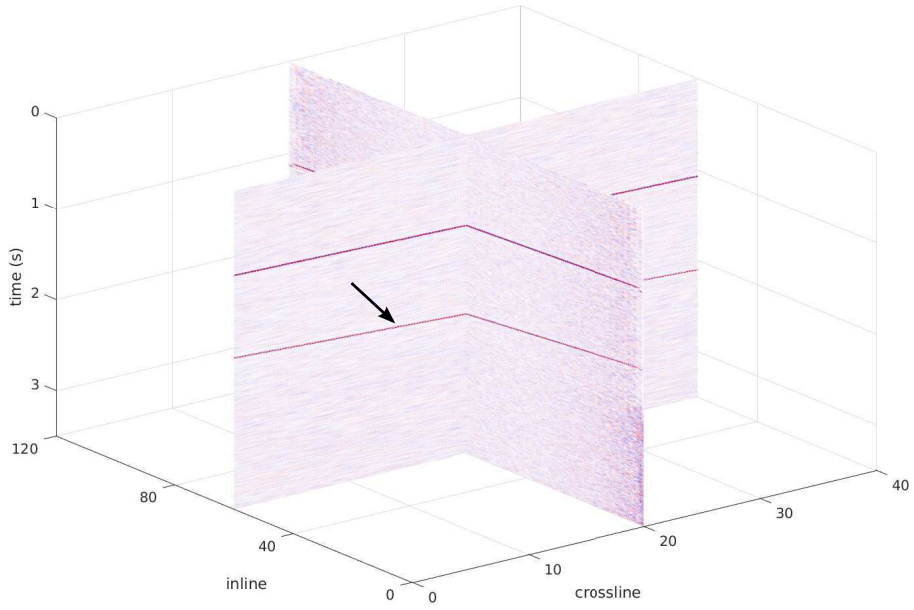

(a)

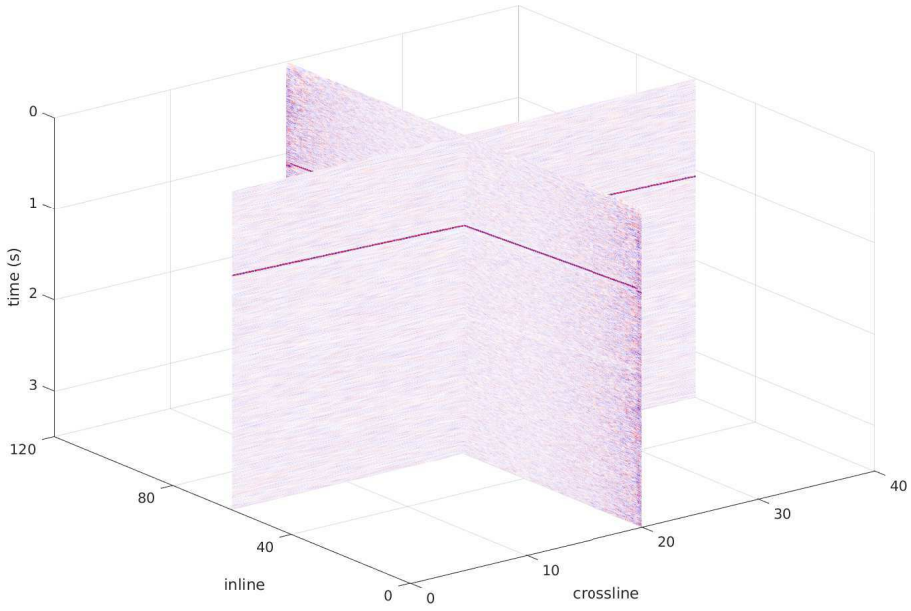

(b)

Figure 2.17: 3D data example. In (a) the stacked section including multiples is displayed. In (b) the corresponding stacked section after multiple attenuation is shown. Multiple which is indicated by an arrow in (a) is attenuated in (b).

2.5 Application in CSP domain

To illustrate and verify the presented zero-offset picking approach in the Common Scatter Point (CSP) domain, I applied it to the Sigsbee2B dataset, which is introduced in Section 2.2. In the first step, I obtained partial migrated prestack data using the CSP operator developed by (Dell, 2012). To do this, I needed a velocity section. This section can be obtained, e.g., from CRS attributes, the code was provided by (Glöckner et al., 2016):

$$V_{mig} = \frac{v_{NMO}}{\sqrt{1 + \frac{v_{NMO}^2}{v_0^2} sin\alpha^2}}, \tag{2.2}$$

where

$$v_{NMO} = \sqrt{\frac{2v_0 R_{NIP}}{tcos\alpha^2}}. \tag{2.3}$$

I applied the CSP data mapping using this velocity section. Then, I stacked the result but multiples were not properly migrated. To obtain a better result, I decided to decrease the range of velocities (Schleicher and Biloti, 2006) and to smooth the velocity using Seismic Unix software. Therefore, I set the velocity search interval from 1400 m/s to 1750 m/s to obtain a proper velocity section. This velocity section is then used for partial migration. Figure 2.18(a) shows the CSP stacked section of Sigsbee2B data using the velocity section which was derived directly form CRS attributes. The multiple which is indicated by an arrow is not properly migrated. Figure 2.18(b) shows the CSP stacked section of Sigsbee2B data using a decreased smoothed velocity section, the multiple, which is indicated by an arrow, is better migrated. Figure 2.19(a) shows the stacked section of CMP data while Figure 2.19(b) illustrates the stacked section of CSP data. In both figures the first order multiple is indicated by an arrow. In Figure 2.19(a), there are lots of diffractions that cause conflicting dip situations, whereas in Figure 2.19(b) all diffractions are focused, so there are less conflicting dip situations. Since picking multiples in a reduced conflicting dip situation is less challenging, especially in automatic picking, it is better to apply the method in a migrated domain.

The method was implemented as described in Section 2.1. Figure 2.20(a) is the stacked section of data before multiple attenuation, first and second order multiples are indicated by arrows. Figure 2.20(b) shows the corresponding section after multiple attenuation. We observe that multiples are attenuated and hardly visible. In conclusion, the result shows the prospect for the future investigation.

In this chapter, I have presented a new method, where multiples are picked manually or automatically. However, in some areas there are not only first layer multiples but also other surface related multiples which are difficult to pick. To solve this problem, I suggest to use additional information like coherency or velocity to differentiate multiples from other events. I will introduce a new approach based on this idea, in the next chapter.

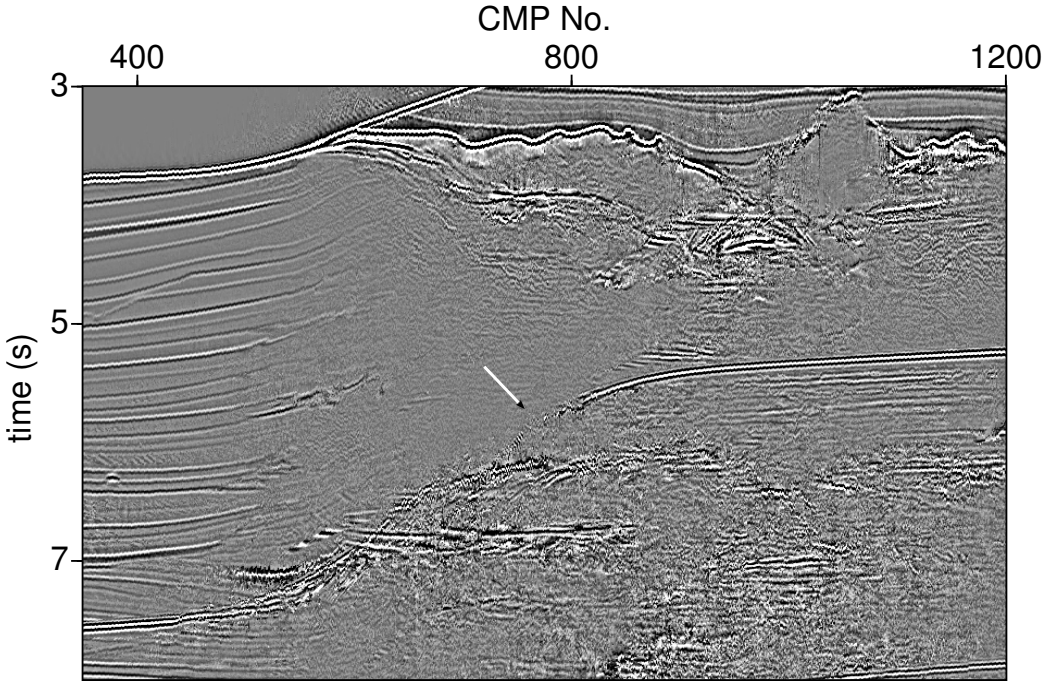

(a)

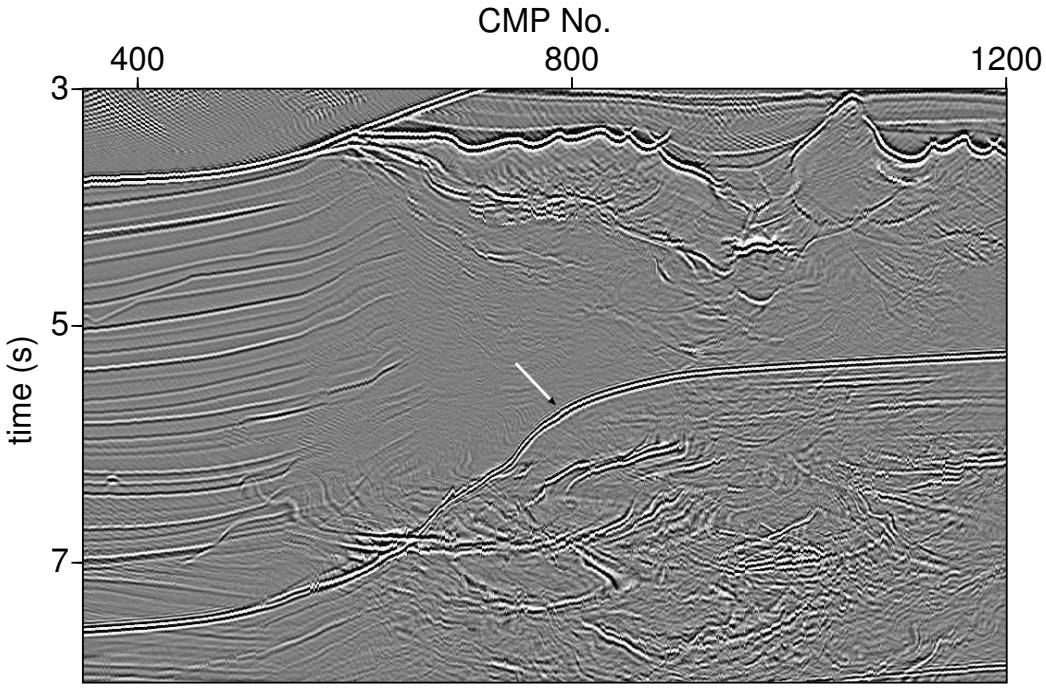

(b)

Figure 2.18: The figure compares the stacked section of Sigsbee2B data in CSP domain obtain from velocity section derived directly from CRS attributes with the stacked section of the CSP data using a decreased smoothed velocity section. In (a) first order multiple, which is indicated by an arrow, is not properly migrated. In (b) The multiple, indicated by an arrow, is better migrated.

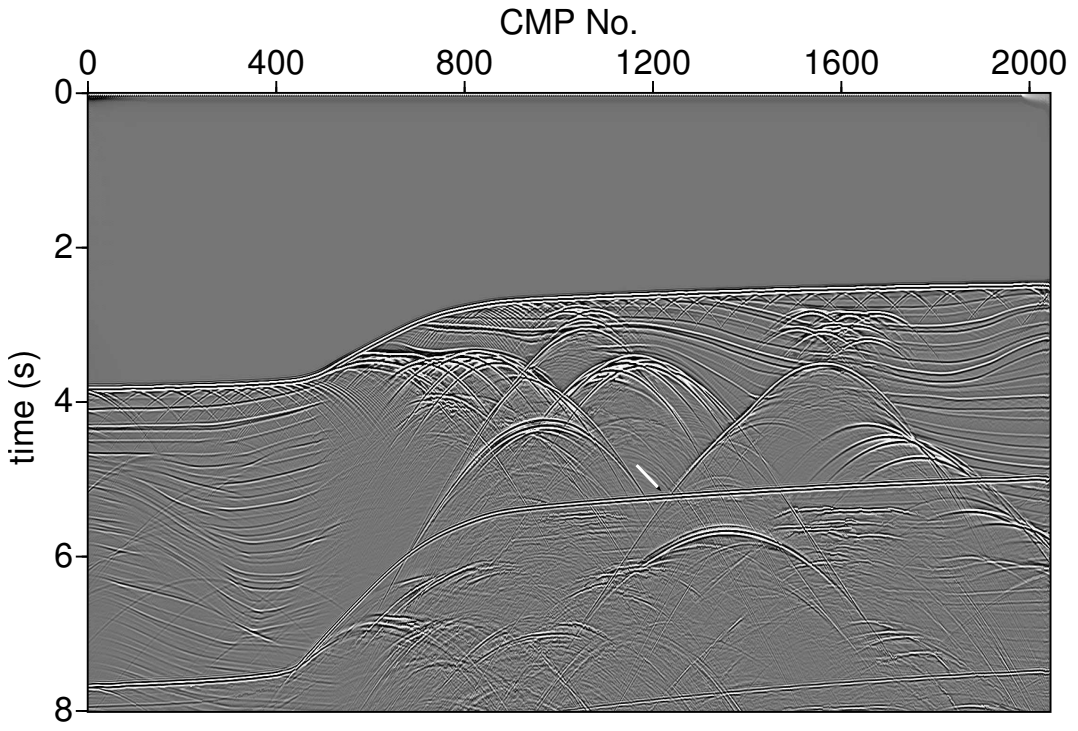

(a)

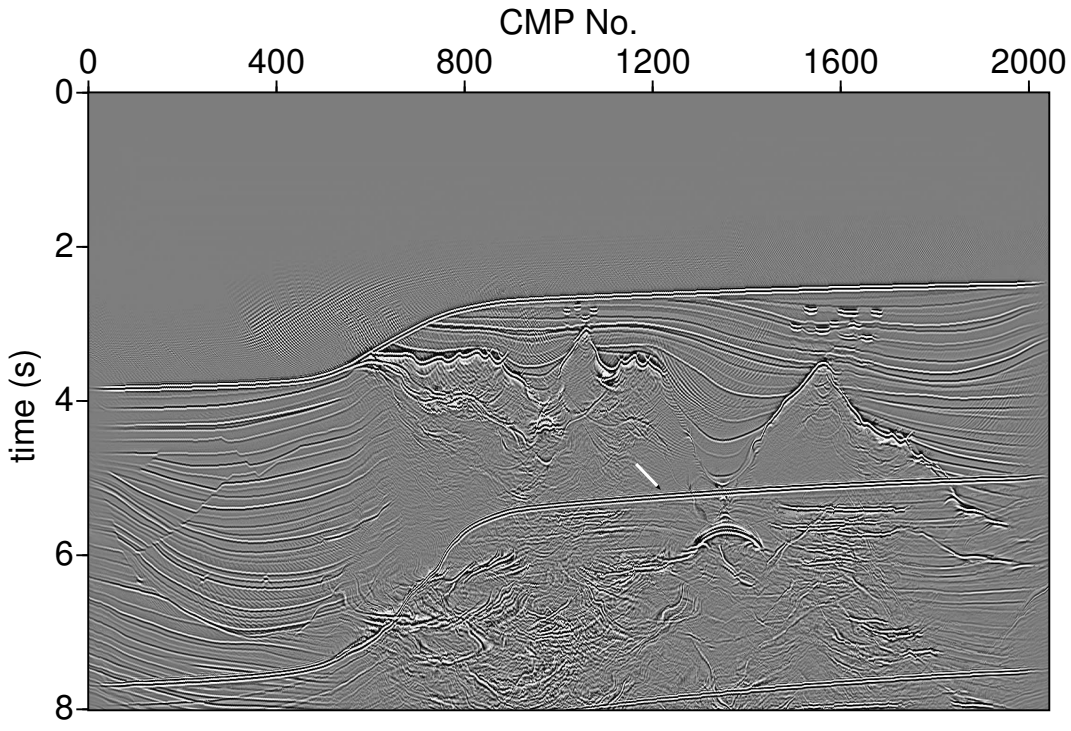

(b)

Figure 2.19: The figure compares the stacked section of Sigsbee2B data in CSP domain with stacked section in CMP domain. (a) which is in CMP domain the is first order multiple is indicated by an arrow conflict with a lot of diffractions. In (b) which is in CSP domain all the diffraction are focused and there is less conflicting dip situation.

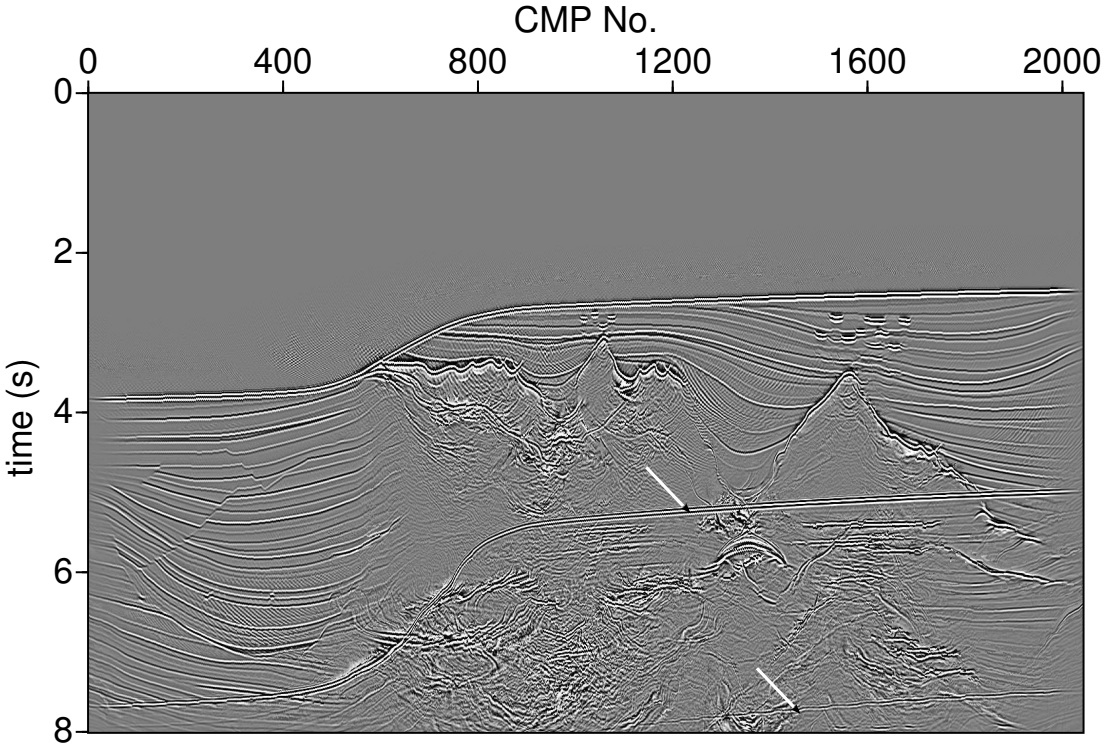

(a)

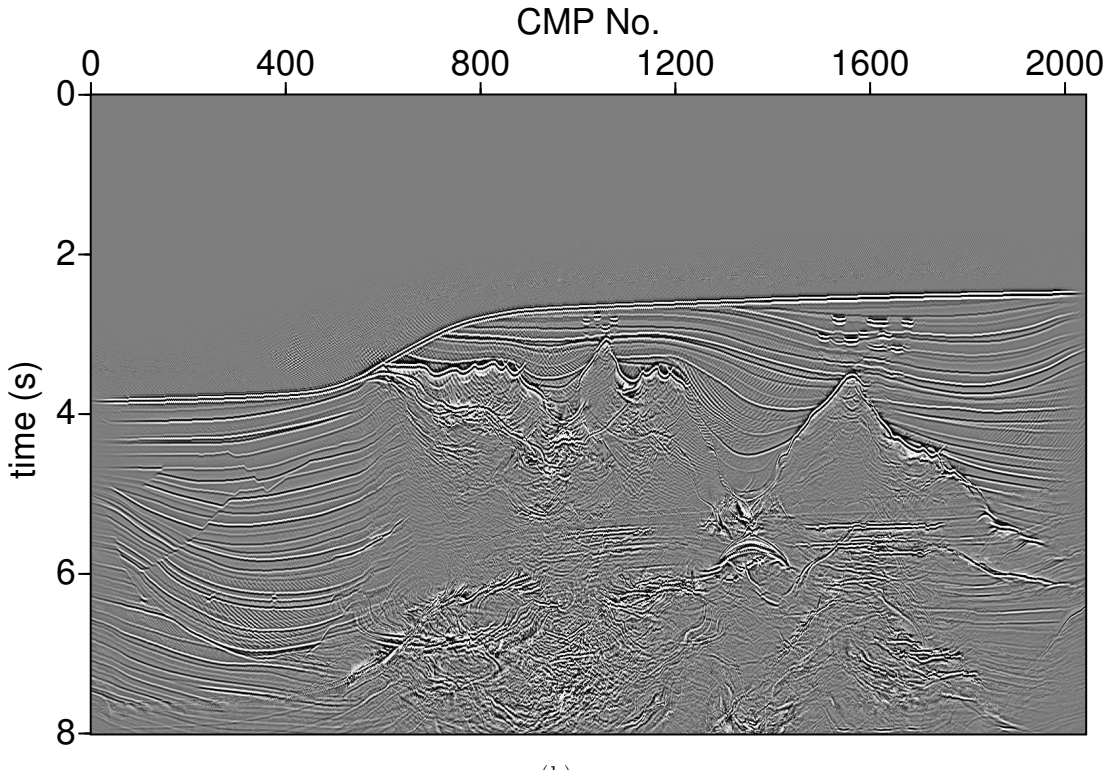

(b)

Figure 2.20: Stacked section of Sigsbee2B data in CSP domain (a) before multiple attenuation multiples are indicated by arrows (b) after multiple attenuation, most of the multiple energy is suppressed.

Chapter 3

Multiple attenuation using additional information as a guide

In the previous chapter, I introduced a method which includes picking multiple events. Picking multiples in some cases was very challenging and we could see some residuals after multiple attenuation. For example, in Figure 3.1, which shows a part of stacked section of TGS data, after the first order multiple (below 3 seconds) the section is covered by other surface related multiples. Picking these multiples is hardly feasible. To solve this issue, I propose to pick multiple events using a coherency section or velocity section instead of picking them manually or automatically.

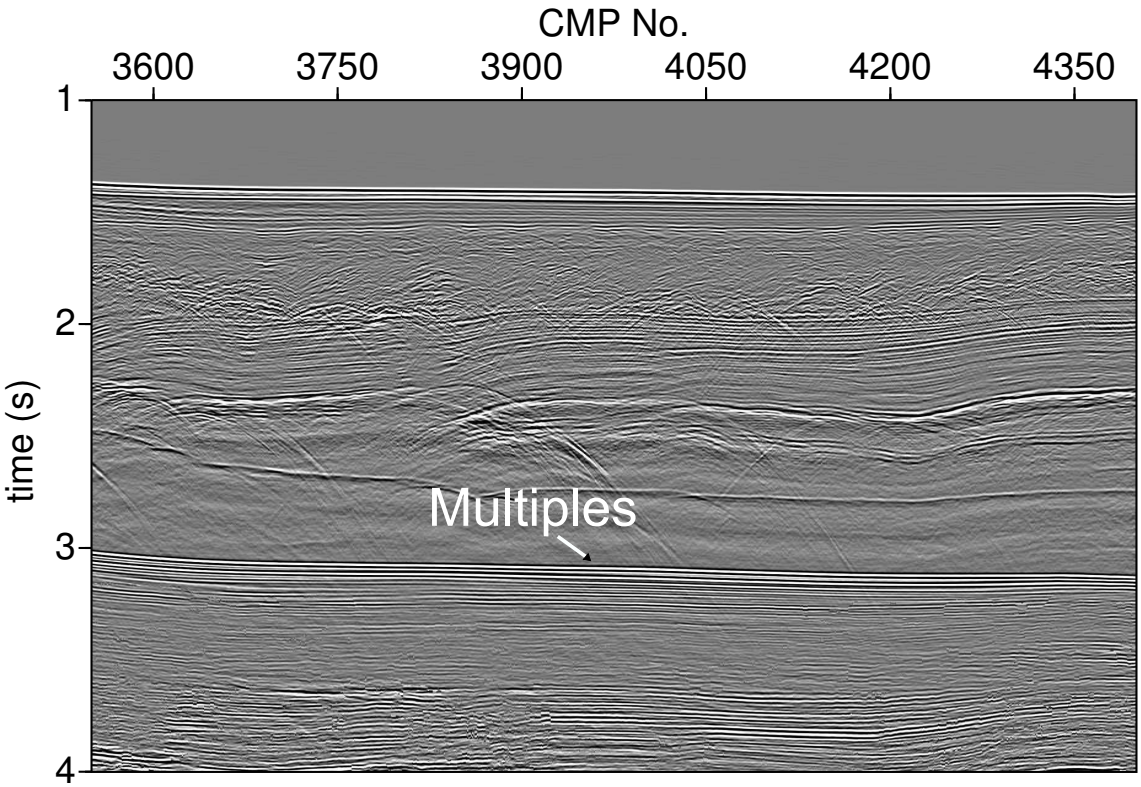

Figure 3.1: The stacked section of the TGS data: after the first order multiple (below 3 seconds) the section is covered by other surface related multiples.

3.1 Multiple attenuation using coherency as a guide

This method is similar to the method which I introduced in the previous chapter. The first step of multiple attenuation using a coherency section, is to obtain a stacked section, a stacking velocity profile, and a coherency section. Since our aim is to obtain a coherency section where multiples have high values, the velocity search interval is adjusted accordingly. For example, if the aim is to attenuate surface related multiples, then I set the velocity search in to a lower range (to illustrate this, an example is provided in the following section). To differentiate between multiples and primaries, a threshold factor is used to cutoff the events with low coherency.

After stacking, the upper part of the first-order multiple is muted to avoid attenuation of primaries. Then, the stacking velocity section, the picked traveltimes, the coherency section, and threshold factor contribute to the estimation of the prestack traveltime of multiples. After multiple prediction in the prestack domain, they are adaptively subtracted from the data.

Since hyperbolic stacking operators are affected by spread length bias, I apply the workflow

separately to two different offset ranges.

3.1.1 Synthetic data example

To illustrate the method, I applied it to the synthetic BP 2004 dataset (Billette and Brandsberg-Dahl, 2005). Figure 3.2 displays the velocity interval of this model. The minimum offset is 125 m, the maximum offset is 8000 m. For the processing, CMPs in the range between 3550 and 3900 were chosen, since in this excerpt the topography of the sea bottom is not complex and the surface related multiples do not conflict with the diffractions. First, I stacked the data tuned to image the multiples. Since our target was surface related multiples, I set the velocity search interval between 1480 m/s to 1550 m/s (the processing parameters are provided in **Appendix D**). To avoid attenuating primaries, I muted the upper part of first order multiples. Figure 3.3(a) shows the coherency section of the data when the stacking is tuned to image multiples properly and Figure 3.3(b) shows the coherency section of the same data when the stacking process is tuned to image primaries. In Figure 3.3(a) multiples have a higher value in comparison to the value of the primaries. This allows us to differentiate between primaries and multiples in the stacked section. As mentioned before, stacking operators are affected by spread length bias. To

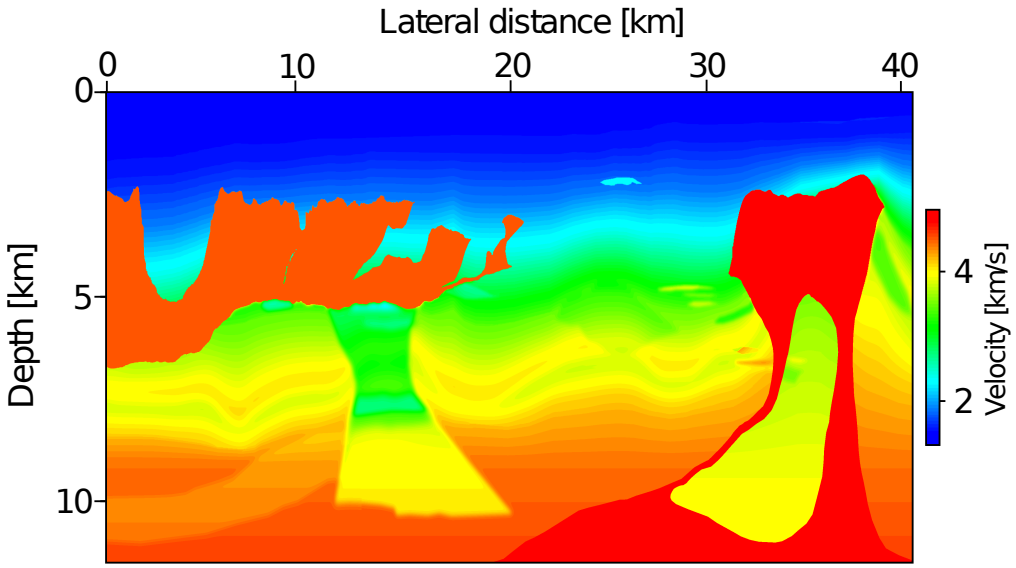

Figure 3.2: Velocity interval of the BP 2004 dataset

resolve this limitation, I applied the method to different offset ranges separately. Since I adjusted the velocity search interval range and the apertures in a way that I could achieve the best possible result for imaging multiples, primaries in this section may not be optimally imaged. Figure 3.4 shows the stacked section using only offsets from 3500 m to 8000 m. After applying the method to both offset ranges, I summed up the data. To visualize the result, I again stack the data but this time the target was to image the primaries. In Figure 3.5(a), the stacked section including multiples is displayed and in Figure 3.5(b) the corresponding stacked section after multiple attenuation is shown. The energy from the

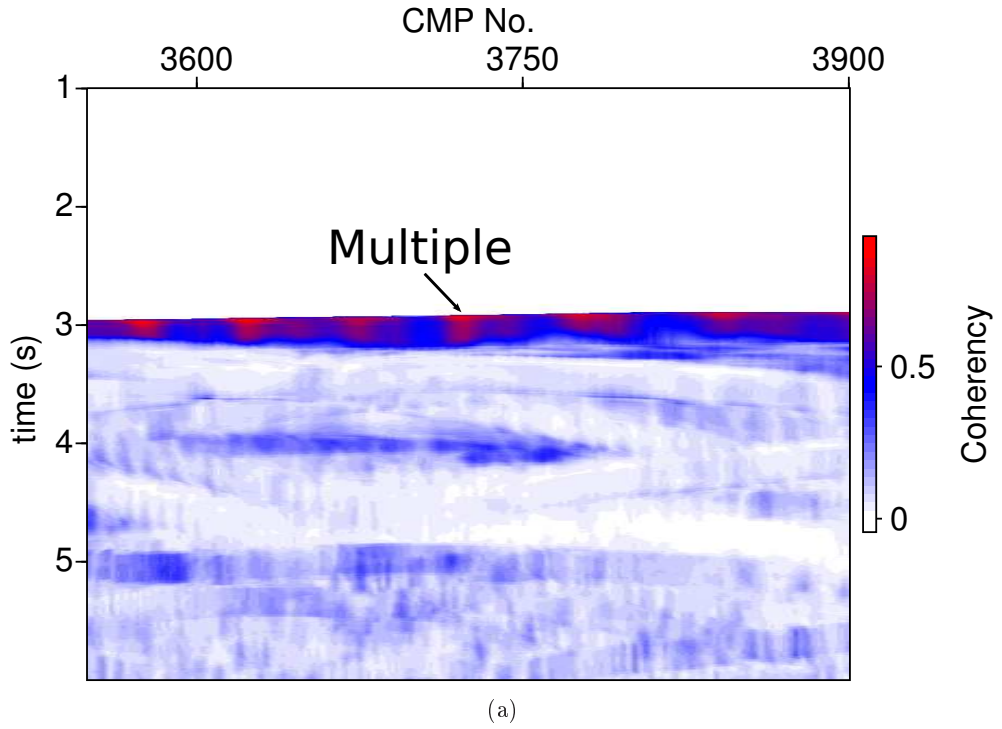

(a)

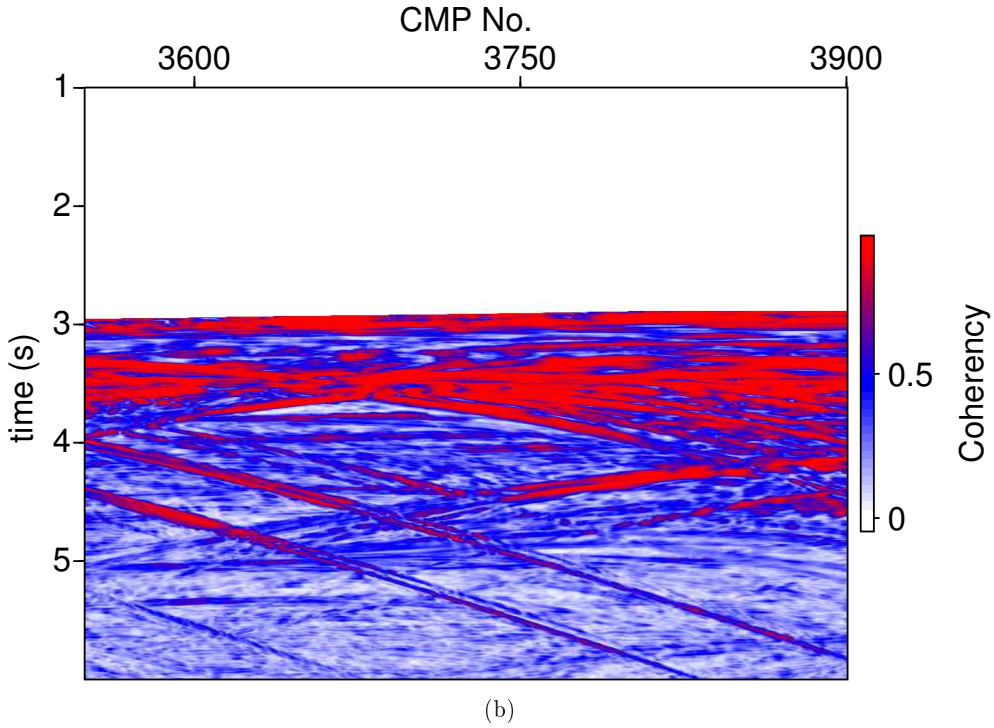

(b)

Figure 3.3: (a) shows the coherency section of the BP 2004 including offsets from 125 m up to 3500 m data of CMPs between 3550 and 3900 when the stacking process is tuned to image multiples properly so that the velocity search interval is adjusted to a lower range (1480 m/s to 1550m/s). (b) shows the coherency section of the data when the stacking process is tuned to image primaries. In (a) multiples have a higher value in comparison to the value of the primaries.

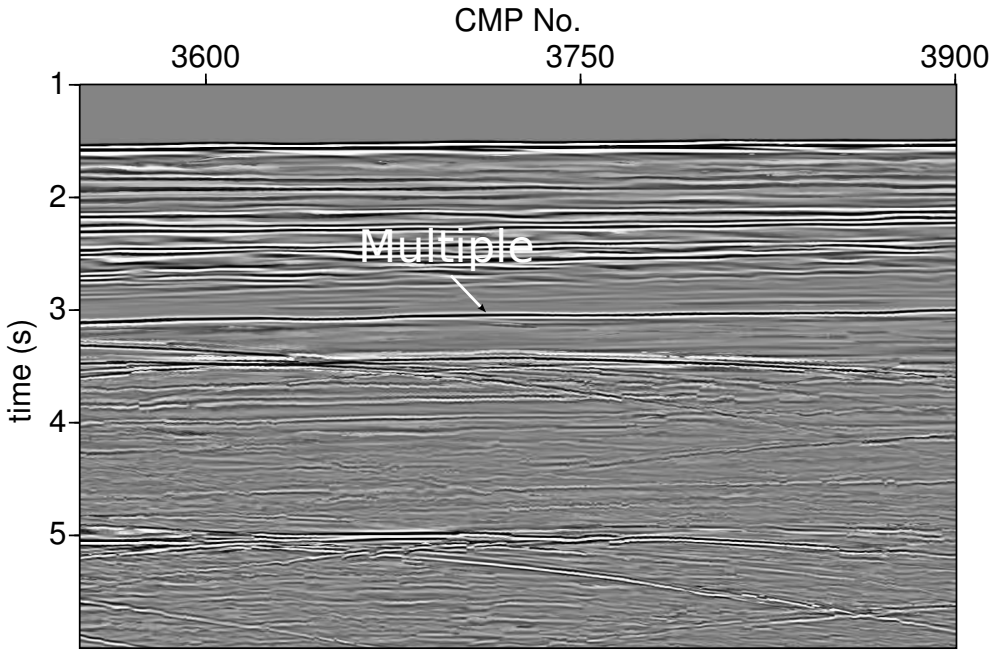

Figure 3.4: The stacked section of the BP 2004 dataset: offsets ranges from 3500 m up to 8000 m. The stacking process is performed, such that multiples are optimally imaged.

first order multiple, which is indicated by an arrow in Figure 3.5(a), is removed and it is not recognizable in the stacked section in Figure 3.5(b). In the following section, I will investigate application of the method to the TGS data.

3.1.2 Field data example

In the next step, the method was applied to the TGS dataset, which is introduced in **Chapter 2**. At first, the stacked section, the corresponding coherency section, and the stacking velocity profile were generated for offset ranges from 150 m to 3638 m. Since in this case our target was to image surface related multiples in marine data, I set the velocity search interval from 1450 m/s to 1550 m/s which is the velocity of water. Then, the upper part of the first order multiple was muted, Figure 3.6(a) is the stacked section of the data and Figure 3.6(b) is the corresponding coherency section. As you can see in the coherency section the multiples have the higher coherency. Then, the stacking velocity profile and the coherency section and the stacked section were used to predict pre-stack traveltimes of multiples. In order to predict multiples for far offsets, the method was applied once again, to the offset ranges from 3638 m to 7338 m. Figure 3.7 shows the stacked section of the far offset data . In Figure 3.8(a), the stacked section before multiple attenuation is presented, and in Figure 3.8(b) the corresponding stacked section after multiple attenuation is shown. Overall, we can see that most of the multiple energy, which is depicted with an arrow in Figure 3.8(a), is removed from the stacked section in Figure 3.8(b). To visualize the result better, a closeup image is provided in Figure 3.9. In Figure 3.9(a) the stacked section of the data CMP's between 3600 and 4400 before multiple attenuation is shown and Figure 3.9(b)

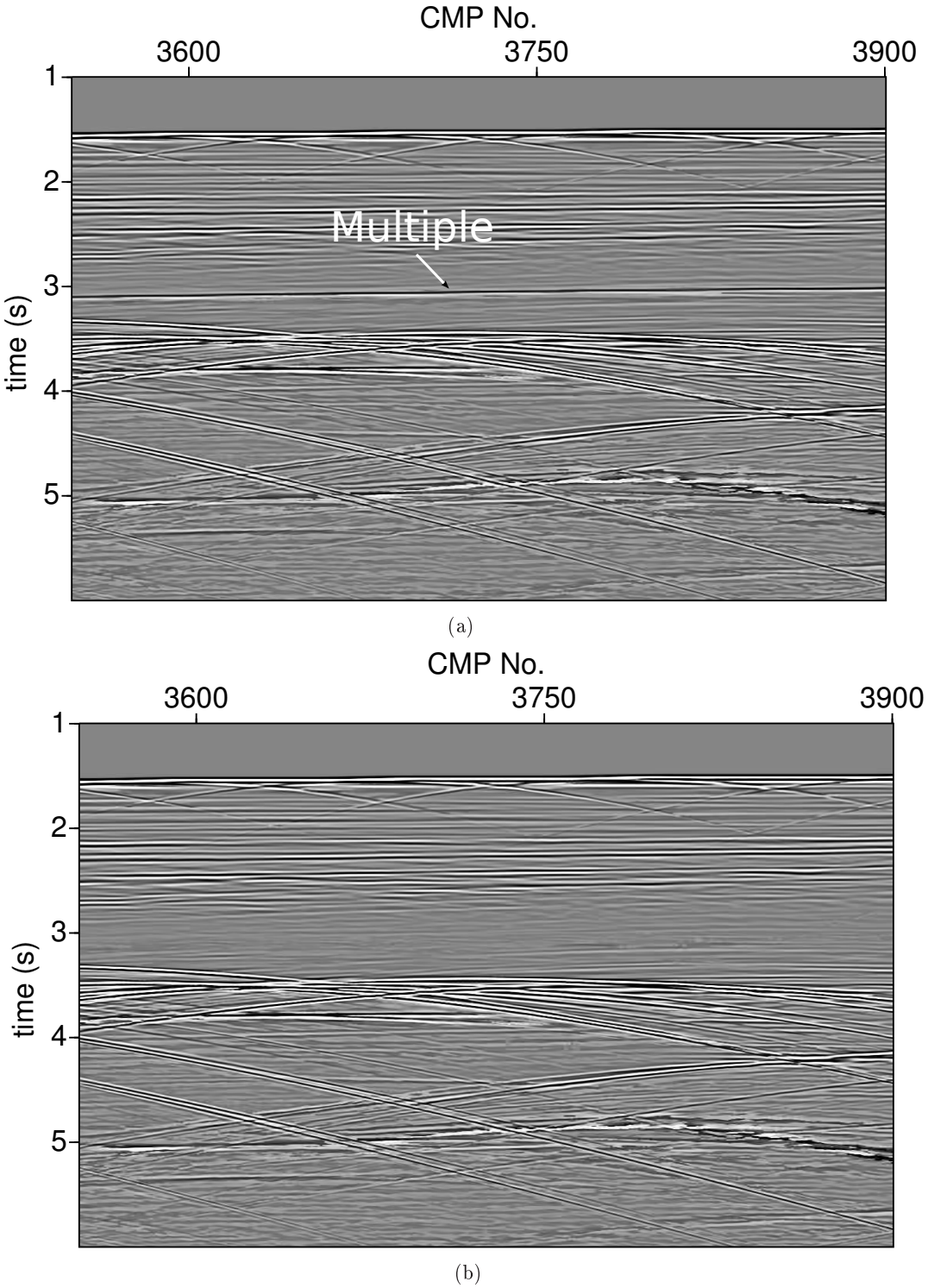

Figure 3.5: The stacked section of the BP 2004 dataset; in (a) the stacked section including multiples is displayed. In (b) the corresponding stacked section after multiple attenuation is shown. The first order multiple (indicated by an arrow in (a)) is removed and it is not recognizable in the stacked section in (b).

is the corresponding section after multiple attenuation. Some events which are shown by arrows in Figure 3.9(b) are revealed after multiple attenuation. Generally, the result in a certain expert of the BP 2004 dataset and TGS data is acceptable but in more complex data the method does not yield a good result. In the next section, I will use the velocity section as a guide, to find a better criterion for picking multiples.

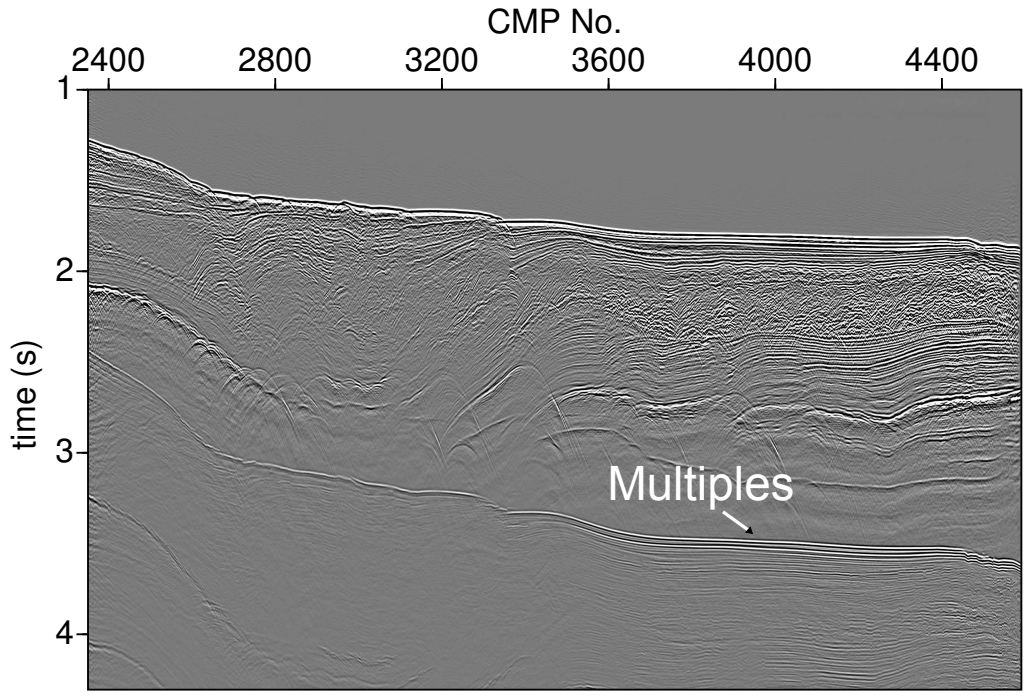

(a)

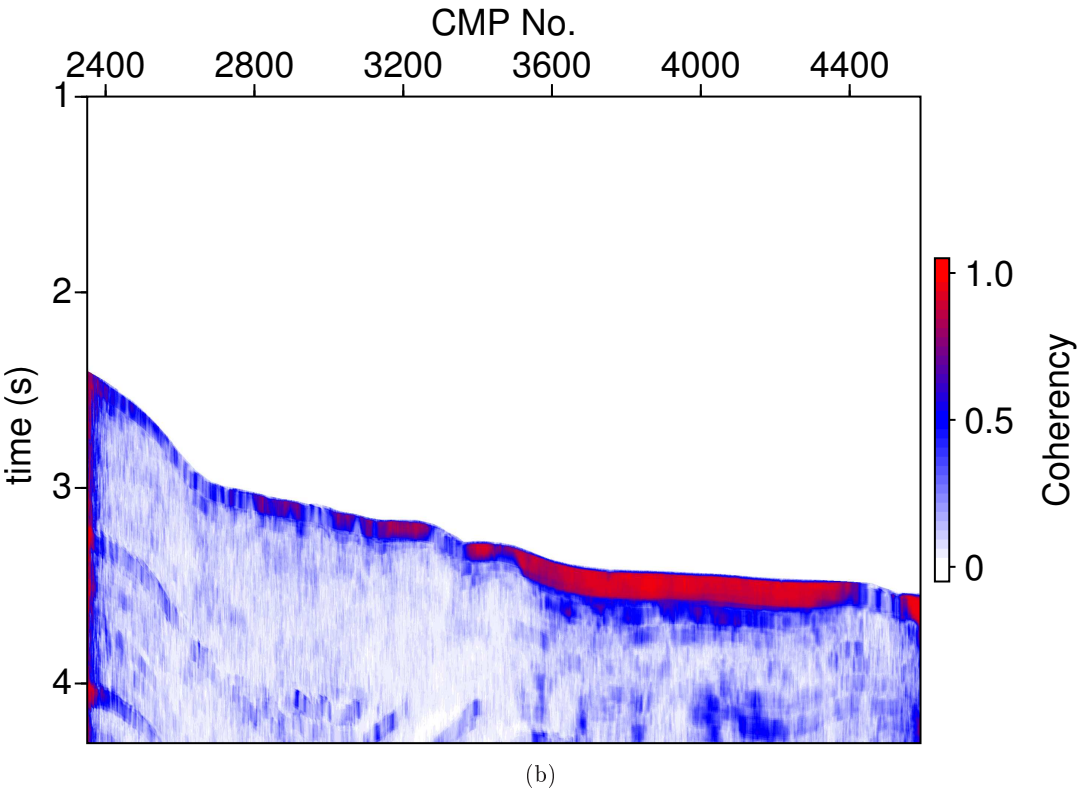

(b)

Figure 3.6: (a) The stacked section of the TGS data including only offsets from 150 m to 3638 m, the velocity search interval is between $1450m/s$ to $1550m/s$. In (b) the corresponding coherency section is displayed.

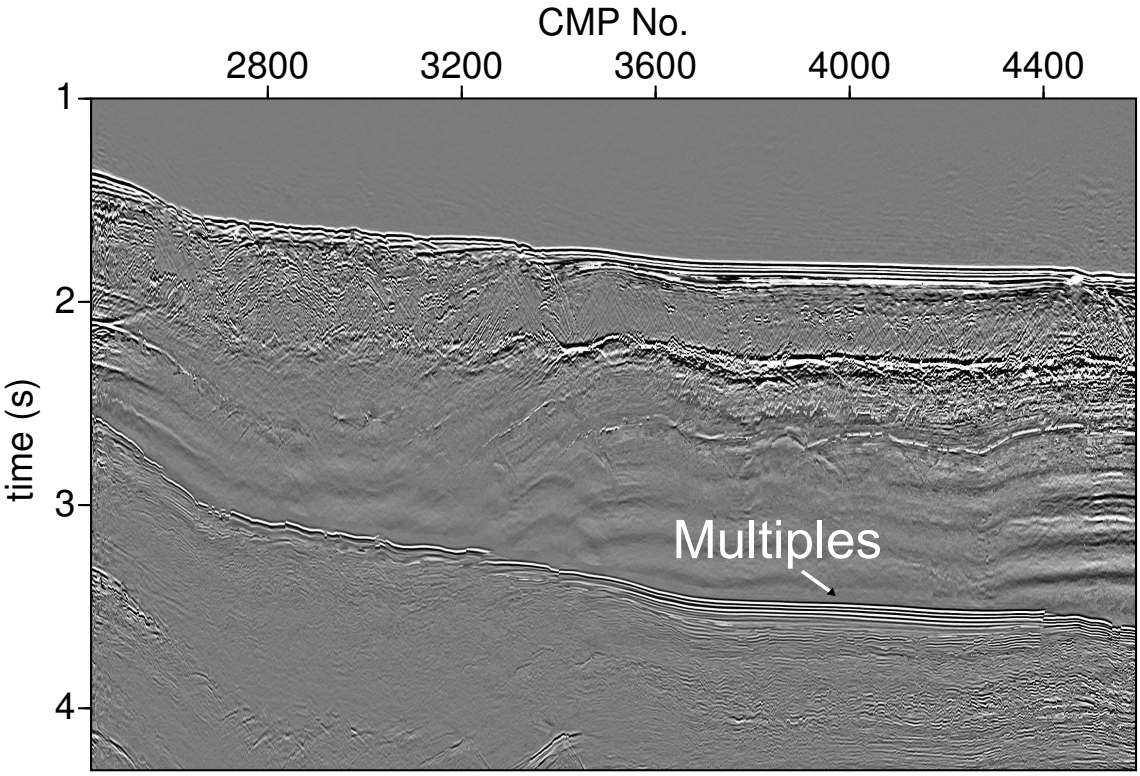

Figure 3.7: The stacked section of the TGS data: offsets from 3638 m to 7338 m. The stacking process has been optimized to image multiples.

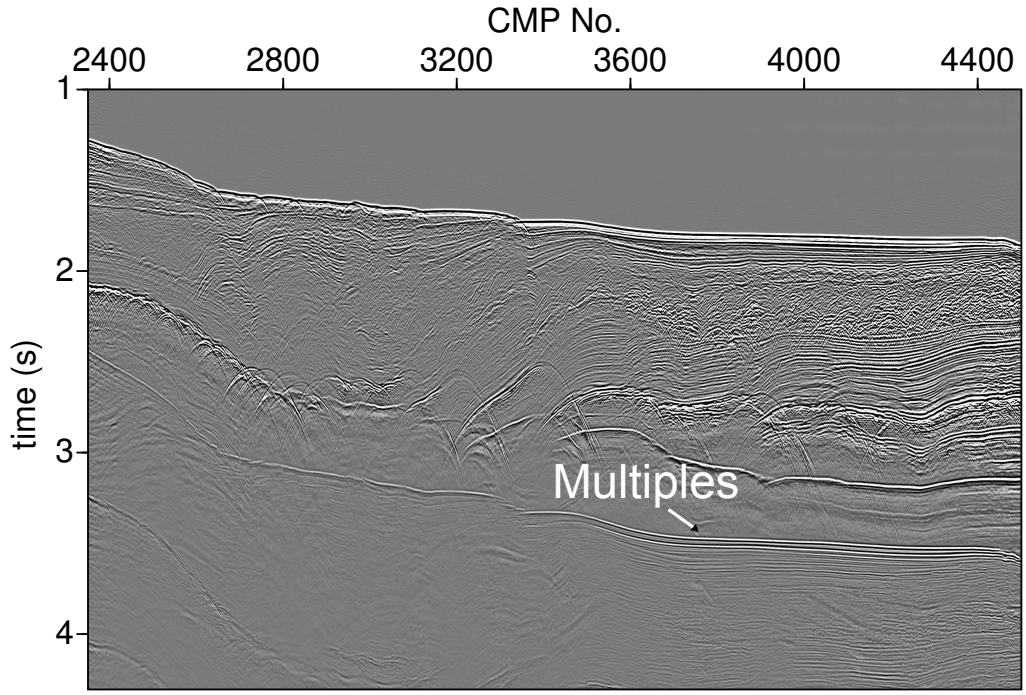

(a)

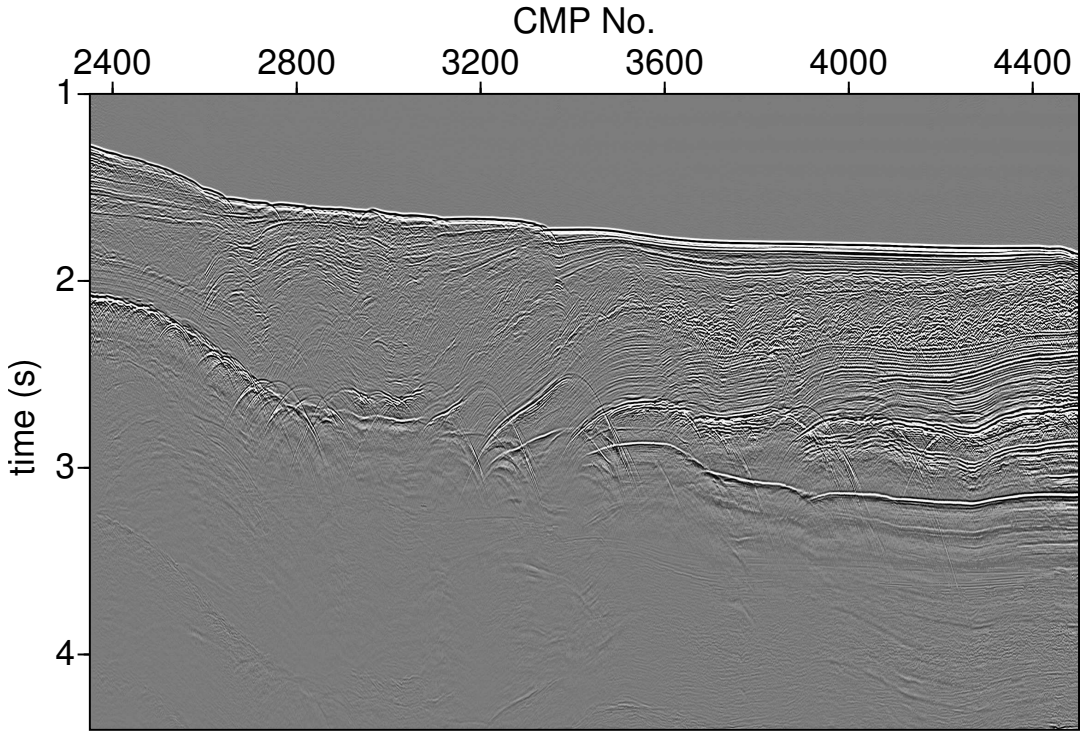

(b)

Figure 3.8: TGS data example. In (a) the stacked section including multiples is displayed. In (b) the corresponding stacked section after multiple attenuation is shown. We can see that most of the multiple energy (indicated by an arrow in (a)) is removed from the stacked section in (b).

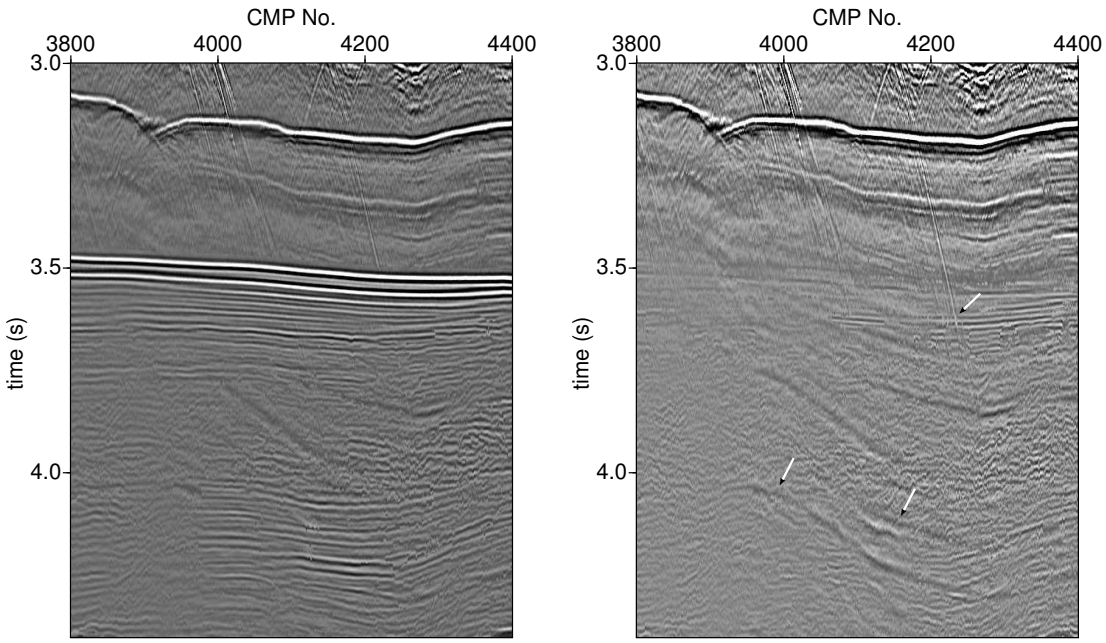

(a) (b)

Figure 3.9: A closeup of the stacked section of the TGS data. In (a) the stacked section including multiples is displayed. In (b) the corresponding stacked section after multiple attenuation is shown. Some events which are shown by arrows in (b) are revealed after multiple attenuation.

3.2 Multiple attenuation using velocity as a guide

In this section, I use velocity as a guide since the coherency method does not work in areas with a lot of diffractions and in case of complex geology. The method is exactly the same as the method I introduced in the previous section. The only difference is that I use the velocity section as a guide to pick the zero-offset traveltime of the events with a certain velocity. In this work, the velocities are provided using a CRS stacking operator which is developed by Walda (2016). This operator includes different algorithms for global optimization like genetic algorithm and differential evolution. Thus, it provides more reliable attributes and stacked sections with higher resolution in comparison with other operators that applied local optimization. Although this operator is quite expensive and time consuming, the multiple attenuation procedure is fast an robust. In the next section, a synthetic data example is provided.

3.2.1 Synthetic data example

To illustrate the method, I again applied it to the synthetic Sigsbee2B dataset which was introduced in **Chapter 2**. After applying CRS stacking workflow, I obtained a stacked section of data and a velocity section as well. It is necessary to mute the upper part of the first order multiple to avoid attenuating primaries because multiples and their related primaries have the same velocity. With the guide of the velocity section zero-offset traveltimes of multiples were picked then the traveltimes of multiples in other offsets were estimated. Afterwards, multiples were adaptively subtracted from the data (the processing parameters are provided in **Appendix D**). The result is shown in Figure 3.10. In Figure 3.10(a), the stacked section including multiples is displayed and in Figure 3.10(b) the corresponding stacked section after multiple attenuation is shown. As you can see most of the multiple energy is attenuated and the result is quite promising. In next step, I apply this method to the field data.

3.2.2 Field data example

In the next step, the workflow was used for attenuating multiples in the TGS dataset which was already introduced in **Chapter 2**. The method was applied according to the described procedure in the previous section (the processing parameters are provided in **Appendix D**). Figure 3.11 shows the velocity section of this data, from this section we can see that multiples have a certain range of velocity (about $1450m/s$ to $1600m/s$), this can be used as a guide to pick the multiples. In Figure 3.12(a), the stacked section before multiple attenuation is presented, and in Figure 3.12(b) the corresponding stacked section after multiple attenuation is shown. Figure 3.13 is a closeup of the result. Some events which are indicated by arrows in Figure 3.13(b), are not visible in Figure 3.13(a), are revealed after multiple attenuation. Figure 3.14 compares the result of multiple attenuation using coherency as an attribute (Figure 3.14(a)) with the result of multiple attenuation using

velocity as an attribute (Figure 3.14(b)). The parameter for multiple attenuation and stacking was the same. there are some residuals of multiples in Figure 3.14(a) which are shown by squares. In general, velocity is a better criterion in comparison to coherency. It yields better results and it is more reliable in the case of complex geology. In this work, I employed the CRS stacking operator (Walda, 2016), To obtain the velocity section, since this operator includes global optimisation, thus, it yields reliable attributes. However, any stacking operator which yields a reliable velocity section, can be used for velocity estimation.

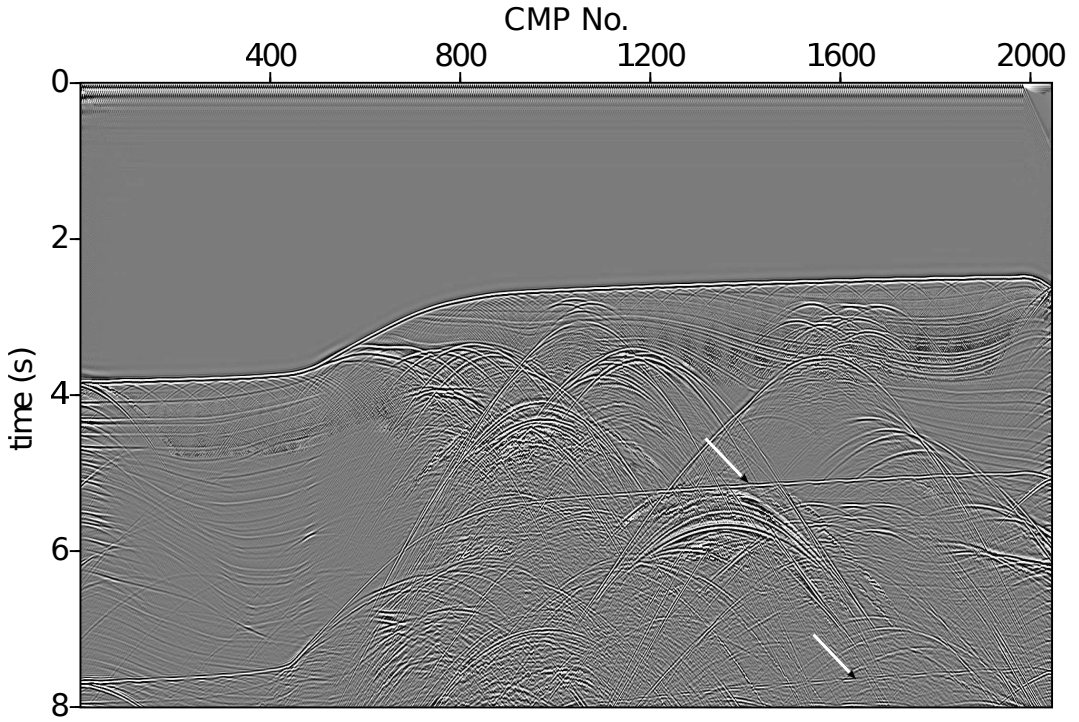

(a)

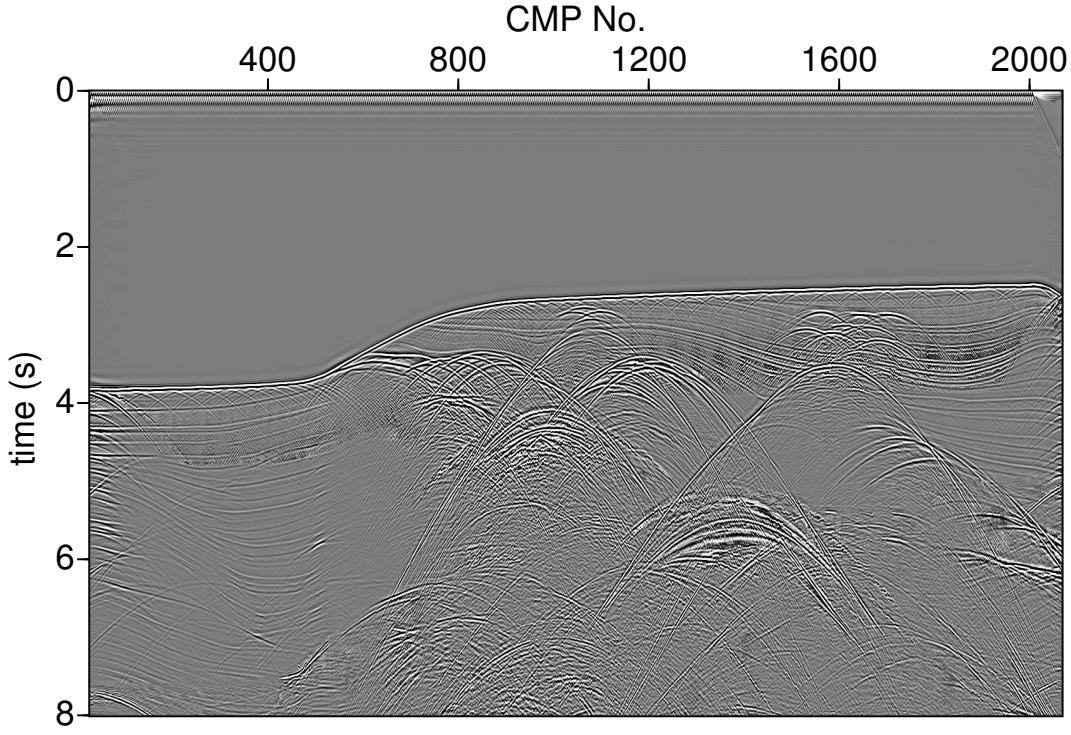

(b)

Figure 3.10: Sigsbee2B dataset. In (a) the stacked section including multiples (indicated by arrows) is displayed. In (b) the corresponding stacked section after multiple attenuation is shown.

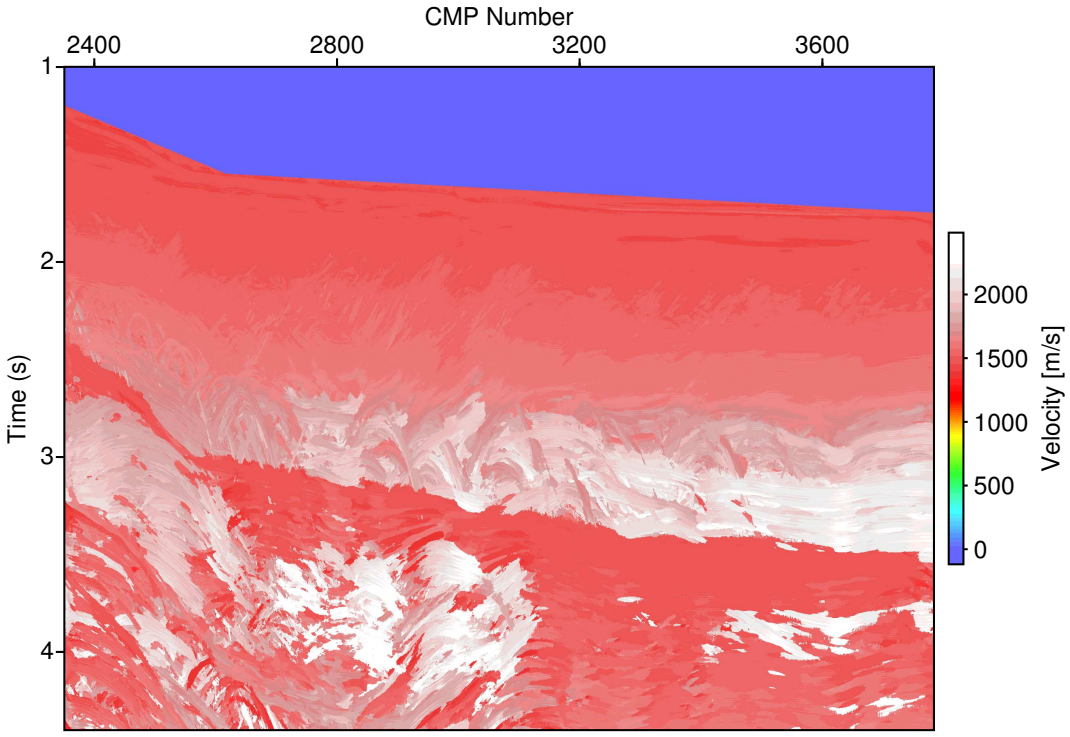

Figure 3.11: The velocity section of the TGS dataset. Multiples have a certain range of velocity (about 1450 m/s to 1600 m/s).

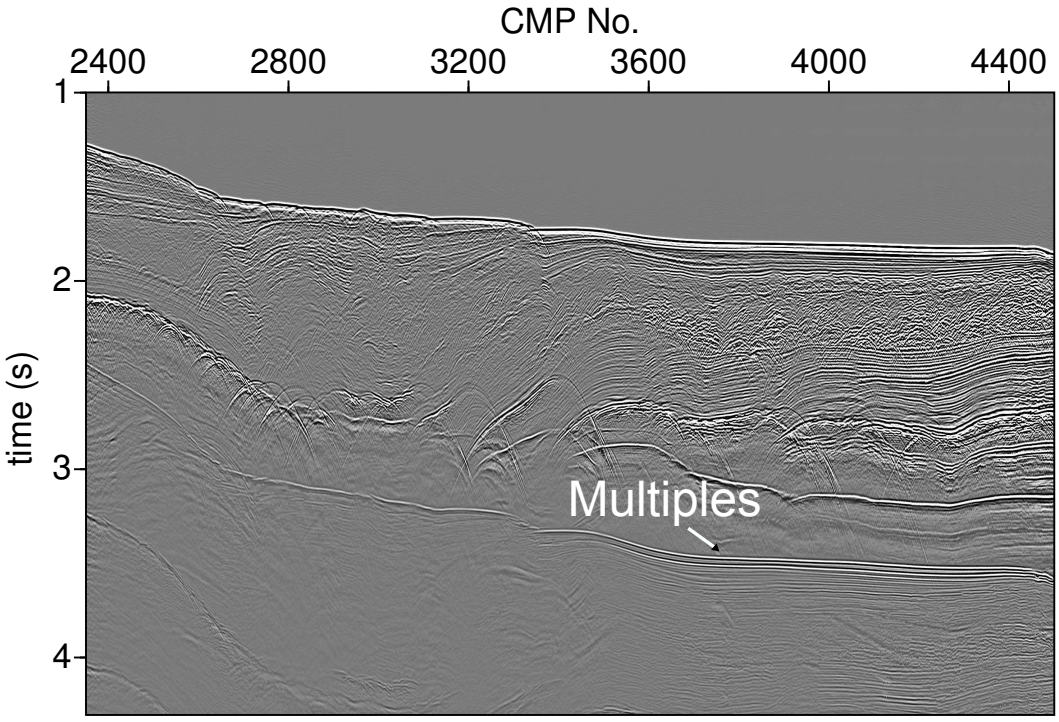

(a)

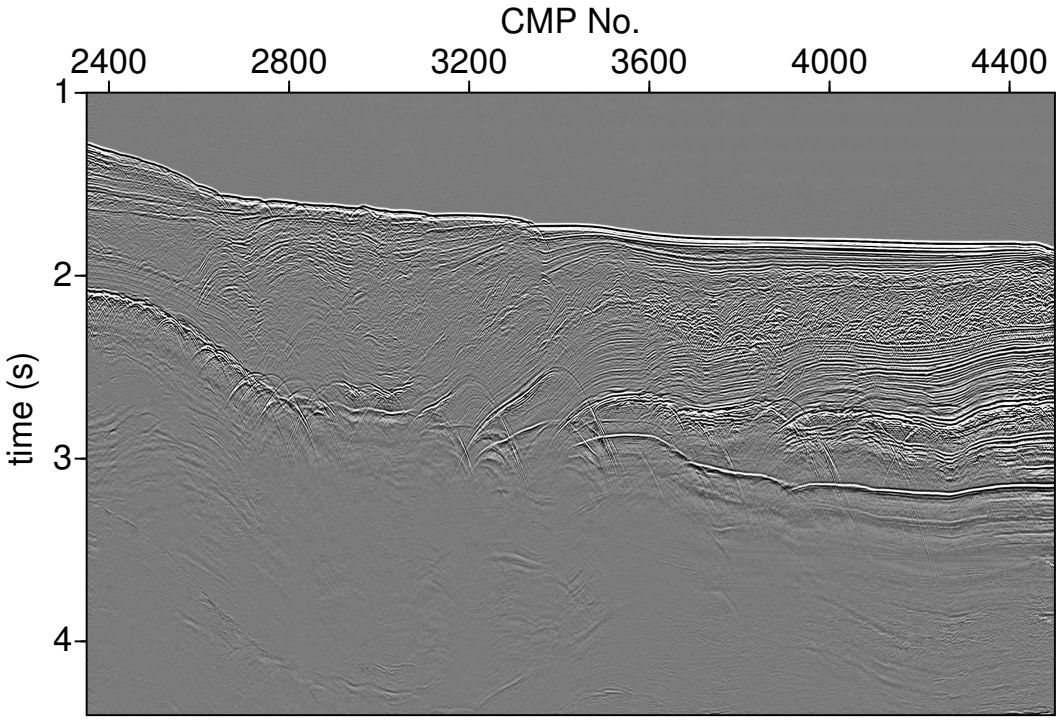

(b)

Figure 3.12: The TGS data example. In (a) the stacked section including multiples is displayed. In (b) the corresponding stacked section after multiple attenuation is shown. We can see that most of the multiple energy (indicated by an arrow in (a)) is removed from the stacked section in (b).

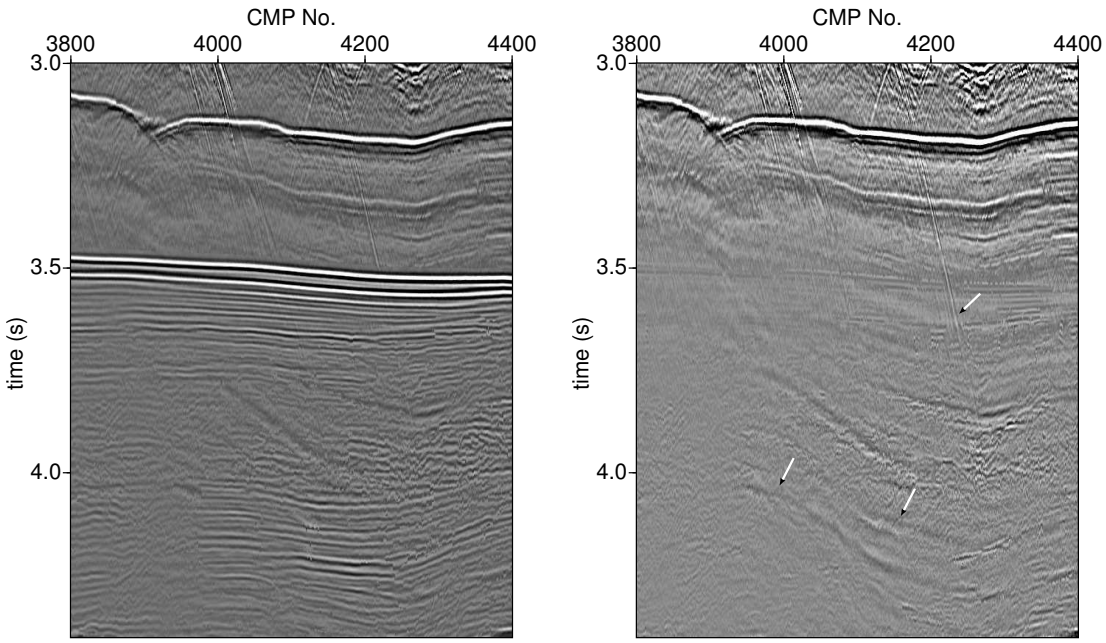

(a) (b)

Figure 3.13: A closeup of the TGS data: CMPs between 3600 and 4400. In (a) the stacked section including multiples is displayed. In (b) the corresponding stacked section after multiple attenuation is shown. Some events which are shown by arrows in (b) are revealed after multiple attenuation.

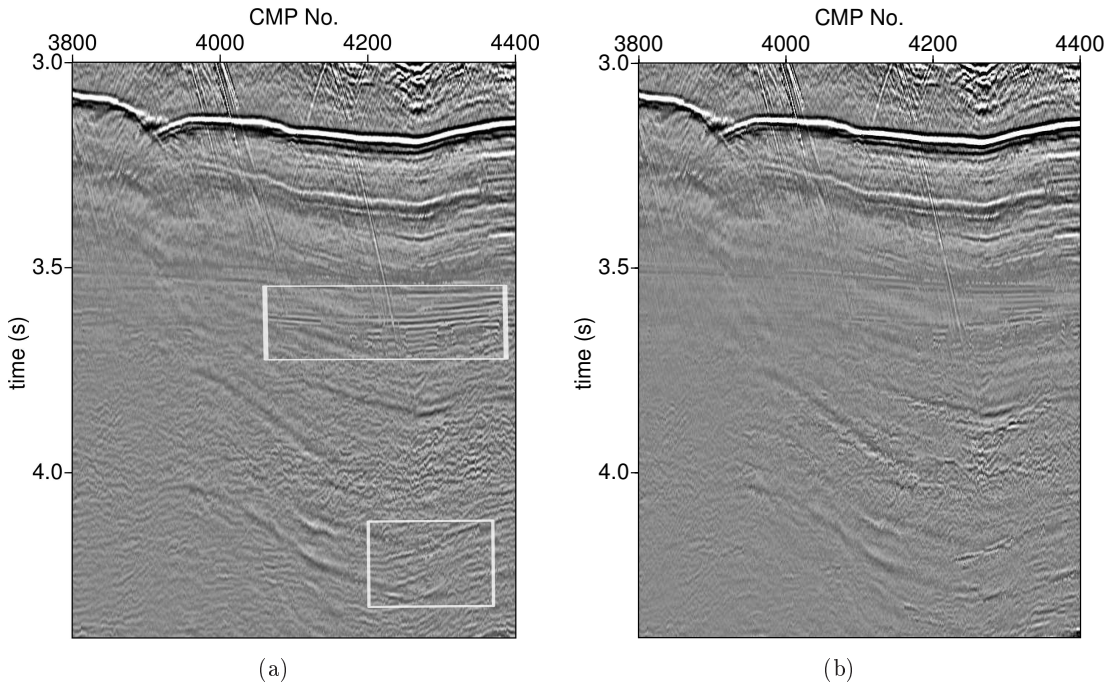

(a) (b)

Figure 3.14: Comparison of the result of multiple attenuation in TGS data CMP's between 3600 and 4400 In (a) the stacked section after multiple attenuation using coherency as a guide is shown. There are some residuals of multiples indicated by squares. In (b) the same stacked section after multiple attenuation using velocity as a guide is displayed.

Chapter 4

Conclusions and Outlook

In seismic processing it is assumed that reflection data only consist of primaries. Thus, multiples are considered as noise in seismic data and should be suppressed prior to migration and stratigraphic interpretation. In the scope of this thesis, I have introduced different interpretational approaches, for prestack multiple attenuation. The key step is to obtain the traveltime of the multiples in the ZO section. For this purpose, multiples can be picked manually or automatically. It is also possible to pick them using additional information such as velocity or coherency. In all the examples, which I have provided in this thesis, the methods were applied within the CMP stacking operator and the targets were surface related multiples.

In zero-offset picking approach multiples were picked manually in 2D examples and automatically in a 3D example. To resolve the spread length bias effect, the data was divided into two different offset ranges and treated separately. Therefore, the method is not limited to a certain range of offsets.

In the presence of conflicting dips and triplications automatic picking is challenging. To solve this issue, I also applied the method to a partly migrated synthetic dataset, where diffractions are focused and there are fewer conflicting dip situations.

In 2D examples, the result were satisfying and showed the potential of the method. The main advantage of the method is its speed and robustness. Furthermore, it can be easily applied to a field data and does not require high computational effort.

To attenuate other surface related multiples as well as first layer multiples, I tried to pick multiples using the coherency section as a guide. The result for synthetic data and marine data was acceptable. However, in the case of complex structures and presence of diffractions, coherency was not a good criterion. To find a better criterion, I used the velocity section instead of the coherency section as guide to pick the multiples. It proved to be a more reliable criterion comparing to coherency and it performed stably in presence of diffractions and complex structures.

In this study, the velocity section were provided using CRS stacking operator which includes global optimisation. Thus, it yields reliable attributes. Nevertheless, any operator which provides a reliable velocity section, can be used for velocity estimation.

To sum up, I proposed different approaches for picking the ZO traveltime of multiples: the manual or automatic picking approach proved to be fast, robust and practical. This method can be applied in CSP domain as well as CMP domain depending on the presence of conflicting dip situations or diffractions. The advantage of this approach is that there is less possibility to attenuate primaries in comparison with the guided approach. However, sometimes the targets are other surface related multiples as well as first layer multiples. In this case, picking multiples is unfeasible because some parts of the section are covered by multiples. In this situation, using attributes would be a pragmatic strategy.

I applied the ZO picking approach within the CMP stacking operator. Any kind of stacking operator can be used including the CRS operator. I suggest using CRS prestack data enhancement (Baykulov and Gajewski, 2009) to obtain a stacked section with high S/N ratio.

The automatic picking approach was investigated on a very simple 3D synthetic dataset. Since automatic picking is not an easy task in conflicting dip situation. I suggest considering the application of the method in more complex 3D data with conflicting dip situations. In this case, it is more reasonable to apply the method in CSP domain to encounter fewer conflicting dip situations.

Multiple identification in the stacked section is an interpretational step and should be done carefully in order to avoid picking primaries instead of multiples. This step can be guided by 1D convolution prediction.

Since the hyperbolic formula is limited to near offsets and is affected by spread length bias. To use this method for larger offsets, I apply the method to two different range of offsets separately. However, it is possible to divide data into more offset ranges to obtain a good result for all offset ranges. Another solution could be using a nonhyperbolic operator for prestack multiple prediction.

The presented method could be applied to any hyperbolic event. However, in this thesis, only surface related multiples were considered. For further investigation, I propose to apply the method to internal multiples as well.

I applied the ZO picking approach in CSP domain to obtain a stacked section with less diffractions and conflicting dip situation. After application of the method in CSP domain data remapping from the CSP domain to the CMP domain for further processing is possible (Yang et al., 2016).

The first step in application the method in CSP domain is to obtain a migration velocity section which can be challenging in presence of dipping multiples. As another option, I suggest using diffraction separated data instead of application the method in CSP domain

(e.g. Dell and Gajewski, 2011; Rad et al., 2016).

To derive the velocity section, which was used as a guide for picking multiples, I employed a CRS stacking operator (Walda, 2016). This operator also generates the stacked section and other attributes in different dip angles, by splitting the search space into different angle search intervals (Walda and Gajewski, 2015c). This means we have access to extra information about the subsurface that can be used in different steps of processing including multiple attenuation.

Appendix A

Reviewing f-k filtering and Radon transform

Before reviewing f-k filtering and Radon transform the concept of normal moveout is defined.

A.1 Normal moveout

The difference between the two-way traveltime at a certain offset and the two-way zero-offset traveltime in a reflection event on a Common Mid Point (CMP) gather is called normal moveout (NMO). Figure A.1 shows a seismic section which is sorted by common midpoint and then corrected for normal moveout. Reflection traveltimes are NMO corrected for every offset, this moveout depends on different factors such as velocity above the reflector, offset, dip of the reflector, and the source-receiver azimuth regarding the dip direction of the reflector. The traveltime is given by (e.g. Yilmaz, 2001) as

$$\Delta t_{NMO} = t - t_0. \tag{A.1}$$

In another way, it can be introduced as

$$\Delta t_{NMO} = t_0[\sqrt{1 + (\frac{x}{v_{NMO} t_0})^2} - 1]. \tag{A.2}$$

For a single horizontal layer medium v_{NMO} is equal to the velocity of the medium above the reflector and for a single dipping-layer medium

$$v_{NMO} = \frac{v}{\cos\phi}, \tag{A.3}$$

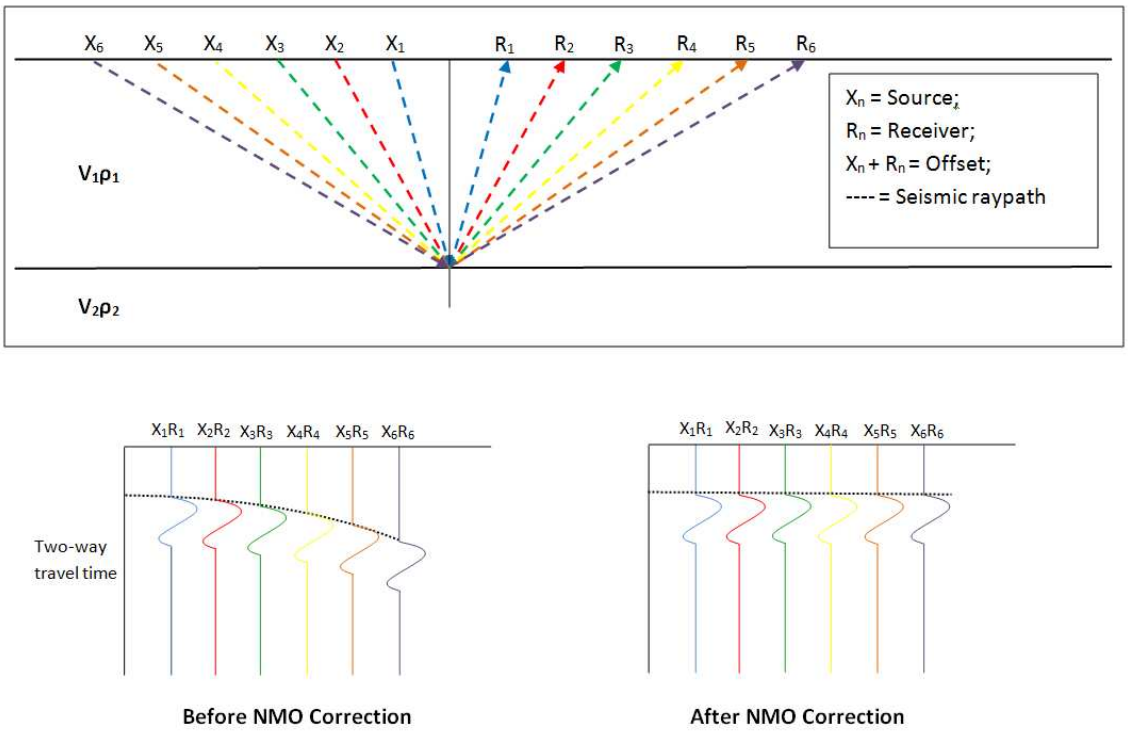

Figure A.1: Seismic data is sorted by common midpoint and then corrected for normal moveout (`https://en.wikipedia.org/wiki/Normal_moveout`).

where ϕ is the dip angle of the reflector. In the case of horizontally stratified media v_{NMO} is equal to v_{rms} which can be obtained by

$$v_{rms}^2 = \frac{1}{t_0}\sum_{i=1}^{N} v_i^2 \Delta\tau_i, \tag{A.4}$$

where v_i is the interval velocity of the ith layer and $\Delta\tau_i$ is the vertical two-way time through the ith layer and $t_0 = \sum_{i=1}^{N} \Delta\tau_i$. In this formula, all velocities from the layers above are incorporated to obtain RMS velocity.
Table A.1 gives a summary of NMO velocities in various earth models. In many cases

Table A.1: NMO velocity for various earth models (Yilmaz, 2001).

Model	NMO Velocity
Single horizontal layer	v
Horizontally stratified earth	v_{rms} provided the spread is small
Single dipping layer	$\frac{v}{\cos\phi}$
Multilayered earth with arbitrary dips	v_{rms} provided the spread is small and the dips are gentle

velocities of waves increase with depth and when a wave travels to the deeper layer, the

average velocity it experiences along the raypath is higher than average velocity in shallower layer. The raypaths of the multiples are different from primaries, as a result, the average velocities which they experience are different. Most of the multiples usually travel through the shallower parts so the velocity they experience is lower than primaries at a certain arrival time. Equation A.2 illustrates that a lower velocity leads to a higher moveout. With a correct velocity model for the primaries we can obtain a correct normal move out and then, after normal moveout correction and before stacking, most of the primaries will be flattened. The events left unflattened are either primaries which were not properly corrected or multiples. Any filter which differentiates between the dip events and flat events can be used for multiple suppression. There are some domains to transform the data and suppress the multiple such as f-k or Radon. After transforming the data back to time domain we will have multiple-attenuated data.

A.2 f-k filtering

In frequency-wavenumber (f-k) domain, frequency (f) is defined as the inverse of the period (T) and the wavenumber (k) is the inverse of the wavelength (λ). f-k stands for frequency-wavenumber filtering. Considering that a wavelength in the space is similar to period length in time, wavenumber is the spatial equivalent of frequency in time.

$$k = \frac{1}{\lambda} \tag{A.5}$$

$$f = \frac{1}{T} \tag{A.6}$$

For data as a function of two coordinates (i.e. time and offset for a CMP gather) the f-k transform is a double Fourier transform over both coordinates. First, data(x,t) are transformed to the temporal frequency domain(e.g. Oppenheim et al., 1983)

$$D(x,f) = \int_{-\infty}^{+\infty} d(x,t) e^{-j2\pi ft} dt, \tag{A.7}$$

and in the second step, a Fourier transform over the spatial coordinate can be applied, which is defined as

$$D(k_x,f) = \int_{-\infty}^{+\infty} D(x,f) e^{+j2\pi k_x x} dx. \tag{A.8}$$

A linear event with dip in time domain will also appear as a linear dip event in frequency domain. If we choose the velocity value which is in the range between the average velocities of primaries and multiples and apply NMO correction, primaries will be overcorrected and multiples will be undercorrected. Then, they will appear in two different quadrants in the f-k plane. We can exploit this to recognize and thus attenuate multiples. Transforming the data again to the time domain and reverse NMO application yield multiple attenuated data (Ryu, 1982). f-k filtering is widely used for separating surface waves from body waves see Embree et al. (1963); March and Bailey (1983); Duncan and Beresford (1994). f-k filtering can be applied to 3D seismic data. In this case data will be transformed into f-k-k domain Peardon and Bacon (1992); Meunier (1999).

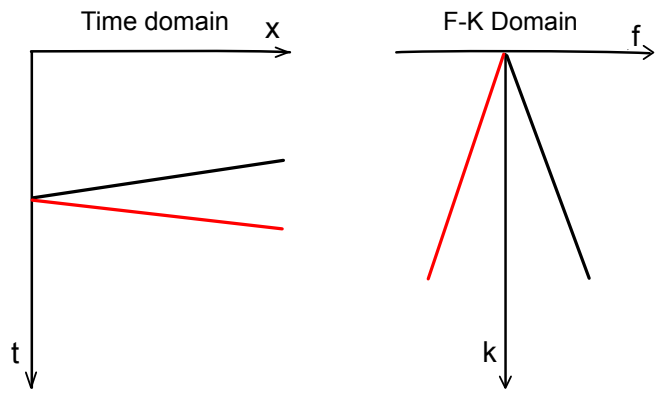

Figure A.2: Simple sketch of event conversion from time domain into frequency-wavenumber domain; event with negative and positive dip angle in time domain appear in two different quadrants in the f-k plane.

A.3 Radon transform

The linear Radon transform which is also called $\tau - p$ or slant stack is given by (Diebold and Stoffa, 1981)

$$m(p_x, \tau) = \int_{-\infty}^{+\infty} d(x, t = \tau + p_x x)dx, \tag{A.9}$$

which implies that the data in time domain is summed up along a straight line with time intercept τ and dip p. Summing up along a line is not always linear and different radon transforms can be derived. For example, parabolic and hyperbolic Radon transforms are widely used, the only difference between them is the mapping operator. The parabolic Radon transform is defined as (Hampson, 1986)

$$m(q, \tau) = \int_{-\infty}^{+\infty} d(x, t = \tau + qx^2)dx, \tag{A.10}$$

and the hyperbolic Radon transform can be expressed as (Thorson and Claerbout, 1985)

$$m(\nu, \tau) = \int_{-\infty}^{+\infty} d(x, t = \sqrt{\tau^2 + \frac{x^2}{\nu^2}})dx. \tag{A.11}$$

The Radon filtering approach is very similar to f-k approach. NMO corrected data are transformed into Radon domain. Then multiples are muted and data will be transformed back into time domain. The disadvantage of f-k filtering and Radon approach is that there should be certain differences between primary moveout and multiple moveout. Applying these methods in near offsets is very difficult because there is very little or no difference in moveout between the two.

Appendix B

Convolution

Convolution of two signals means that one signal is reversed in time and moved along the other signal. At each lag, elements are multiplied in vertical direction. Then, the resulting products are added. To illustrate this I have provided an example, Figure B.1 and Table B.1 show the convolution of the source wavelet $(\frac{1}{2}, 1)$ with the reflectivity sequence $(-\frac{1}{2}, 0, 1)$ Convolution of two signals $a(t)$ and $b(t)$ in a continuous situation is defined as

Table B.1: Convolution of the source wavelet $(\frac{1}{2}, 1)$
with the reflectivity sequence $(-\frac{1}{2}, 0, 1)$

Reflectivity sequence					Output response
	$-\frac{1}{2}$	0	1		
1	$\frac{1}{2}$				$-\frac{1}{4}$
	1	$\frac{1}{2}$			$-\frac{1}{2}$
		1	$\frac{1}{2}$		$\frac{1}{2}$
			1	$\frac{1}{2}$	1

$$c(t) = a(t) * b(t) = \int_{-\infty}^{+\infty} a(\tau) b(t-\tau) d\tau, \tag{B.1}$$

where the asterisk denotes convolution. Convolution in frequency domain is a scalar multiplication (e.g. Oppenheim et al., 1983).

$$C(f) = A(f)B(f). \tag{B.2}$$

This shows convolution is a commutative operation, it means interchanging the order of the input has no effect on the result.

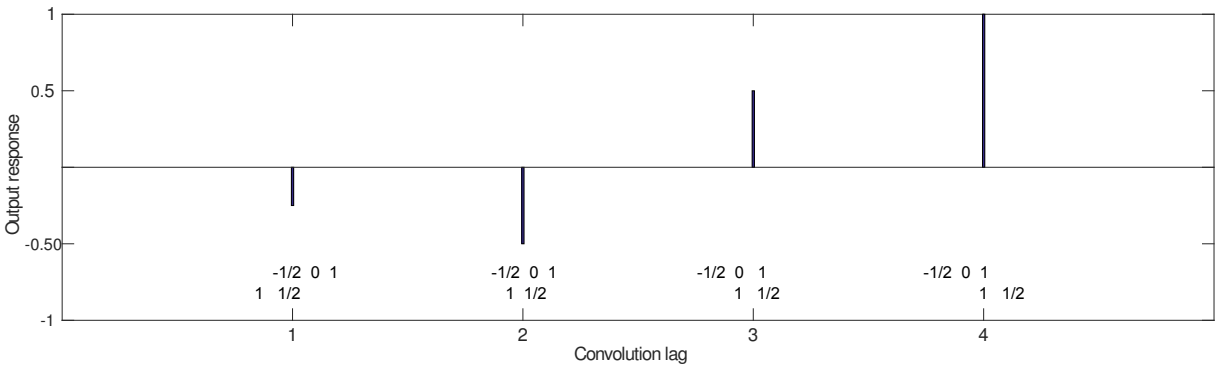

Figure B.1: Convolution of the source wavelet $(\frac{1}{2}, 1)$ with the reflectivity sequence $(-\frac{1}{2}, 0, 1)$

Appendix C

Correlation

Correlation is an operation that is used to measure the similarity or time alignment of two signals. To do this, one signal is moved along the other signal and at each lag elements are multiplied in vertical direction then the resulting products are added. The time lag at which they have the highest similarity is defined. Crosscorrelation is correlation of two different signals and measures how much these two signals are similar to each other. Correlation of a time series with itself is called autocorrelation. Table C.1 shows the crosscorrelation of the following wavelets:
Wavelet 1 : $(1, 1, -2, -1, 0)$
Wavelet 2 : $(0, 1, 1, -2, -1)$
Wavelet 2 is obtained by shifting wavelet 1 by one sample. From the Table C.1 and Figure C.1(a) we can see that the time lag with the most similarity between the two signals is observed at lag -1. This means that if wavelet 2 shifts one sample back in time then these two wavelets have the most similarity. If the order of these two wavelets is interchanged, the crosscorrelation result would be different. In this case, which is illustrated in the Table C.2 and Figure C.1(a), the time lag where these two wavelets depict the most similarity is 1.

Table C.1: Crosscorrelation of the wavelet $(1, 1, -2, -1, 0)$ with $(0, 1, 1, -2, -1)$

				1	1	-2	-1	0					Output	Lag
0	1	1	-2	-1									-1	-4
	0	1	1	-2	-1								-3	-3
		0	1	1	-2	-1							1	-2
			0	1	1	-2	-1						7	-1
				0	1	1	-2	-1					1	0
					0	1	1	-2	-1				-3	1
						0	1	1	-2	-1			-1	2
							0	1	1	-2	-1		0	3
								0	1	1	-2	-1	0	4

Table C.2: Crosscorrelation of the wavelet$(0, 1, 1, -2, -1)$ with $(1, 1, -2, -1, 0)$

				0	1	1	-2	-1					Output	Lag
1	1	-2	-1	0									0	-4
	1	1	-2	-1	0								0	-3
		1	1	-2	-1	0							-1	-2
			1	1	-2	-1	0						-3	-1
				1	1	-2	-1	0					1	0
					1	1	-2	-1	0				7	1
						1	1	-2	-1	0			1	2
							1	1	-2	-1	0		-3	3
								1	1	-2	-1	0	-1	4

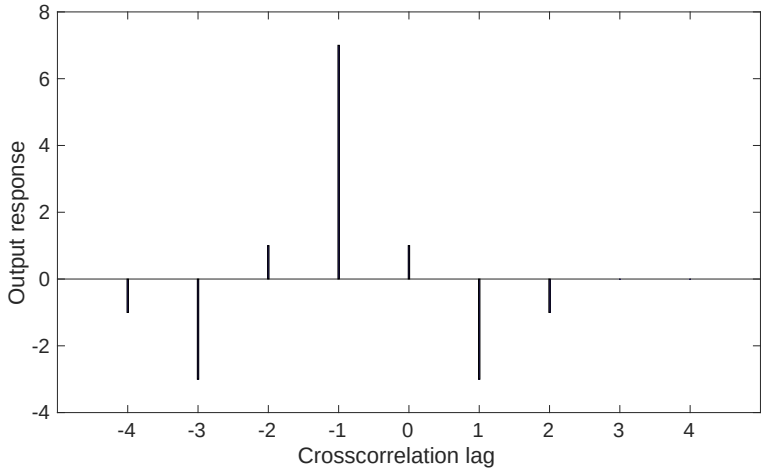

(a)

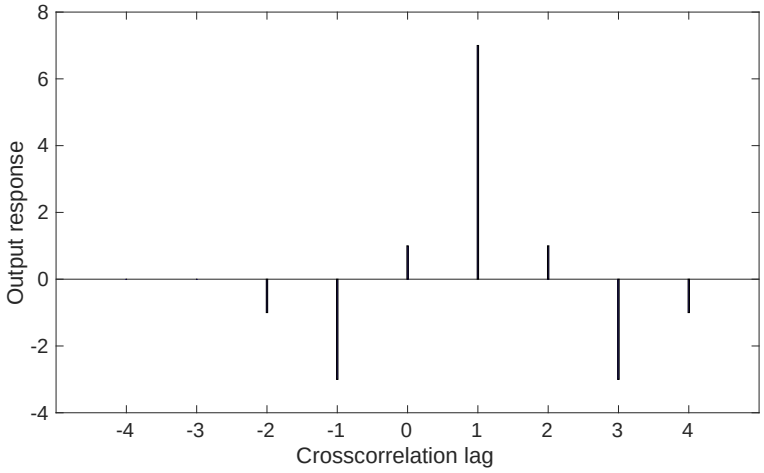

(b)

Figure C.1: a) ilustrate the crosscorrelation of the wavelet $(0, 1, 1, -2, -1)$ with $(1, 1, -2, -1, 0)$ the most similarity between the two signals is observed at lag -1 while b) ilustrate the crosscorrelation of the wavelet $(0, 1, 1, -2, -1)$ with $(1, 1, -2, -1, 0)$ the most similarity between the two signals is observed at lag 1.

Table C.3: Autocorrelation of the wavelet $(0, 1, 1, -2, -1)$

													Output	Lag
				0	1	1	-2	-1						
0	1	1	-2	-1									0	-4
	0	1	1	-2	-1								-1	-3
		0	1	1	-2	-1							-3	-2
			0	1	1	-2	-1						1	-1
				0	1	1	-2	-1					7	0
					0	1	1	-2	-1				1	1
						0	1	1	-2	-1			-3	2
							0	1	1	-2	-1		-1	3
								0	1	1	-2	-1	0	4

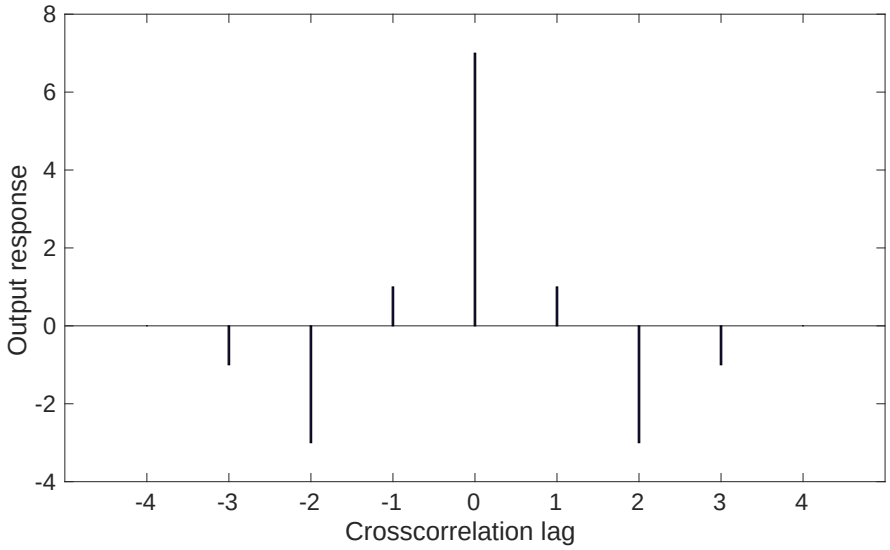

Figure C.2: The autocorrelation of the wavelet $(0, 1, 1, -2, -1)$. The maximum output is observed at lag zero and the result is symmetric.

Table C.3 and Figure C.2 show the output of different lags of autocorrelation of the wavelet 2. The maximum output is obtained at zero lag and the result is symmetric. Correlation of two signals $a(t)$ and $b(t)$ in a continuous situation is defined as

$$\phi_{ab}(t) = \int_{-\infty}^{+\infty} a(\tau)b(t+\tau)d\tau, \tag{C.1}$$

where the symbol ϕ denotes correlation. Correlation in frequency domain is a scalar multiplication of one signal with the complex conjugate of the second one (e.g. Oppenheim

et al., 1983)

$$\phi_{ab}(f) = A(f)B^*(f). \tag{C.2}$$

It implies correlation is not a commutative operation, which means that if the order of two inputs is changed then the result becomes its complex conjugate. In other words, correlation reverses in time direction

$$\phi_{ba}(f) = \phi^*_{ab}(f) = B(f)A^*(f). \tag{C.3}$$

Therefore, it is valid that

$$\phi_{ba}(t) = \phi_{ab}(-t), \tag{C.4}$$

and

$$\phi_{aa}(t) = \phi_{aa}(-t). \tag{C.5}$$

It means that autocorrelation of a signal is symmetric in time. Thus, only the calculation of one side of autocorrelation lags is sufficient.

Appendix D

Processing parameters

Table D.1: CMP search parameters: Sigsbee2B

Parameters for stacking multiples, offsets from 0 m to 4500 m	
Coherence measurement	Semblance
Coherency	5
Minimum offset aperture	1000 m at 0.002 s
Maximum offset aperture	3000 m at 8 s
Lower moveout velocity constraints	1450 m/s
Upper moveout velocity constraints	1700 m/s
Parameters for stacking multiples, offsets from 4500 m to 7000 m	
Coherence measurement	Semblance
Coherency	10
Minimum offset aperture	4800 m at 0.002 s
Maximum offset aperture	6000 m at 8 s
Lower moveout velocity constraints	1450 m/s
Upper moveout velocity constraints	1700 m/s
Parameters for stacking primaries	
Coherence measurement	Semblance
Coherency	5
Minimum offset aperture	1000 m at 0.002 s
Maximum offset aperture	3000 m at 8 s
Lower moveout velocity constraints	1450 m/s
Upper moveout velocity constraints	6000 m/s

Table D.2: CMP search parameters: TGS data

Parameters for stacking multiples, offsets from 150 m to 3638 m	
Coherence measurement	Semblance
Coherency	15
Minimum offset aperture	1000 m at 0.002 s
Maximum offset aperture	1500 m at 3.5 s
Lower moveout velocity constraints	1450 m/s
Upper moveout velocity constraints	1550 m/s
Parameters for stacking multiples, offsets from 3638 m to 7338 m	
Coherence measurement	Semblance
Coherency	20
Minimum offset aperture	4000 m at 0.002 s
Maximum offset aperture	5500 m at 3.5 s
Lower moveout velocity constraints	1450 m/s
Upper moveout velocity constraints	1550 m/s
Parameters for stacking primaries	
Coherence measurement	Semblance
Coherency	5
Minimum offset aperture	720 m at 0.002 s
Maximum offset aperture	3750 m at 3.5 s
Lower moveout velocity constraints	1450 m/s
Upper moveout velocity constraints	6000 m/s

Table D.3: CMP search parameters: BP 2004 dataset

Parameters for stacking multiples, offsets from 0 m to 3500 m	
Coherence measurement	Semblance
Coherency	15
Minimum offset aperture	1000 m at 0.006 s
Maximum offset aperture	2000 m at 6 s
Lower moveout velocity constraints	1480 m/s
Upper moveout velocity constraints	1550 m/s
Parameters for stacking multiples, offsets from 3500 m to 8000 m	
Coherence measurement	Semblance
Coherency	15
Minimum offset aperture	4800 m at 0.006 s
Maximum offset aperture	5000 m at 6 s
Lower moveout velocity constraints	1480 m/s
Upper moveout velocity constraints	1550 m/s
Parameters for stacking primaries	
Coherence measurement	Semblance
Coherency	5
Minimum offset aperture	1000 m at 0.2 s
Maximum offset aperture	2500 m at 8 s
Lower moveout velocity constraints	1450 m/s
Upper moveout velocity constraints	5000 m/s

Table D.4: Parameters which was used for adaptive subtraction of multiples in Sigsbee2B dataset in CMP domain

Operator length (in n of samples)	10
size of time windows (in number of samples)	50
size of space windows	2
overlap of time windows	1
overlap of space windows	1
Relative stabilization factor	0.001
Norm	2

Table D.5: Parameters which was used for adaptive subtraction of multiples in Sigsbee2B dataset in CSP domain

Operator length (in number of samples)	15
size of time windows (in number of samples)	200
size of space windows	2
overlap of time windows	1
overlap of space windows	1
Relative stabilization factor	0.001
Norm	2

Table D.6: Parameters which was used for adaptive subtraction of multiples in TGS dataset

Operator length (in number of samples)	10
size of time windows (in number of samples)	80
size of space windows	2
overlap of time windows	1
overlap of space windows	1
Relative stabilization factor	0.001
Norm	2

Table D.7: Parameters which was used for adaptive subtraction of multiples in BP 2004 dataset

Operator length (in n of samples)	10
size of time windows (in number of samples)	80
size of space windows	2
overlap of time windows	1
overlap of space windows	1
Relative stabilization factor	0.001
Norm	2

Table D.8: CSP data mapping parameters: Sigsbee2B dataset

Minimum offset aperture	-7932.0
Maximum offset aperture	0
Minimum xtarget	3055.62
Maximum xtarget	27424.38
Minimum ttarget	0
Maximum ttarget	8.0
Minimum taper radius	300
Maximum taper radius	3500
Minimum aperture radius	700
Maximum aperture radius	7500
dx	11.43
v	1480

Table D.9: CRS parameters: Sigsbee2B dataset Walda (2016).

General parameters	
Dominant frequency	20 Hz
Coherence measurement	Semblance
Coherence time window	56 ms
Velocity constraints	
Near surface velocity	1500 m/s
Lower moveout velocity constraints	1400 m/s
Upper moveout velocity constraints	6000 m/s
Search apertures	
Minimum midpoint aperture	300 m at 2 s
Maximum midpoint aperture	500 m at 11 s
Minimum offset aperture	750 m at 2 s
Maximum offset aperture	3000 m at 11 s
Conflicting dip handling	
Number of dip intervals	17
Dip intervals in °	[-90,-45], [-45,-30], [-30,-20], [-20, -12.5], [-12.5,-7.5], [-7.5,-3], [-3,3], [3, 7.5] ,[7.5,12.5], [12.5,20], [20,30], [30,45], [45,90]
Global optimization parameters	
Algorithm	Differential evolution
Number of individuals	20
Crossover probability	74.55 %
Differential weight	0.9362
Minimum number of iterations	30
Maximum number of iterations	200
Number of allowed stagnated iterations	10
Local optimization parameters	
Lower coherence threshold	1.00 at 0 s
Upper coherence threshold	1.00 at 10 s
Maximum Number of iterations	100
Minimum deviation required	10^{-5}
Transformation radius of R_N	100 m
Initial variation of emergence angle	2 °
Initial variation of R_{NIP}	3 %
Initial variation of R_N	4 °

Table D.10: CRS search parameters: TGS data Walda (2016).

General parameters	
Dominant frequency	40 Hz
Coherence measurement	Semblance
Coherence time window	26 ms
Velocity constraints	
Near surface velocity	1480 m/s
Lower moveout velocity constraints	1300 m/s
Upper moveout velocity constraints	4000 m/s
Search apertures	
Minimum midpoint aperture	300 m at 0 s
Maximum midpoint aperture	500 m at 5 s
Minimum offset aperture	750 m at 0 s
Maximum offset aperture	3000 m at 5 s
Conflicting dip handling	
Number of dip intervals	17
Dip intervals in °	[-90,-45], [-45,-22.5], [-22.5,-15], [-15, -10], [-10,-7], [-7,-4], [-4,-2], [-2, -0.75] ,[-0.75,0.75], [0.75,2], [2,4], [4,7], [7,10], [10,15], [15,22.5], [22.5, 45], [45,90]
Global optimization parameters	
Algorithm	Differential evolution
Number of individuals	20
Crossover probability	74.55 %
Differential weight	0.9362
Minimum number of iterations	30
Maximum number of iterations	200
Number of allowed stagnated iterations	10
Local optimization parameters	
Lower coherence threshold	1.00 at 0 s
Upper coherence threshold	1.00 at 5 s
Maximum Number of iterations	100
Minimum deviation required	10^{-5}
Transformation radius of R_N	100 m
Initial variation of emergence angle	2 °
Initial variation of R_{NIP}	3 %
Initial variation of R_N	4 °

Table D.11: CRS stacking parameters: TGS data Walda (2016).

Stacking parameters	
Minimum midpoint aperture	50 m at 0 s
Maximum midpoint aperture	150 m at 5 s
Minimum offset aperture	100 m at 0 s
Maximum offset aperture	3000 m at 5 s
Velocity tolerance for multiple prediction	5 %
Diffraction separation	
Minimum midpoint aperture	50 m at 0 s
Maximum midpoint aperture	150 m at 5 s
Minimum offset aperture	750 m at 0 s
Maximum offset aperture	3000 m at 5 s
Diffraction weight threshold	0.5
Partial stacks	
Regularized receiver interval	25 m
Minimum local midpoint aperture	50 m at 0 s
Maximum local midpoint aperture	150 m at 5 s
Local offset aperture	50 m
Migration	
Minimum midpoint aperture	1000 m at 0 s
Maximum midpoint aperture	2000 m at 5 s
Minimum offset aperture	2000 m at 0 s
Maximum offset aperture	4000 m at 5 s

Appendix E

List of publications

Vefagh, M. and Gajewski, D. (2014). A zero-offset picking approach for pre-stack multiple attenuation. Annual Report, Wave Inversion Technology Consortium, 18:272-280.

Vefagh, M. and Gajewski, D. (2015). A coherency guided method for pre-stack multiple attenuation. Annual Report, Wave Inversion Technology Consortium, 19:289-296.

Vefagh, M. , Düümmong, S. and Gajewski, D. (2015). A zero-offset picking approach for pre-stack multiple attenuation. In SEG Annual Meeting. Expanded abstracts.

List of Figures

List of Tables

References

Bancroft, J. C., Geiger, H. D., and Margrave, G. F. (1998). The equivalent offset method of prestack time migration. *Geophysics*, 63:2042–2053.

Barros, T., Ferrari, R., Krummenauer, R., and Lopes, R. (2015). Differential evolution-based optimization procedure for automatic estimation of the Common Reflection Surface traveltime parameters. *Geophysics*, 80:WD189–WD200.

Baykulov, M. and Gajewski, D. (2009). Prestack seismic data enhancement with partial Common Reflection Surface (CRS) stack. *Geophysics*, 74:V49–V58.

Berkhout, A. J. and Verschuur, D. (1997). Estimation of multiple scattering by iterative inversion, part I: Theoretical considerations. *Geophysics*, 62:1586–1595.

Bickel, S. H. and Natarajan, R. R. (1985). Plane-wave Q-deconvolution. *Geophysics*, 50:1426–1439.

Billette, F. and Brandsberg-Dahl, S. (2005). The 2004 BP velocity benchmark. In *EAGE Annual Meeting*. Expanded abstracts.

Clauzon, G., Suc, J. P., Gautier, F., Berger, A., and Loutre, M. F. (1996). Alternate interpretation of the Messinian salinity crisis: Controversy resolved? *Geology*, 24:363–366.

Dell, S. (2012). *Seismic processing and imaging with diffractions*. PhD thesis.

Dell, S. and Gajewski, D. (2011). Common Reflection Surface based workflow for diffraction imaging. *Geophysics*, 76:S187–S195.

Dell, S., Gajewski, D., and Vanelle, C. (2009). Common Scatter Point data mapping. *Annual Report, Wave Inversion Technology Consortium*, 13:43–57.

Dell, S., Gajewski, D., and Vanelle, C. (2010). An automatic time imaging using Common Scatter Point gathers. In *SEG Annual Meeting*. Expanded abstracts.

Diebold, J. B. and Stoffa, P. L. (1981). The traveltime equation, tau-p mapping, and inversion of common midpoint data. *Geophysics*, 46:238–254.

Dümmong, S. (2010). *Seismic data processing with an expanded Common Reflection Surface workflow*. PhD thesis.

Dümmong, S. and Gajewski, D. (2008). A multiple suppression method via CRS attributes. In *SEG Annual Meeting*. Expanded abstracts.

Duncan, G. and Beresford, G. (1994). Slowness adaptive f-k filtering of prestack seismic data. *Geophysics*, 59:140–147.

Embree, P., Burg, J. P., and Backus, M. M. (1963). Wide-band velocity filtering the pie-slice process. *Geophysics*, 28:948–974.

Glöckner, M., Schwarz, B., Vanelle, C., and Gajewski, D. (2016). Kinematic time demigration with an automatically generated velocity model. In *EAGE Annual Meeting*. Expanded abstracts.

Gradmann, S., Hübscher, C., Ben-Avraham, Z., Gajewski, D., and Netzeband, G. (2005). Salt tectonics off northern Israel. *Marine and Petroleum Geology*, 22:597–611.

Hale, D. (2009). A method for estimating apparent displacement vectors from time-lapse seismic images. *Geophysics*, 74:V99–V107.

Hampson, D. (1986). Inverse velocity stacking for multiple elimination. *Canadian Journal of Exploration Geophysics*, 22:44–55.

Hubral, P. (1983). Computing true amplitude reflections in a laterally inhomogeneous earth. *Geophysics*, 48:1051–1062.

Hubral, P. and Krey, T. (1980). *Interval velocities from seismic reflection time measurements*. Society of Exploration Geophysicists.

Kelamis, P. and Verschuur, D. (1996). Mulitple elimination strategies for land data. In *EAGE Annual Meeting*. Expanded abstract.

Krijgsman, W., Hilgen, F., Raffi, I., Sierro, F., and Wilson, D. (1999). Chronology, causes and progression of the Messinian salinity crisis. *Nature*, 400:652–655.

Landa, E., Belfer, I., and Keydar, S. (1999). Multiple attenuation in the parabolic τ-p domain using wavefront characteristics of multiple generating primaries. *Geophysics*, 64:1806–1815.

Leinbach, J. (1995). Wiener spiking deconvolution and minimum-phase wavelets: A tutorial. *The Leading Edge*, 14:189–192.

Levinson, N. (1947). The Wiener RMS (Root Mean Squar) error criterion in filter design and prediction. *Journal of Mathematics and Physics*, 25:261–278.

Mann, J. (2002). *Extensions and Applications of the Common Reflection Surface Stack Method*. Logos Verlag Berlin.

March, D. and Bailey, A. (1983). A review of the two-dimensional transform and its use in seismic processing. *First break*, 1:9–21.

Mayne, W. H. (1962). Common Reflection Point horizontal data stacking techniques. *Geophysics*, 27:927–938.

Meunier, J. (1999). 3D geometry, velocity filtering and scattered noise. In *SEG Annual Meeting*. Expanded abstracts.

Müller, T. (1999). *Seismic imaging without explicit knowledge of the velocity model*. PhD thesis, TH Karlsruhe.

Neidell, N. and Taner, M. (1971). Semblance and other coherency measures for multichannel data. *Geophysics*, 71:482–497.

Nelder, J. A. and Mead, R. (1965). A simplex method for function minimization. *The computer journal*, 7:308–313.

Netzeband, G., Gohl, K., Hübscher, C., Ben-Avraham, Z., Dehghani, G., Gajewski, D., and Liersch, P. (2006a). The levantine basin-crustal structure and origin. *Tectonophysics*, 418:167–188.

Netzeband, G., Hübscher, C., and Gajewski, D. (2006b). The structural evolution of the messinian evaporites in the levantine basin. *Marine Geology*, 230:249–273.

Oppenheim, A. V., Willsky, A. S., and Young, I. T. (1983). *Signals and Systems*. Prentice Hall.

O'Doherty, R. F. and Anstey, N. A. (1971). Reflection on amplitudes. *Geophysical Prospecting*, 19:430–458.

Peardon, L. and Bacon, C. (1992). An introduction to f-k-k techniques. *First Break*, 10:113–123.

Perez-Careta, E., Torres-Cisneros, M., Avina-Cervantes, J., Debeir, O., Ibarra-Manzano, O., Aguilera-Gomez, E., Perez-Pantoja, E., and Negrete-Romero, G. (2008). Cell recognition and tracking using nonlinear crosscorrelation. In *Digest of the leos summer topical Meetings*.

Rad, P. B., Gajewski, D., and Vanelle, C. (2016). Diffraction separation based on the projected first fresnel zone. In *EAGE Annual Meeting*. Expanded abstracts.

Robinson, E. A. (1957). Predictive decomposition of seismic traces. *Geophysics*, 22:767–778.

Robinson, E. A. (1967). Predictive decomposition of time series with application to seismic exploration. *Geophysics*, 32:418–484.

Ryu, J. V. (1982). Decomposition (decom) approach applied to wave field analysis with seismic reflection records. *Geophysics*, 47:869–883.

Schleicher, J. and Biloti, R. (2006). Dip correction for coherence-based time migration velocity analysis. *Geophysics*, 72:S41–S48.

Schwarz, B. (2011). *A new nonhyperbolic multi-parameter stacking operator*. Diploma thesis.

Stoughton, D., Stefani, J., and Michell, S. (2001). 2D elastic model for wavefield investigations of subsalt objectives, deep water gulf of mexico. In *EAGE Annual Meeting*. Expanded abstracts.

Thorson, J. R. and Claerbout, J. F. (1985). Velocity-stack and slant-stack stochastic inversion. *Geophysics*, 50:2727–2741.

Verschuur, D. (2006). *Seismic multiple removal techniques*. EAGE Publications.

Verschuur, D., Berkhout, A., and Wapenaar, C. (1992). Adaptive surface related multiple elimination. *Geophysics*, 57:1166–1177.

Walda, J. (2016). *Determination and application of wavefront attributes*. PhD thesis.

Walda, J. and Gajewski, D. (2015a). Common Reflection Surface stack improvement by differential evolution and conflicting dip processing. In *SEG Annual Meeting*. Expanded abstracts.

Walda, J. and Gajewski, D. (2015b). Global optimization of the CRS operator using a genetic algorithm. In *EAGE Annual Meeting*. Expanded abstracts.

Walda, J. and Gajewski, D. (2015c). Handling the conflicting dip problem in the CRS/iCRS methods. In *EAGE Annual Meeting*. Expanded abstracts.

Webster, G. M. (1978). *Deconvolution*, volume 1. Society of Exploration Geophysicists.

Wiener, N. (1964). *Extrapolation, Interpolation, and Smoothing of Stationary Time Series*. The MIT Press.

Yang, Y., Vanelle, C., and Gajewski, D. (2016). A new kinematic time demigration approach based on the CSP method. In *EAGE Annual Meeting*. Expanded abstracts.

Yilmaz, Ö. (2001). *Seismic data analysis*, volume 1. Society of Exploration Geophysicists.

Acknowledgments

- I have literally no words to express my gratefulness to Prof. Dr. Dirk Gajewski for giving me the chance and accepting me as PhD student, supervision of this work. His door was always open for me when questions about my current working topics occurred. He gave me the opportunity to produce this work and allowed me to participate in many geophysical conferences around the globe.
- I am also grateful to PD. Dr. Claudia Vanelle for the co-supervision of my thesis and also for teaching me how to give presentation. Special thank for the proofreading of this thesis.
- I would like to thank Stefan Dümmong, Alex Müller, and Eric Verschuur for providing me with the codes that I needed.
- I am very great full to Dr. Oksana Zhebel, Dela Spickermann, and Marie Voß for proofreading of this thesis. All remaining mistakes are mine.
- I also like to say thank you to Dr. Ekkehart Tessmer for managing of my computer requirements.
- I am as well grateful to Prof. Dr. Christian Hübscher, Dr. Sergius Dell, Dr. Benjamin Schwarz, Robert Pfau, Yan Yang, Ivan Abakumov, Martina Glöckner, and Jan Walda for fruitful technical discussion.
- I would like to say thank you to Paola Dal Corso who always helped me with administration issues.
- I am very grateful to the applied seismic working group for interesting discussions, good advices and support, and for providing a friendly environment.
- I gratefully acknowledge the Wave Inversion Technology (WIT) consortium for financial support.
- I like to thank BP company for providing BP 2004 synthetic dataset, Subsalt Multiple Attenuation and Reduction Technology Joint Venture (SMAART JV) for Providing Sigsbee2B dataset, and TGS company for providing the Eastern Mediterranean dataset.
- I also would like to thank CWP Seismic Unix for providing seismic cods. NORSAR and Schlumberger for providing the softwares that I used in this thesis.

- My special thanks goes to Dr. Ali Dehghani and his lovely wife Mrs. Ashraf Dehghani for their support in every difficult situation.
- Obviously, I like to thank my family for their long distance support throughout my PhD. At the end I like to thank my husband for always supporting and encouraging me.

Eidesstattliche Versicherung

Eidesstattliche Versicherung
Declaration on oath

Hiermit erkläre ich an Eides statt, dass ich die vorliegende Dissertationsschrift selbst verfasst und keine anderen als die angegebenen Quellen und Hilfsmittel benutzt habe.

I hereby declare, on oath, that I have written the present dissertation by my own and have not used other than the acknowledged resources and aids.

Hamburg, den 8. November 2016
City and date

Unterschrift
Signature Manizheh Vefaghnematollahy